GEOLOGICA ULTRAIECTINA

Mededelingen van de
Faculteit Aardwetenschappen
Universiteit Utrecht

No. 196

Chemical osmosis in natural clayey materials

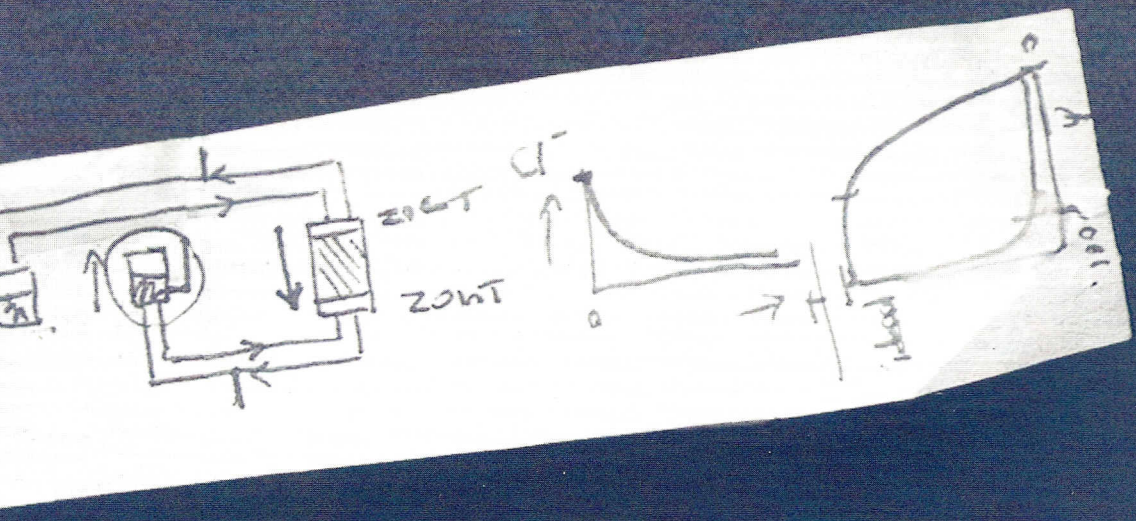

Thomas JS Keijzer

GEOLOGICA ULTRAIECTINA

MEDEDELINGEN VAN DE
FACULTEIT AARDWETENSCHAPPEN
UNIVERSITEIT UTRECHT

No. 196

Chemical osmosis in natural clayey materials

Thomas JS Keijzer

ISBN 90–5744–053–9

Chemical osmosis in natural clayey materials

Chemische osmose in natuurlijke kleiige materialen

(met een samenvatting in het Nederlands)

PROEFSCHRIFT

TER VERKRIJGING VAN DE GRAAD VAN DOCTOR
AAN DE UNIVERSITEIT UTRECHT
OP GEZAG VAN DE RECTOR MAGNIFICUS, PROF. DR H.O. VOORMA,
INGEVOLGE HET BESLUIT VAN HET COLLEGE VAN PROMOTIES
IN HET OPENBAAR TE VERDEDIGEN
OP MAANDAG 27 NOVEMBER 2000 DES OCHTENDS TE 10.30 UUR

door

Thomas Jillerd Simon Keijzer
geboren op 16 september 1966, te Bramsche

PROMOTOR Prof. Dr CH van der Weijden
Faculteit Aardwetenschappen
Projectgroep Geochemie
Universiteit Utrecht

CO-PROMOTOR Dr Ir JPG Loch
Faculteit Aardwetenschappen
Projectgroep Geochemie
Universiteit Utrecht

The research described in this thesis was carried out at the Faculty of Earth Sciences, Projectgroup Geochemistry, Universiteit Utrecht, Budapestlaan 4, PO Box 80021, 3508 TA Utrecht, the Netherlands. This study was partly financed by the Directorate General for Public Works and Water Management (*Rijkswaterstaat*).

Voorkant – Chemische osmose uitgelegd op de achterkant van een kassabon.
Cover – Chemical osmosis explained on the backside of a supermarket receipt.

Misschien is niets geheel waar, en zelfs dat niet.

Multatuli – Idee 1

Contents

Introduction

Osmosis? Isn't that the very well known, but also poorly understood subject from biology class in secondary school? The 'emergency exit' for every question asked during the biology lesson? What has osmosis to do with earth sciences? Both biology and earth sciences include the study of materials capable of separating the transport of solutes from the transport of solvents. These materials exhibit semipermeable properties. Biology shows that the membrane walls of plant and animal cells are capable of restricting the passage of salts, or sugar in biology class, but allow water to pass in or out of the cell depending on the solution in which the cells are placed. The most famous membrane is the pig bladder which served as an example of semipermeability for countless generations of scientists in several scientific disciplines (e.g. Kruyt & Overbeek, 1965). Earth sciences can show that clays or sediments with high clay content are capable to act as a semipermeable membrane under certain conditions.

In earth sciences semipermeable properties were recognised at the end of the nineteenth and beginning of the twentieth century. Becker (1893) suggested that natural high concentration of metals might be the result of membrane processes. Briggs (1902) was probably the first who gave an experimental demonstration of the semipermeable properties of clays by passing different salts through the sedimentated clay fraction of a soil. That semipermeable properties may have a profound effect on large geological systems, and might be held responsible for observed highly saline ground waters, was suggested by Russel (1933) and later by De Sitter (1947). A short abstract by Berry and Hanshaw (1960) on the formation of brines in the subsurface, and Hanshaw's thesis (Hanshaw, 1962) initiated a multitude of studies into the semipermeable behaviour of predominantly shales and bentonites. During the sixties and seventies various studies were aimed to determine the properties and circumstances that are favourable for a natural material to act as a semipermeable membrane. Models were proposed based on the anion exclusion or salt sieving properties of the clay either by the Donnan theorem, like the Teorell–Meyer–Siever model (e.g. Hanshaw, 1962) and the Fritz–Marine Membrane Model (e.g. Fritz, 1986), or by the diffuse double layer theory (Kemper, 1972; Bresler, 1973; Bolt, 1982b). Studies on the impact

of this separation of transport of the solute and the solvent in geological systems were limited to the laboratory determination of the retention order of different cations (e.g. Kharaka & Berry, 1973) or isotopic fractionation (e.g. Fritz & Whitworth, 1994). The relative unfamiliarity of the geologist with semipermeability and its impact on the tools he or she uses to study geochemical and geological systems stems from the lack of field situations where beyond reasonable doubt its impact is shown. A number of studies suggested or suspected the occurrence of semipermeability on the processes observed. Semipermeability was suggested to play a role in the development of brine formation waters (e.g. Russell, 1933; De Sitter, 1947; Graf, 1983), the occurrence of unrealistic high aquifer pressures (e.g. Marine & Fritz, 1981), and the shift of isotopic fractionation in sediment cores (Boulegue *et al.*, 1990). In soil physics, osmosis was traditionally associated with the swelling of clays (e.g. Bolt & Miller, 1955; Warkentin *et al.*, 1957).

Only recently, Neuzil (2000) was able to demonstrate that an *in situ* shale is capable of osmotic water transport, thus proving that on a field scale semipermeability can have an effect on the transport of water and solutes. This observation raises concerns about the impact semipermeability can have when large salt concentration differences are separated by horizontally extended clay layers, a common situation in the subsurface of the western parts of the Netherlands. A potential osmotic system was already identified in the *Haarlemmermeer Polder* near Amsterdam by De Haven (1982). He concluded that osmotic phenomena should be considered in the analysis of water balance. However, this advice was never explored in the description and modelling of ground water in these salt/fresh water systems. As the exploitation of the western parts of the Netherlands intensifies, solutions for the disposal of waste and the containment of contaminants focus on the application of clay barriers to prevent the undesirable transport of pollutants. This raises the question whether clays, or depots for permanent storage of contaminated clayey sediments, can be used without the knowledge of, or insight in the semipermeable properties of these materials.

SCOPE OF THIS STUDY

The main objective of the study presented in this thesis is to develop and apply laboratory instrumentation that enables the direct measurement of the semipermeability of natural contaminated materials. The semipermeability of natural clays, its importance and possible impact on the transport of contaminants, was first discussed in the Netherlands within the framework of the environmental aspects of permanent harbour sludge depots (Van den Berg & Loch, 1993). One of the main depots,

De Slufter near the Port of Rotterdam, is constructed in a salt water aquifer without a bottom liner. The clayey harbour sludge itself is thought to act as a low permeable layer, restricting advective transport of contaminants. However, the design possibly also enables the sludge layer to act as a semipermeable membrane. Semipermeability can induce water transport by chemical osmosis, and subsequently transport of contaminants out of the sludge into the aquifer. As a consequence, the design criteria regarding water and pollutant fluxes from the depot as laid down in Dutch legislation may be exceeded. Other man made situations where semipermeability of clays can have a profound effect on the transport of contaminants may exist in landfill sites. Here clay barriers, often consisting of bentonite or a sand–bentonite mixture, are applied to prevent emissions from the landfill.

Against this background the samples investigated in this study are natural clays —bentonite— and clayey contaminated sediments —harbour sludge— under conditions closely related to those encountered in the Netherlands.

OUTLINE OF THIS THESIS

The theoretical framework of semipermeability of natural clayey materials is discussed in **Chapter 1**. This chapter is also intended to give the reader a comprehensive overview of the available models and will introduce the terminology. It includes a detailed overview of the research carried out on semipermeability of natural earth materials, and addresses the role this may have on processes observed in geological systems. **Chapter 2** introduces and discusses the samples used in the experiments. **Chapter 3** contains a short description of the historical development of instrumention used for research of osmotic phenomena. Moreover, it describes a novel design based on a flexible wall permeameter used in this study. The design criteria are formulated and a description of the instrumentation is given together with the general experimental procedures. Its performance during several tests on clay and non–clay samples are discussed. The apparatus was used to determine the semipermeability of a commercially available Wyoming bentonite. The results of these experiments are discussed in **Chapter 4**. Experiments were done on loose and more compacted samples of bentonite. Results were compared with the semipermeability predicted by three available models, and discussed within the context of earlier experiments on bentonite. In **Chapter 5** the experiments on the semipermeability of harbour sludge are presented and discussed. Again the applicability of the theory is compared with the experimental observations, and the relative importances of the factors that make the sludge a semipermeable membrane are discussed. As there is little to no reference work done on

unconsolidated sediments the results are compared with shales. **Chapter 6** reports the fate of polycyclic aromatic hydrocarbons in the samples of harbour sludge when subjected to a small advective flux. Polycyclic aromatic hydrocarbons are an example of contaminants that may be transported by advection due to osmosis. Their nonionic hydrophobic character permits transport through the barrier that is semipermeable by its charge properties. The last chapter, **Chapter 7**, discusses advantages and disadvantages of the instrumentation developed for this study. A synthesis is given of the experimental work and the implications it has on the storage of harbour sludge in depots. The applicability of the models to 'messy', natural samples is discussed.

1 Chemical osmosis in natural clayey materials: A review

1.1 INTRODUCTION

This chapter is intended to provide the reader with a short but comprehensive overview of the behaviour of clays as natural semipermeable membranes. It also gives a summary of the research carried out on this subject as well as the terminology and theory behind so–called coupled transport which includes chemical osmosis. Additionally, the role of osmotic processes in natural systems is discussed.

Clay minerals

Clay minerals are made up of combinations of two simple structural units, the silica tetrahedron and the octahedron. In the octahedron divalent ions like Mg^{2+} and Fe^{2+} as well as Al^{3+} are bound to oxygen in six fold coordination. These units are assembled in sheets with the general formula $(Si_2O_5^{2-})_n$ for the tetrahedron and $(Al_2(OH)_6)_n$ or $((Fe \text{ or } Mg)_3(OH)_6)_n$ for the octahedron sheet. When a clay mineral consists of one octahedral and one tetrahedral sheet a so–called 1:1 layer or platelet is formed as in the mineral kaolinite. If an octahedral sheet is sandwiched between two tetrahedral sheets, a 2:1 platelet is formed as in montmorillonite, a member of the smectite group. The different clay minerals are thus characterised by the differences in stacking of these sheets and the manner in which the successive two– or three–sheet platelets are held together. Differences between minerals within a clay mineral group result from differences within the crystal structure of the tetrahedral and octahedral sheet, known as isomorphic substitution. Isomorphic substitution is the presence of a cation other than the Si^{4+} in the ideal tetrahedral and Al^{3+} in the ideal octahedral sheet. Common is the substitution of Al^{3+} for Si^{4+} in the tetrahedral sheet and Mg^{2+} or Fe^{2+} for Al^{3+} in the octahedral sheet. As a result of these substitutions, most clay surfaces have a net negative surface charge under natural conditions. In some clays, e.g. in kaolinite, the negative charge is mainly the result of broken bonds along non–cleavage surfaces.

To preserve electrical neutrality the negative charge of the clay particle is balanced by the attraction of cations which are held between the layers and on the surface of the particles. While electrostatically attracted the concentration of these cations or counter–ions diminishes with increasing distance from the clay particle surface (Figure 1.1). The charged clay surface together with the counter–ions in the pore water form the diffuse double layer. The pore water outside the double layer region is referred to as the equilibrium or free solution. In the idealised form this is known as the Gouy–Chapman double layer (Mitchell, 1993). The cations in the double layer are subjected to opposing forces. Electrostatic forces attract the cations towards the charged clay surface, whereas by diffusion they tend to move away from the surface. Simultaneously, the anions or co–ions with the same charge as the clay surface are repelled from the surface. Diffusion from the equilibrium solution towards the surface counteracts the electric repulsion of anions. At equilibrium the average concentration of the ions at a known distance from the clay surface is a function of the concentration in the equilibrium concentration (Horseman *et al.*, 1996). Furthermore, the double layer is influenced by the valency of the counter–ions and the temperature (Mitchell, 1993).

Clay as a semipermeable membrane

Semipermeability is defined as the ability of a material to prevent the passage of a solute without affecting the passage of the solvent (Mitchell, 1993). The ability of a clay to act as a semipermeable membrane arises when the double layers of adjacent clay platelets overlap (Figure 1.2). This overlap can be the result of compaction of the

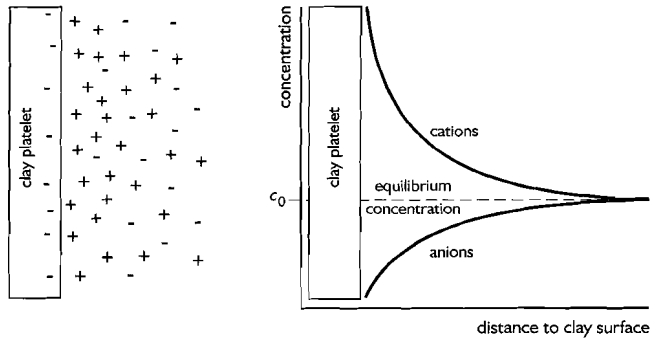

Figure 1.1 Distribution of cations and anions adjacent to a clay platelet according to the diffuse double layer theory (after Mitchell, 1993).

clay under an overburden load. It results in an even higher concentration of cations and lower concentration of anions in the double layer with respect to the equilibrium solution (Figure 1.2). The water film present in the narrow pore between the clay layers is thus completely dominated by the overlapping double layers, and the electrical restrictions they impose. Anions attempting to migrate through the narrow aqueous film are repelled by the negative charge of the clay platelets. This effect is known as 'negative adsorption' or Donnan Exclusion (Mitchell, 1993; Horseman *et al.*, 1996). In order to maintain electrical neutrality in the external solution cations will tend to remain with their co–ions. Thus, their movement across the clay will also be restricted (Fritz, 1986).

The above mechanism holds for charged membranes such as clays. There are, however, also uncharged semipermeable membranes. In these uncharged membranes rejection of a solute is on the basis of size or mobility. The result is that lighter, smaller or more mobile components are less restricted during their passage of the membrane than the heavier or larger ones (Whitworth, 1993). Semipermeable properties of clays with essentially no charge, like kaolinite, arise predominantly from their size exclusion properties.

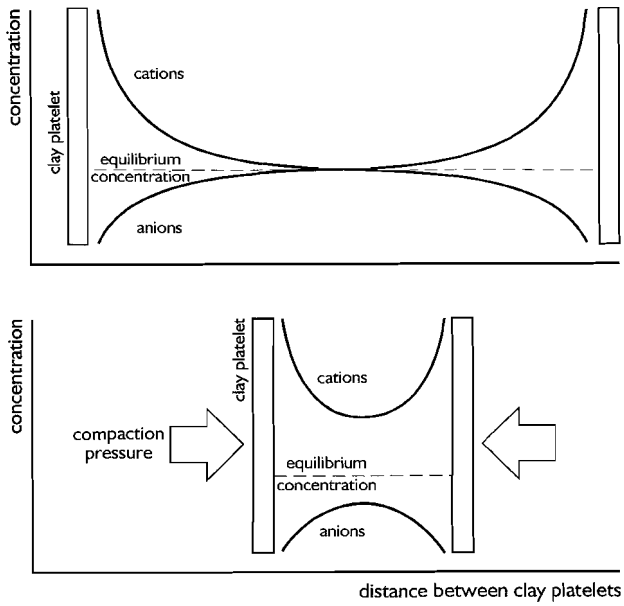

Figure 1.2 Distribution of cations and anions adjacent to a clay platelet; **top** in a completely dispersed situation without overlap of the double layers, and **bottom** with overlap e.g. as a result of compaction.

1.2 TRANSPORT PHENOMENA

Flow laws and coupled flow

According to Mitchell (1993) each flux in soils and sediments relates linearly to its corresponding driving force, provided that the flow process does not change the state of the soil, according to:

$$J_i = L_{ii} X_i \tag{1.1}$$

where J_i is the flux of a component —be it water, electrons, solutes or heat— L_{ii} is the conductivity coefficient for the specific flux, and X_i the corresponding driving force. When written for the water flux Eq. 1.1 becomes:

$$Q_h = K_h\, i \tag{1.2}$$

and is known as Darcy's law in which Q_h is the flux of water in $m{\cdot}s^{-1}$, K_h the hydraulic conductivity $m{\cdot}s^{-1}$, and i the hydraulic pressure gradient. In most cases, however, even when only one driving force is present it can result in simultaneous flows of different types. For example, when pore water flows under a hydraulic gradient, it can induce a concurrent flow of solutes by advection. This simultaneous

Table 1.1 Direct and coupled flow phenomena. The direct flows with their flow laws are given in the shaded cells (Alexander, 1990; Mitchell, 1993).

flow	gradient			
	hydraulic	temperature	electrical	chemical
fluid	hydraulic flow *Darcy's law*	thermo–osmosis	electro–osmosis	chemical osmosis
heat	convective heat flow	thermal conduction *Fourier's law*	Peltier effect	Dufour effect
current	streaming current	Seebeck effect	electric current *Ohm's law*	diffusion and membrane potentials
ion	streaming current	Soret effect	electro–phoresis	diffusion *Fick's law*

flow is called coupled flow. Thus, a gradient of one type can cause the flow of another type according to (Katchalsky & Curran, 1965; Mitchell, 1993):

$$J_i = \sum_{j=1}^{n} L_{ij} X_j \tag{1.3}$$

in which J_i is the flux of type i, L_{ij} is the coupling coefficient and X_j the driving force of type j. The coupled flows are given in Table 1.1 as well as the normal, direct flows. Sets of equations for the description of coupled flow as a result of different driving forces can be subsequently derived (Groenevelt & Bolt, 1969; Yeung, 1990; Yeung & Mitchell; 1993).

Of all phenomena listed in Table 1.1, only those induced by a hydraulic or a chemical gradient are considered in the current study.

Chemical osmosis

Non–hydraulically driven fluid flow is generally denoted as osmosis. Chemical osmosis, or chemico–osmosis, refers to the flow of water induced by a chemical difference across a semipermeable membrane e.g. a compacted clay layer. In an imaginary experiment using an open U–tube (Figure 1.3), an initial situation is given in which a semipermeable membrane separates aqueous solutions of different concentrations with no initial hydraulic pressure difference. Transport of water will occur as a result of this chemical difference until a hydraulic pressure difference is established equal to the osmotic pressure difference between the two solutions (Figure 1.3). The osmotic pressure difference between two solutions can be calculated using:

$$\Delta\pi_0 = \frac{RT}{\bar{V}_w} \ln \frac{a_w^{low}}{a_w^{high}} \tag{1.4}$$

here $\Delta\pi_0$ is the osmotic pressure difference in Pa between the equilibrium solutions. Due to the excess of counterions in the overlapping double layers of compacted clays and clay rich materials, the osmotic pressure in the interstitial water between the clay platelets (π) differs from that in the equilibrium solution (π_0). Furthermore, R is the gas constant (8.31451 $J \cdot K^{-1} \cdot mol^{-1}$), T the absolute temperature, $\bar{V}_w$ the partial molar volume of water ($m^3 \cdot mol^{-1}$), and a_w is the activity of the water at the low (a_w^{low}) and high (a_w^{high}) concentration side of the membrane. Thus the actual driving

force is not the concentration gradient of the salt, but the activity gradient of the water across the membrane. The activity of water at different concentrations can be found using (Robinson & Stokes, 1959):

$$\ln a_W = -\frac{\nu m W_w}{1000}\phi \tag{1.5}$$

in which ϕ is the molal osmotic coefficient, ν is an integer representing the number of ions in which the electrolyte dissociates, e.g. for NaCl ν equals 2, m is the molality of the solution in mol·kg^{-1}, and W_W is the molar mass of the solvent in kg·mol^{-1}. The value of ϕ is unique for each electrolyte and a function of the temperature. Robinson and Stokes (1959) have tabulated values of ϕ for a large number of electrolytes and temperatures. However, the value for a_W at low concentrations can also be estimated by (Alexander, 1990):

$$a_W = 1 - 0.017\nu m \tag{1.6}$$

Reverse osmosis

Reverse osmosis or hyperfiltration refers to hydraulically driven water transport in the presence of a counteracting osmotic gradient. Reverse osmosis occurs when a hydraulic pressure in excess of the osmotic pressure is present at the salt water side of the semipermeable membrane (Figure 1.3). The direction of flow is reversed with respect to the flow of water during chemical osmosis. Thus, during reverse osmosis water flows across the membrane from the high to the low solute concentration side.

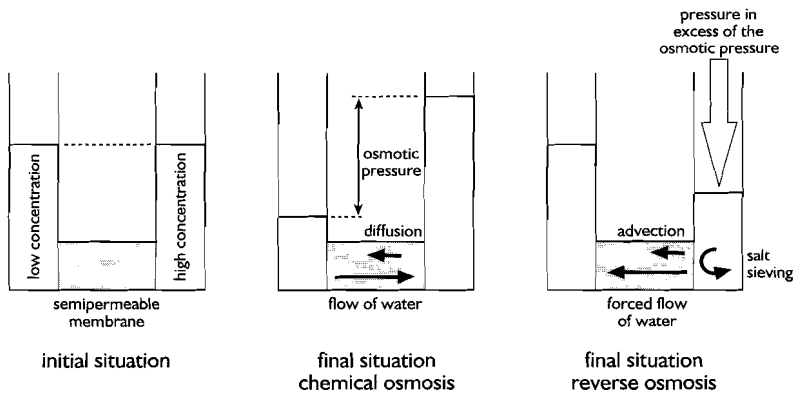

Figure 1.3 Imaginary experiment using a U-tube showing the principles of chemical osmosis and reverse osmosis.

Reverse osmosis is commonly applied in industrial processes, e.g. for desalination (Merten, 1966) or the removal of inorganic and organic solutes from surface and ground waters (Sun *et al.*, 1995; Kaštelan–Kunst *et al.*, 1997). The technique was also used for the investigation of semipermeable membrane properties of natural clayey materials (e.g. Milne *et al.*, 1964; Kharaka & Berry, 1973; Demir, 1988) and their industrial application (Ishiguro *et al.*, 1995)

1.3 IDEAL AND NON–IDEAL SEMIPERMEABLE MEMBRANES

Before describing the behaviour of semipermeable membranes in a mathematical way, membrane ideality should be first discussed. In natural systems semipermeable membranes are seldom ideal, most membranes do not restrict the passage of all the solutes present in the solvent as it passes the membrane. In addition, diffusion of solutes as a result of the chemical gradient occurs. Such membranes are non–ideal and are sometimes referred to as 'leaky' membranes. An ideal membrane completely restricts the passage of solutes through its structure. As an illustration the development of a hydraulic head across an ideal and non–ideal semipermeable membrane is given in Figure 1.4.

Based on the assumption that under stationary conditions the thermodynamic forces acting across a semipermeable membrane are counterbalanced by the total sum of mechanical friction, Katchalsky and Curran (1965) —using the framework of irreversible thermodynamics— derived a series of expressions for the transport of ions and solution through semipermeable membranes.

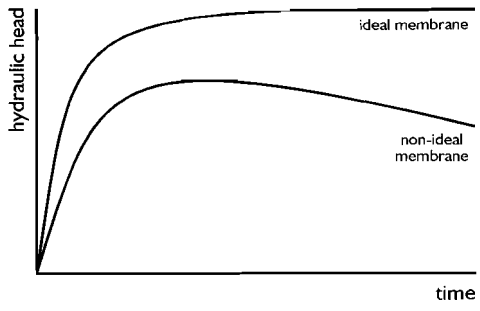

Figure 1.4 Schematic representation of the development of a hydraulic head across an ideal and non–ideal semipermeable membrane (after Katchalsky & Curran, 1965).

For an isothermal, iso–electrical system the flux of solvent (J_v, in $m \cdot s^{-1}$) and solute (J_s, in $mol \cdot m^{-2} \cdot s^{-1}$) perpendicular to the membrane are given by (Katchalsky & Curran, 1965; Fritz, 1986):

$$J_v = L_p(\Delta p - \sigma \Delta \pi_o) \tag{1.7}$$

$$J_s = \bar{c}_s(1-\sigma)J_v + \omega \Delta \pi_o \tag{1.8}$$

in which $\bar{c}_s$ is the average solute concentration across the membrane in $mol \cdot m^{-3}$, σ is the reflection coefficient, ω is the solute permeability coefficient in $mol \cdot N^{-1} \cdot s^{-1}$, $\Delta \pi_o$ is the osmostic pressure difference across the membrane in the equilibrium solution, L_p is the hydraulic permeability coefficient in $m^3 \cdot N^{-1} \cdot s^{-1}$ and Δp is the hydraulic pressure difference across the membrane in Pa. The three phenomenological coefficients in Eq. 1.7 and 1.8 —σ, ω and L_p— can be experimentally determined and are useful in describing membrane behaviour.

Hydraulic permeability coefficient, L_p

The hydraulic permeability coefficient is a measure of the mechanical filtration capacity of a membrane. This coefficient relates the fluid discharge through a membrane in response of a pressure difference (Fritz, 1986). The hydraulic permeability coefficient L_p in $m^3 \cdot N^{-1} \cdot s^{-1}$ for a semipermeable membrane is not equal to the hydraulic permeability, K_h in $m \cdot s^{-1}$, as it includes the effect of membrane thickness. The hydraulic permeability coefficient is related to K_h according to (Fritz, 1986):

$$L_p = \frac{K_h}{\rho g x} \tag{1.9}$$

in which ρ is the fluid density in $kg \cdot m^{-3}$, g is the gravitational constant (9.8066 $m \cdot s^{-2}$) and x is the thickness of the membrane in m. When there is no osmotic pressure across the membrane L_p can be measured from the ratio of J_v over Δp.

Solute permeability coefficient, ω

The solute permeability coefficient controls the rate at which the solute diffuses across a semipermeable membrane as a result of a chemical gradient. For an ideal membrane, the value of ω equals 0, whereas for non–ideal membranes it has a positive value which is highest for a membrane without semipermeable properties. It differs

from the normal Fickian diffusion coefficient because it incorporates the physical and electrical impedance of the membrane to the diffusion path (Fritz & Whitworth, 1994). The solute permeability coefficient ω in $mol \cdot N^{-1} \cdot s^{-1}$ is related to the Fickian diffusion coefficient D_0 in $m^2 \cdot s^{-1}$ through:

$$\omega = \frac{D_0}{RTx\tau} \tag{1.10}$$

where R is the gas constant (8.31451 $J \cdot K^{-1} \cdot mol^{-1}$), T is the absolute temperature, x is the thickness of the sample in m, and τ is the tortuosity of the membrane. The tortuosity is defined as L_e/L, which is the ratio of the actual effective distance of flow through the sample (L_e) and the straight line or macroscopic distance of the membrane (L). This definition yields values for τ above 1 (Fritz & Marine, 1983; Fritz & Whitworth, 1994).

Reflection coefficient, σ

In natural systems semipermeable membranes are seldom ideal. The non–ideality of a membrane is expressed as the reflection coefficient σ which is defined as the ratio of the developed hydraulic pressure over the applied osmotic pressure after equilibrium, i.e. at zero solution flux (Katchalsky & Curran, 1965):

$$\sigma = \left(\frac{\Delta p}{\Delta \pi_0} \right)_{J_v = 0} \tag{1.11}$$

An ideal membrane has a reflection coefficient of 1, whereas for non–ideal membranes the value varies between 0 and 1. In porous media without semipermeability the reflection coefficient equals 0. The reflection coefficient is the most informative parameter as it can be used to predict the hydraulic pressure that is induced across a membrane as the result of a chemical gradient. There are several synonyms for ideality found in the literature. Most commonly encountered are the osmotic efficiency, ranging from 0–1 or 0–100 %, and the membrane or filtration efficiency with values between 0–100 %.

There are a host of factors influencing the ideality of natural clayey semipermeable membranes of which the type of clay, its cation exchange capacity and exchangeable cations, the compaction and the salt concentration in the equilibrium solution are the most important. In Table 1.2 (p. 21) an overview of the influencing factors determined in laboratory experiments is listed.

Several models have been published over the years for the prediction of the reflection coefficient in natural systems based on the framework of irreversible thermodynamics as formulated by Katchalsky and Curran (1965). Three models will be introduced here and will be referred to throughout this thesis: the Fritz–Marine Membrane Model, the model by Kemper and Bresler, and the model by Groenevelt and Bolt.

1.4 FRITZ–MARINE MEMBRANE MODEL

The Fritz–Marine Membrane Model (FMMM – Marine & Fritz, 1981; Fritz & Marine, 1983; Fritz, 1986) is a refinement of the Teorell–Meyer–Siever model (TMS) for the potential distribution across a charged membrane based on the Donnan concept of a diffuse double layer (Hanshaw, 1962; Kaharaka & Berry, 1973). According to the authors the FMMM is modified for the mineralogy and porosity found under geological conditions. The expression derived for σ in this model is:

$$\sigma = 1 - \frac{K_s(R_w + 1)}{\left[\left(R_w \frac{\overline{C}_a}{\overline{C}_c} + 1\right) + R_{wm}\left(R_m \frac{\overline{C}_a}{\overline{C}_c} + 1\right)\right] n} \tag{1.12}$$

in which K_s is a measure for the salt exclusion properties of the semipermeable membrane given by (Fritz, 1986):

$$K_s = \frac{\overline{C}_a}{\overline{c}_s} \tag{1.13}$$

where $\overline{C}_a$ is the anion concentration in the membrane pores in mol·cm^{-3} and $\overline{c}_s$ is the average concentration in mol·cm^{-3} of both solutions separated by the membrane. The cation concentration, $\overline{C}_c$, in moles per cm^3 of membrane is given by:

$$\overline{C}_c = \overline{C}_a + \mathrm{CEC}\,\rho_p(1 - n) \tag{1.14}$$

where $\overline{C}_a$ can be found using:

$$\overline{C}_a = -\tfrac{1}{2}\mathrm{CEC}\,\rho_p(1-n) + \tfrac{1}{2}\sqrt{\mathrm{CEC}^2\,\rho_p{}^2(1-n)^2 + 4\overline{c}_s{}^2 n^2} \tag{1.15}$$

in which CEC is the cation exchange capacity in $\mathrm{mol_c \cdot g^{-1}}$, ρ_p is the particle density of the membrane material in $\mathrm{g \cdot cm^{-3}}$, and n is the porosity of the membrane.

Equation 1.12 contains a set of friction ratio coefficients which will be discussed below. Firstly, R_m is the ratio of the friction coefficient (f) of the cations (c) and anions (a) with the solid membrane structure (m), thus $R_m = f_{cm}/f_{am}$. It relates the tendencies of the charged species to be retarded by frictional resistance by the membrane walls. Assuming that the frictional resistance is a pure physical phenomenon, and thus independent of electrostatic effects between the ions, the value for R_m can be approximated by taking the ratio of the hydrated radii of the ions. This results for the $\mathrm{NaCl{+}H_2O}$ system in a value of R_m between 1.13 and 1.80 (Kharaka & Berry, 1973; Fritz, 1986; Marcus, 1997). Secondly, R_{wm} is the ratio of the friction coefficients of the anions with the matrix of the membrane and with the water (w) in the membrane, $R_{wm} = f_{am}/f_{aw}$. For a compact membrane $R_{wm} > 1$, whereas R_{wm} equals 0 when there is little frictional resistance as in loosely compacted membranes. For membranes with a porosity above 40 % the value for R_{wm} is taken to be 0 (Fritz & Marine, 1983). Finally, R_w is the ratio of the friction coefficients for the ions with the water in the membrane, $R_w = f_{cw}/f_{aw}$. If it is assumed that the frictional resistance of the cation and anion with the water in the membrane structure is equivalent to that in the free solution, the reciprocal of the transport number (t_0) of the cation equals $R_w + 1$ (Fritz & Marine, 1983), thus:

$$\frac{1}{t_0^{cation}} = R_w + 1 \tag{1.16}$$

The transport number is a measure for the percentage of charge that is transported by the cation or anion when the mobilities of the ions in solution differ. For the $\mathrm{NaCl{+}H_2O}$ system the value for $t_0^{Na} \approx 0.38$ throughout the concentration range of 0–3 $\mathrm{mol \cdot L^{-1}}$, thus R_w is approximately 1.63.

The dependency of the reflection coefficient on the porosity for various clay minerals with different cation exchange capacities is clearly illustrated by the FMMM (Figure 1.5). Also clearly shown is the change in ideality for a membrane with the decrease in the average solute concentration across the membrane as was experimentally found by several investigators (Berry, 1969; Kharaka & Berry, 1973; Kharaka & Smalley, 1976).

1.5 THE REFLECTION COEFFICIENT ACCORDING TO KEMPER–BRESLER

A relation for the salt exclusion properties for interacting double layers based on the Gouy–Chapman theory of the diffuse double layer was published by Kemper and Rollins (1966), and in a somewhat different form by Bresler (1973). Both authors determined the dependence of the reflection coefficient on basis of the water film thickness and the salt exclusion factor from the diffuse double layer theory. They assume a uniform distribution of the water film over the full surface area of a completely dispersed clay. According to Bresler (1973) this results in:

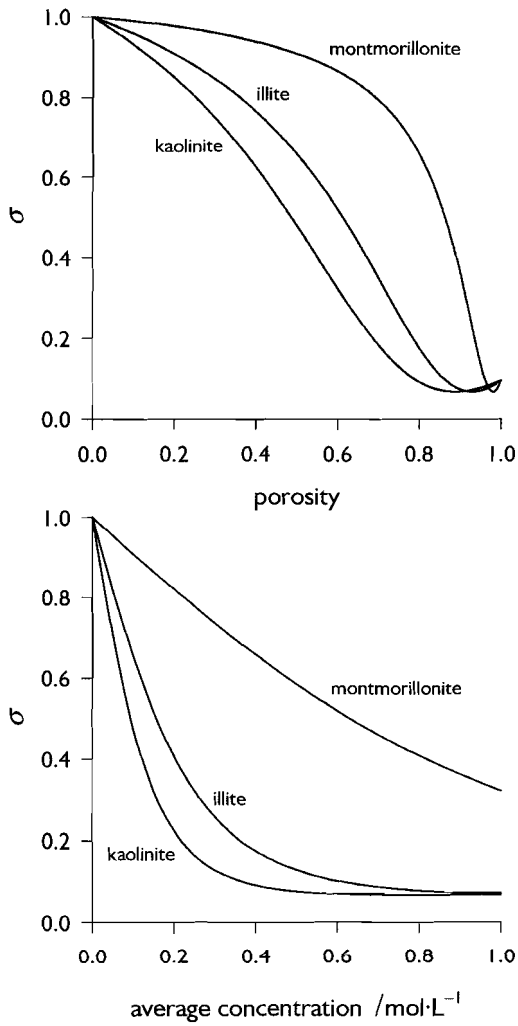

Figure 1.5
The reflection coefficient, σ, according to the Fritz–Marine Membrane Model (FMMM); **top** σ as a function of the porosity at an average concentration of 0.1 $mol \cdot L^{-1}$, and **bottom** σ as a function of the average concentration at a given porosity of 0.5. Curves were calculated using Eq. 1.12 for monomineral membranes made of kaolinite, illite or montmorillonite with values for the CEC of respectively 15, 25 and 100 $cmol_c \cdot kg^{-1}$. R_{wm} was taken at a constant value of 0.1 throughout the porosity range, R_m was 1.8 and R_w equalled 1.63.

$$\sigma = 1 - \frac{c(y_b)}{c_0} \tag{1.17}$$

where $c(y_b)$ is the anion concentration in mol·L^{-1} at y_b. y Is a dimensionless potential function from the DDL and its value is calculated for the thickness of the water film b, and c_0 is the equilibrium concentration in mol·L^{-1}. Kemper (1972) derived a similar relation:

$$\sigma = 1 - e^{(-y_b)} \tag{1.18}$$

Both equations yield identical curves (Figure 1.6) and values for the reflection coefficient for the same sample, therefore both models will be regarded as one model and are referred to as the Kemper–Bresler model.

Bresler (1973) plotted σ as a function of the normalised parameter $b\sqrt{c_0}$, however, in Figure 1.6 the reflection coefficient is plotted for a given water film thickness, as a function of the equilibrium concentration comparable to the method used by Kemper (Kemper & Rollins, 1966; Kemper, 1972).

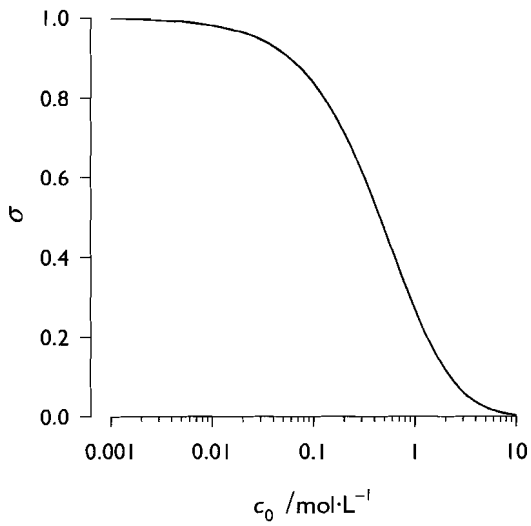

Figure 1.6 Reflection coefficient as a function of the equilibrium concentration according to Kemper (1972) and Bresler (1973) for a bentonite. The graph shows two overlapping curves calculated with Eq. 1.17 and 1.18. For the bentonite a CEC of 100 cmol$_c$·kg^{-1}, a surface area of 800 m^2·g^{-1}, a porosity of 0.5 and an occupation with a monovalent cation was used.

1.6 THE REFLECTION COEFFICIENT ACCORDING TO GROENEVELT–BOLT

Using the framework supplied by the thermodynamics of irreversible processes Groenevelt and Bolt also derived a relation for the reflection coefficient. They assumed that the distribution of the ions in the interacting double layers follows the corrected Gouy–Chapman theory (Bolt, 1955; Van Olphen, 1963) of the planar diffuse double layer (Groenevelt & Bolt, 1969; 1972; Bolt, 1982b). The salt exclusion properties of clays originate from the diffuse double layers on the particles and are dependent on the clay mineralogy and the ionic composition. They assume a mono-mineral, monoionic system where the clay is completely dispersed. Anion exclusion is assumed to take place within a mobile water layer extending from the shear plane —at distance x_s from the clay particle surface— to the truncation plane, x_t (Figure 1.7). The shear plane is defined as the location where the viscosity of the water changes

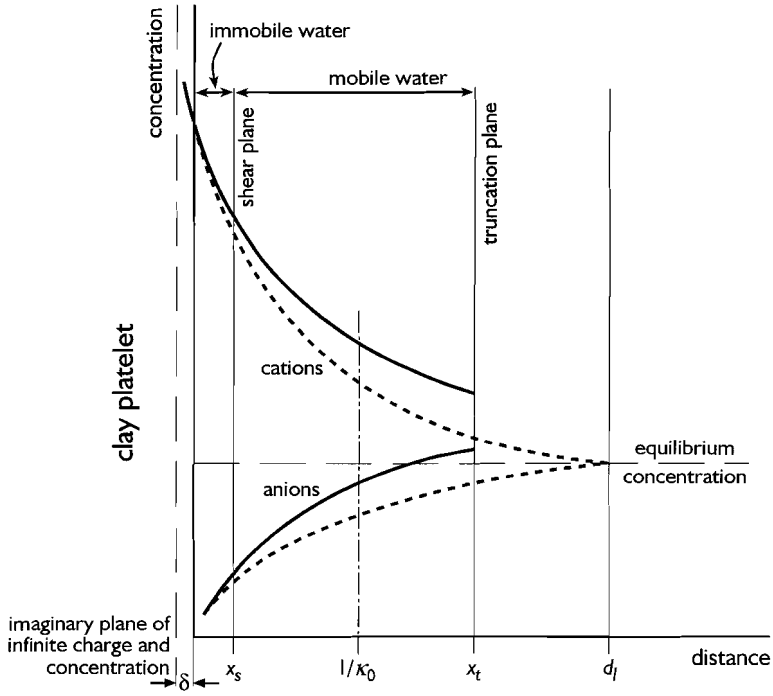

Figure 1.7 Schematic representation of the distribution of the ions in a normal (dotted lines) and truncated (solid lines) double layer. The position of the immobile and mobile water adjacent to the clay platelet for the truncated double layer according to the model by Groenevelt and Bolt is also indicated.

from very high values, directly adjacent to the clay platelet, to its bulk value in the pore (Groenevelt & Bolt, 1972). Truncation of the double layer occurs when removal of water forces both counterions and co–ions into a liquid layer of decreased thickness (Bolt, 1982a) e.g. as the result of compaction or decrease in water content by evaporation. Thus, the mobile water layer between the shear and truncation plane is taken as an approximation of the thickness of the diffuse double layer. The immobile water layer between the surface of the platelet and the distance x_s does not participate in the salt exclusion. This results in a relation between the reflection coefficient and the diffuse double layer properties according to:

$$\sigma = \frac{3}{(\kappa_0 d_l)^3}\left\{\kappa_0 d_l \int_{t_s}^{t_d} \ln\left(\frac{t}{t_s}\right)\frac{4t}{(1+t)^2}\,d(\ln t) + \frac{1}{2}\int_{t_s}^{t_d} \ln^2\left(\frac{t}{t_s}\right)\frac{4t}{(1+t)^2}\,d(\ln t)\right\} \qquad (1.19)$$

for which the analytical solution can be derived:

$$\sigma = \frac{12}{(\kappa_0 d_l)^3}\left[\kappa_0 d_l\left\{\ln(1+t_s) - \frac{\kappa_0 d_l}{2}\frac{t_d}{1+t_d}\right\} - \sum_{n=1}^{\infty}\frac{-t_d{}^n}{n^2} + \sum_{n=1}^{\infty}\frac{-t_s{}^n}{n^2}\right] \qquad (1.20)$$

in which κ_0 is the Debye–Hückel reciprocal thickness for a given equilibrium solution of a diffuse double layer in m^{-1}, and d_l is the thickness of a liquid film on a charged surface in m. The value for κ_0 can be calculated using (Bolt, 1982b):

$$\kappa_0 = \sqrt{\beta I_0} \qquad (1.21)$$

where β is a constant given by $2F^2/\varepsilon_0\varepsilon_r RT$ in which F is the Faraday constant ($96.4853 \cdot 10^3$ C·mol^{-1}), R is the gas constant (8.31451 J·K^{-1}·mol^{-1}), ε_0 is the permittivity of the vacuum ($8.85419 \cdot 10^{-12}$ C·V^{-1}·m^{-1}), ε_r is the dielectric constant of water (78.54 at 298.15 K), and T the absolute temperature; at 298.15 K $\beta \approx 10.80 \cdot 10^{15}$ m·mol^{-1}. I_0 is the ionic strength of equilibrium solution in mol·m^{-3}. Furthermore, t represents the mathematical expression $\left(\sqrt{u}-1\right)/\left(\sqrt{u}+1\right)$, in which u is the Boltzmann accumulation factor for monovalent counterions in the diffuse double layer. At $x = x_s$ and $x = x_t$ the values of t_s and t_d are given by:

$$t_s = e^{(-\kappa_0 \delta)} \qquad (1.22)$$

$$t_d = e^{(-\kappa_0 (d_l + \delta))} \qquad (1.23)$$

δ Is the absolute distance of the imaginary plane of infinite charge and potential behind the surface of the clay particle in m (Mitchell, 1993 – see also Figure 1.7). For a 1:1 electrolyte, like NaCl, it can be calculated using by $\delta = 4/\beta\Gamma$ for solutions upto 1 mol·L^{-1}, where Γ is the counter charge per unit surface area in mol$_c$·m^{-2}. The reflection coefficient is plotted against $\kappa_0 d_l$ (Figure 1.8) which is the normalised double layer thickness corrected for the presence of the immobile water layer from $x=0$ to $x=x_s$. The curves are valid for $\kappa_0 d_l > 1$ and represent the salt exclusion properties of clays with a 'thin' water film (Bolt, 1982b).

A solution for a limited case, useful for obtaining a first estimate can be found by (Bolt, 1982b):

$$\sigma = \frac{12}{(\kappa_0 d_l)^2} - \frac{\pi^2}{(\kappa_0 d_l)^3} \tag{1.24}$$

which is valid for $\kappa_0 d_l > 5$ and $\kappa_0 \delta < 0.01$, thus for clays with a 'thick' water film (Figure 1.8).

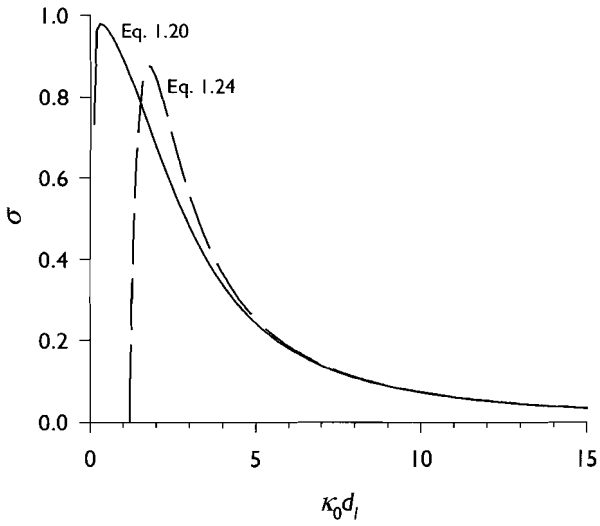

Figure 1.8 The reflection coefficient as a function of the normalised mobile film thickness, $\kappa_0 d_l$, at zero streaming potential according to the model by Groenevelt and Bolt. The solid curve represents σ for 'thin' water films ($\kappa_0 d_l > 1$), the dashed line represents σ for $\kappa_0 d_l > 5$ or 'thick' water films.

1.7 CHEMICAL OSMOSIS IN NATURAL MATERIALS

Laboratory studies

Two of the earliest studies to demonstrate chemical osmosis in clay rich natural material were by Kemper (1961) and Young and Low (1965). The data by Young and Low were obtained from a shale with 8–10 % clay size material in which illite and kaolinite were the most abundant. Water transport was observed as volume flow in a calibrated standpipe. Kemper (1961) demonstrated that a hydraulic pressure can be induced by separating solutions of different salt concentrations by a shale. He also showed that the clay fraction of the shale was a better semipermeable membrane than the shale itself. Since then various investigators have shown that the semipermeable properties of natural material are affected by a whole range of properties of the sample or sample material (Table 1.2). The most popular sample materials in these studies

Table 1.2 Experimentally determined factors affecting the ideality of natural clayey membranes (after Alexander, 1990; Whitworth, 1993; Keijzer *et al.*, 1994).

observations	study	membrane type
High flow rates cause a decrease in membrane efficiency.	Milne *et al.*, 1964	bentonite
A decrease of the input fluid pressure increases the membrane efficiency.	Milne *et al.*, 1964; Kharaka, 1973	bentonite
Ideality increases with increasing ion exchange capacity of the membrane material.	Kharaka & Berry, 1973; Kharaka & Smalley, 1976	bentonite, kaolinite and shale
Ideality increases with increasing compaction pressure.	Kharaka & Berry, 1973	bentonite, shale
Membrane efficiency increases with a decrease in the solution concentration.	Berry, 1969; Kharaka & Berry, 1973; Kharaka & Smalley, 1976	bentonite, kaolinite and shale
Ideality of membranes with orientated fabric is higher than those with random fabric.	Benzel & Graf, 1984	smectite
Ideality is not effected by the membrane thickness.	Benzel & Graf, 1984	smectite
Ideality increases with temperature.	Haydon & Graf, 1986	smectite

were shales, kaolinite and bentonite. Shales are of interest in hydrological systems for the assessment of anomalous hydraulic pressures (e.g. Graf, 1983; Neuzil, 1986). Bentonite is of interest because of its use as a low permeable barrier in waste containment and is a typical charged membrane (e.g. Yeung *et al.*, 1992; Keijzer *et al.*, 1997; 1999). Kaolinites were studied as they are examples of clays in which semipermeability is mainly based on size exclusion properties (e.g. Olsen, 1969; 1972).

A short introduction and description of different types of experimental instrumentation used in these laboratory studies are given in Chapter 3.

Field observations

There are a number of observations indicating that coupled processes are not only important on a laboratory scale but also take place on a field scale. In several field situations high salinity aquifer waters may have developed by osmosis (Russel, 1933; De Sitter, 1947; Berry & Hanshaw, 1960; Hanshaw & Hill, 1969; Wood, 1976; Marine & Fritz, 1981). According to Graf (1983) abnormally high hydraulic heads of aquifers, i.e. pressures that cannot be explained with the assumptions of standard hydrogeological models (Horseman *et al.*, 1996) can be explained by chemical osmosis. Until recently the attribution of abnormal pressures to chemical osmosis was controversial (Neuzil, 1986) because other possible causes such as hydrocarbon accumulation, smectite dehydration and cementation or tectonic deformation may be held responsible (Horseman *et al.*, 1996; Osborne & Swarbrick, 1997). In addition it was suggested that the presence of fractures prevents a shale from exhibiting semipermeable properties by supplying a short–circuiting route (Osborne & Swarbrick, 1997). However, a long term *in situ* field experiment on the cretaceous Pierre Shale, USA, shows water transport between boreholes in accordance with an applied chemical gradient (Neuzil, 1994; 2000). As the author states, "*It is clear that osmotic pumping of pore fluids has occurred in this experiment, showing that the Pierre Shale* in situ *has the properties of an osmotic membrane*". This represents the first direct *in situ* observation of the semipermeable properties of a natural clay rich material. Neuzil (1998) also states that as shales lack large scale fracturing no mechanism is present to short–circuit osmosis.

Osmotic phenomena occur in geological systems of various degrees of consolidation. De Haven (1982) analysed data from wells in the *Haarlemmermeer Polder*, the Netherlands, and concluded that osmotic potentials should be considered in the water balance analysis. In the coastal area of the Netherlands aquifers of different chemical composition are often separated by clay layers, and water transport as a result of osmostic gradients can occur (Loch & Keijzer, 1996).

Geological significance of coupled flow

Evidence collected from the literature indicates that membrane properties may have a significant impact on a wide range of geochemical and geological processes on both the laboratorium and field scale.

Hanshaw and Zen (1965) argued that osmotic pressure gradients can be responsible for anomalous high pressures in shale beds which can lead to overthrust faulting of the shale.

Fractionation of isotopes of lithium, oxygen, chlorine and carbon was shown to occur under laboratory conditions through clays and shales when subjected to (reverse) osmosis (Coplen & Hanshaw, 1973; Campbell, 1985; Fritz *et al.*, 1987; Phillips & Bentley, 1987; Demir, 1988; Boulegue *et al.*, 1990; Fritz & Whitworth, 1994). Boulegue *et al.* (1990) showed that two cores taken by the Ocean Drilling Program (ODP) in the Indian Ocean show characteristics directly related to reverse osmosis, resulting in a shift in isotopic composition of the pore water. Another debate in marine science, the formation of deep water brines in the Eastern Mediterranean Sea may be explained by osmotic water flow according to Camerlenghi (1988).

Fritz and Eady (1985) showed that calcite can precipitate from originally undersaturated solutions forming a calcite cement by hyperfiltration through clay membranes. Also the formation of certain sedimentary copper deposits in New Mexico USA, may be the result of membrane induced heavy metal precipitation as a result of hyperfiltration of an undersaturated solution through the shale (DeRosa *et al.*, 1997; Whitworth & DeRosa, 1997).

Electro–osmosis has recently been introduced as a remediation technique for sites contaminated with heavy metals (Acar & Alshawabkeh, 1993; Everwijn *et al.*, 1992; Van Cauwenberghe, 1997; Chung & Kang, 1999). Traditonally it was used as a technique for the stabilisation of 'quick clays' (Bjerrum *et al.*, 1967). According to Veder (1979) electro–osmotical processes in soils can be responsible for slope instability and slope failure. More generally, applications of electrokinetic phenomena such as electro–osmosis and electrophoresis in soils are discussed by Yeung and co–workers (Yeung *et al.*, 1992; Yeung & Mitchell, 1993; Yeung, 1994; Yeung & Datla, 1995).

As several countries are looking for repository sites for the long term disposal of high level radioactive waste in low permeable strata, like shales or granite backfilled with bentonite, coupled transport phenomena are critically reviewed as possible driving forces for water and radionuclides. Recently, Soler (1999) reviewed the different coupled flow processes for the Opalinus Clay, Switzerland. He concluded that coupled transport will have only a small effect on radionuclide transport at the time of expected canister failure (>1000 yr). On a shorter time scale the effects are less

well understood. However, some of the coupling phenomena will work in favor of —thermo–osmosis— and others against —chemical osmosis— the release of radionuclides from a repository.

It should be noted that geological membranes are not limited to clay rich materials. As discussed earlier, membrane properties can also arise from differences in ion mobilities and size in so–called uncharged semipermeable membranes. Based on a comparison between pore sizes of chalks and commercially available uncharged membranes, e.g. cellulose acetate, Whitworth (1993) concluded that chalks may prove to be relatively efficient geological membranes.

2 Sample description

2.1 INTRODUCTION

Two different bentonites and two harbour sludge samples from the Port of Rotterdam, the Netherlands, which were used throughout this study, are discussed in this chapter. The bulk properties and the mineralogical characterisation based on (geo)chemical and analytical techniques will be given and evaluated.

A short introduction on bentonite

The term bentonite was first applied by Knight (1898) to a particular, plastic and highly colloidal clay found near Fort Benton in Wyoming, USA. This clay has the unique characteristic of swelling to several times its original volume when placed in water, and to form gels with water even when the amount of clay in such gels is relatively small. It was shown that this bentonite was formed by the *in situ* alteration of volcanic ash and therefore the definition of bentonite was limited as such (Grim, 1953). There are, however, nowadays also bentonites known from the hydrothermal alteration of igneous rocks. As a result the definition of bentonite does no longer include the origin; currently it is defined as *"any natural material composed predominantly of the clay minerals of the smectite group whose properties are controlled by these minerals"* (Grim & Güven, 1978). The minerals most commonly found in bentonite are montmorillonite with a representative formula $(½Ca,Na)_{0.7}(Al_{3.3}Mg_{0.7})_4[Si_8O_{20}](OH)_4 \cdot nH_2O$, or beidellite with a representative formula $(½Ca,Na)_{0.7}(Al_4)_4[(Si_{7.3}Al_{0.7})O_{20}](OH)_4 \cdot nH_2O$ (Deer *et al.*, 1992). Based on the major cation on the exchange complex of the mineral, two major varieties of bentonite are distinguished (Hosterman & Patterson, 1992). Firstly, the sodium or Wyoming bentonite consisting of montmorillonite or beidellite with predominantly Na^+ as exchangeable cation. This bentonite is the high swelling variety. It is traditionally used in drilling mud and found a more recent use as material for low permeable barriers for waste disposal sites. Secondly, the calcium or southern

bentonite which is a low or non-swelling clay, consisting of montmorillonite or beidellite with Ca^{2+} as the major cation on the exchange complex. This variety is often used as a filling agent.

2.2 SAMPLES

Harbour sludge samples

The harbour sludge samples were retrieved from locations in the *Beerkanaal* (BK) and *Beneden Merwede*-river (BMR) in the port of Rotterdam, the Netherlands (Figure 2.1), during autumn of 1993. Selection of the sampling locations was based on the expected contamination with polycyclic aromatic hydrocarbons (PAH – see Chapter 6) and the differences in mineralogical composition. The BK sample was deposited in a brackish environment influenced by the tidal regime of the North Sea, which may result in low PAH contamination and is expected to have a large clay size fraction. The BMR sample is from a fresh water environment, having potentially a high contamination with PAH as a result of its proximity to industrial sites and a relatively large influence of river transported material and contaminants. The clay content is expected to be lower than at the BK site. These sites represent two different types of harbour sludge disposed in the main harbour sludge depot *De Slufter* (Figure 2.1). The samples were stored under dark, anaerobic conditions at 4°C until used in the experiments described in Chapter 5 and 6.

Figure 2.1 Locations of the *Beerkanaal* (BK) and *Beneden Merwede*-river (BMR) sampling sites in the Port of Rotterdam, the Netherlands. The location of the harbour sludge depot *De Slufter* is also indicated.

Ankerpoort Wyoming bentonite

The Ankerpoort Wyoming bentonite (AWy) is a commercially available Na–montmorillonite marketed under the name of Colclay A90™ (Ankerpoort, Geertruidenberg, NL). In all experiments described in this thesis in which AWy was used, it was from batch number 61203.

Source clay Wyoming bentonite

The Source clay Wyoming bentonite (SWy–2) was obtained from the Source Clay Repository of the Clay Minerals Society (University of Missouri, Columbia, USA) and is a Na–montmorillonite which originates from Crook County, Wyoming, USA. It replaces the well known source clay bentonite SWy–1 used in the earlier work on membrane phenomena. The SWy–2 is used in this thesis as a reference material.

2.3 ANALYTICAL METHODS

Mineralogy

Several techniques were used to determine the mineralogical composition of the bentonites and of the clay size fraction (<2 μm) of the harbour sludge samples. It is this fraction that determines the ability of the sludge to act as a semipermeable membrane.

X–ray diffractograms (XRD – Phillips PW1710; CuKα radiation, $1.5418 \cdot 10^{-10}$ m) were made of oriented samples after the removal of carbonates and organic matter. For the harbour sludge samples also semi–quantative XRD analyses were performed by the University of Amsterdam, Landscape and Environmental Research Group.

Fourier Transform InfraRed spectra (FTIR – Perkin Elmer Paragon 1000) in the mid–infrared, 400–4000 cm^{-1}, were collected. Fifty scans were recorded for each spectrum with a spectral resolution of 1 cm^{-1} on KBr pellets or self supporting thin films.

Cation exchange capacity and specific surface area

For a clay or clay rich sediment to act as a semipermeable membrane the Cation Exchange Capacity (CEC), the cation occupation of the exchange complex and the Specific Surface Area (A_s) are of importance (Chapter 1).

Table 2.1 Sample properties of the Ankerpoort (AWy) and Source clay Wyoming bentonite (SWy–2).

		AWy	SWy–2	
cation exchange capacity		68.3 ± 1.3	69.6 ± 0.7	$cmol_c \cdot kg^{-1}$
cation occupation by	Na^+	48.4 ± 0.3	38.3 ± 0.2	$cmol_c \cdot kg^{-1}$
	K^+	1.4 ± 0.1	1.8 ± 0.1	$cmol_c \cdot kg^{-1}$
	Ca^{2+}	23.5 ± 0.9	22.6 ± 0.4	$cmol_c \cdot kg^{-1}$
	Mg^{2+}	4.2 ± 0.2	15.1 ± 0.2	$cmol_c \cdot kg^{-1}$
organic matter content		0.20	na	wt%
carbonate content		0.79	1.92	wt%
particle density in		2.64	2.65	$g \cdot cm^{-3}$
specific surface area	N_2–BET	47 ± 4	47 ± 2	$m^2 \cdot g^{-1}$
	EGME	556 ± 13	538 ± 22	$m^2 \cdot g^{-1}$

na not analysed

Table 2.2 Sample properties of the *Beerkanaal* (BK) and the *Beneden Merwede*–river (BMR) harbour sludge samples.

		BK	BMR	
cation exchange capacity		24.2 ± 0.3	14.9 ± 0.5	$cmol_c \cdot kg^{-1}$
cation occupation by	Na^+	30.8 ± 0.7	0.4 ± 0.1	$cmol_c \cdot kg^{-1}$
	K^+	2.8 ± 0.1	nd	$cmol_c \cdot kg^{-1}$
	Ca^{2+}	12.4 ± 0.2	16.7 ± 0.5	$cmol_c \cdot kg^{-1}$
	Mg^{2+}	10.0 ± 0.2	1.5 ± 0.2	$cmol_c \cdot kg^{-1}$
organic matter content		2.30	2.10	wt%
carbonate content		35.2	18.0	wt%
particle density		2.46	2.58	$g \cdot cm^{-3}$
particle size fraction	>60 μm	3	46	%
	2–60μm	41	28	%
	<2 μm	56	26	%
specific surface area	N_2–BET	30 ± 4	32 ± 3	$m^2 \cdot g^{-1}$
	EGME	167 ± 1	184 ± 14	$m^2 \cdot g^{-1}$

nd not detected

The CEC and cation occupation were determined by extraction with 0.01 $mol \cdot L^{-1}$ silver thiourea (AgTU – Merck, Darmstadt, GE) using 250 or 500 mg of sample diluted with 2.0 g washed sand (Van Reeuwijk, 1995). The sand was previously heated to 900°C to remove traces of organic matter and carbonates. The cation concentration in the supernatant solution was determined using Inductively Coupled Plasma Atomic Emission Spectrometry (ICP–AES – ARL 34000). The A_s was measured using the N_2–BET method (Carlo Erba/Fisons Sorptomatic 1990) on 0.1 g of bentonite and harbour sludge (Greene–Kelly, 1964; Aylmore *et al.*, 1970). Additionally sorption of ethylene glycol monoethyl ether (EGME – Merck, Darmstadt, GE) was also used to obtain values for the A_s. Approximately 1 ml of EGME was added to 0.5 g P_2O_5 dried (Merck, Darmstadt, GE) samples, placed under vacuum above anhydrous $CaCl_2$ (Merck, Darmstadt, GE) for ten days and weighed (Van Reeuwijk, 1995).

Organic matter and carbonate content

The organic matter content was determined by the Walkley–Black method (Allison, 1965) in which 1 $mol \cdot L^{-1}$ $K_2Cr_2O_7$ is added to 0.5 g sample and the oxidation reaction is facilitated by the heat generated by the addition of concentrated H_2SO_4. The carbonate content was determined by using the Scheibler method, shaking the sample with 1 $mol \cdot L^{-1}$ HCl and volumetrically measuring the release of CO_2.

Table 2.3 Weight percentages of the clay minerals present in the clay size fraction of the two harbour sludge samples determined by semi–quantative XRD analyses.

minerals	BK	BMR
	%	%
smectite	37	28[1)]
illite	38	47
kaolinite	15	15
chlorite	10	10
quartz	± 5	± 5
feldspar	traces	traces

1) might contain interstratifications of illite/smectite and vermiculite/smectite

Particle density and particle size distribution

The particle density was determined using a specific gravity flask or pycnometer with hexane as the liquid phase (Blake, 1965). The particle size distribution was determined using a Malvern Particle Sizer 2600, after removal of organic matter and carbonate.

2.4 RESULTS AND DISCUSSION

Bentonite properties and mineralogy

From X–ray diffractograms it was inferred that the bentonite samples mainly consisted of montmorillonite (Figure 2.2). Both bentonites contain traces of quartz, probably less than 1 %. Other mineral phases that might be expected in bentonite, such as cristobalite, biotite, and plagioclase (Deer *et al.*, 1992) were not found.

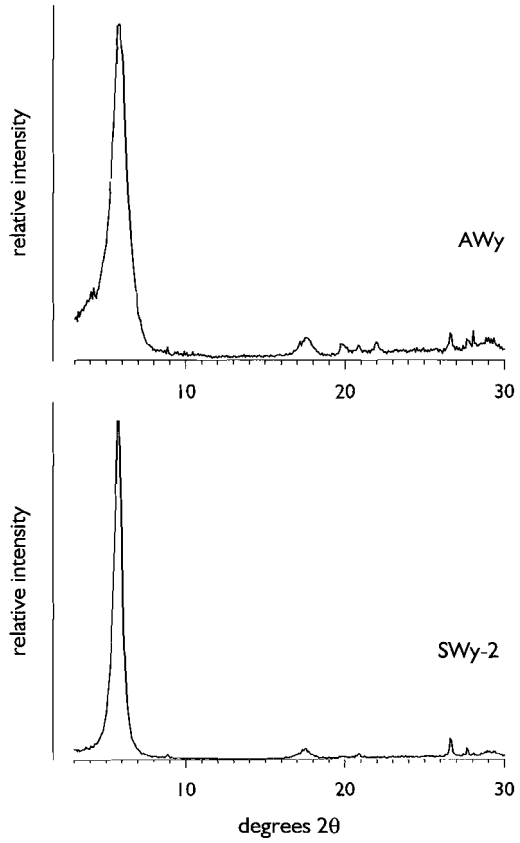

Figure 2.2
X–ray diffractograms of the Ankerpoort Wyoming bentonite (AWy) and the source clay (SWy–2) after saturation with Mg.

For both bentonites the CEC was determined around 70 $cmol_c \cdot kg^{-1}$ (Table 2.1), which is at the lower end of the range reported in the literature. Mitchell (1993) lists CEC's for montmorillonites between 80–150 $cmol_c \cdot kg^{-1}$. Of the available adsorption sites two third is occupied by Na^+, which therefore is the major cation on the exchange complex (Table 2.1). Ideally, the occupation by the different cations should add up to approximately the value of the CEC, however, for our bentonites the total cation occupation exceeds the value for the CEC by approximately 12 %. This is probably the result of the method used to determine the cation occupation and CEC, in the presence of carbonates in the clays (Table 2.1). Although the AgTU–method should be suitable for calcareous soils (Van Reeuwijk, 1995) the measured Ca^{2+} occupation may have been influenced by $CaCO_3$ solubilisation.

The A_s of the bentonites correlates well with literature values for N_2–BET surface areas between 15–150 $m^2 \cdot g^{-1}$ (Green–Kelly, 1964; Aylmore *et al.*, 1970;

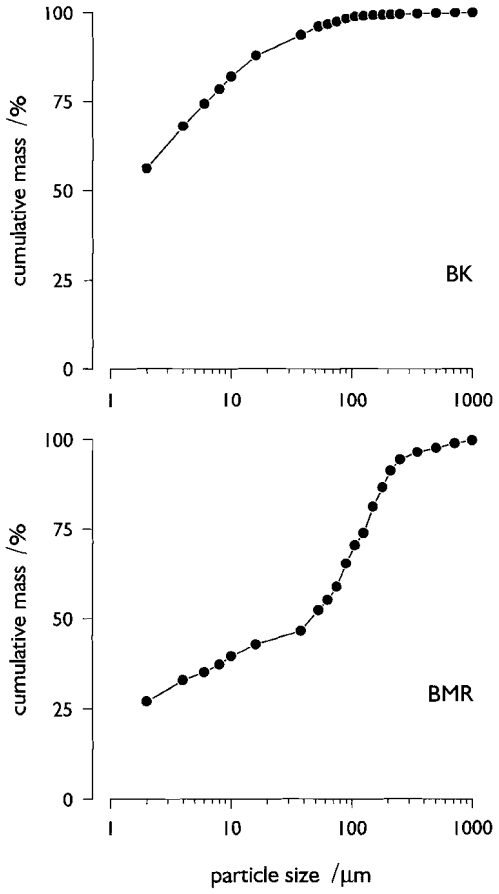

Figure 2.3
Particle size distribution for the two harbour sludge samples.

Churman & Burke, 1991; Mitchell, 1993). However, the N_2–BET method gives the external or primary A_s because N_2 only adsorbs onto the surface of assemblies of the silicate layers, and not on the interlayer surfaces (Aylmore *et al.*, 1970; Churchman *et al.*, 1991; Feller *et al.*, 1992; Padmanabhan & Mermut, 1995). EGME yields the secondary or total A_s as EGME also adsorbs at the interparticle surfaces (Mitchell, 1993). The measured secondary surface areas compare well with literature values (Mitchell, 1993; Petersen *et al.* 1996) but are again at the lower end of the reported range of 550–850 $m^2 \cdot g^{-1}$. However, there is a clear correlation between the CEC and secondary A_s (Churchman & Burke, 1991), and therefore our low secondary A_s–values are not unreasonable.

Bulk properties of the harbour sludge samples

The bulk properties show that the harbour sludge samples differ mainly in their clay and carbonate content (Table 2.2). The high clay content (Figure 2.3) and carbonate content of the BK–site clearly reflect its position further downstream

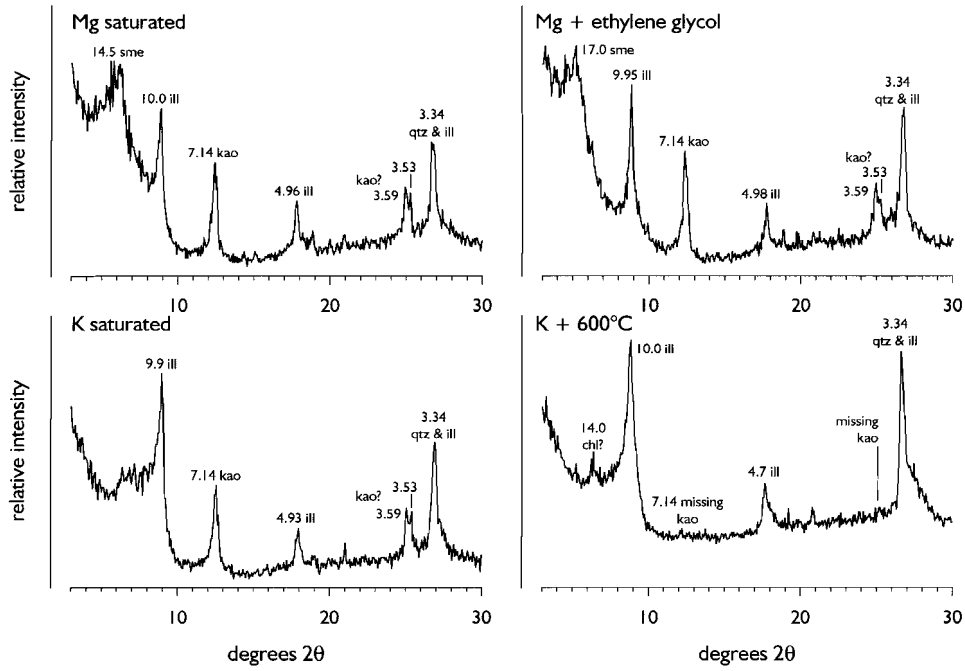

Figure 2.4 X–ray diffractograms of the clay size fraction of BK with designation of the different peaks to various minerals and their spacing in 10^{-10} m; sme=smectite, chl=chlorite, ill=illite, kao=kaolinite and qtz=quartz.

relative to the BMR site. The higher clay content is also reflected in the measured values for the CEC (Table 2.2). The major cation on the exchange complex of BK is Na^+, whereas BMR predominantly contains Ca^{2+}.

Kuijper *et al.* (1990) report physical properties for sediments in coastal areas and major waterways of the Netherlands. The organic carbon content and total clay content of the samples from BK and BMR fall in their reported range. However, our samples exhibit higher CEC and EGME A_s–values. This can be explained by the higher smectite content of the samples (Table 2.3). According to Kuijper *et al.* (1990) illite is the major clay mineral with only small amounts, generally below 10 wt%, of smectites.

Mineralogy of the clay size fraction of the harbour sludges

Based on the X–ray diffractograms it was concluded that the main minerals in the fraction <2 μm of the sludges were clay minerals from the smectite group, illite and kaolinite (Figures 2.4 & 2.5). The semi–quantative analysis confirmed this

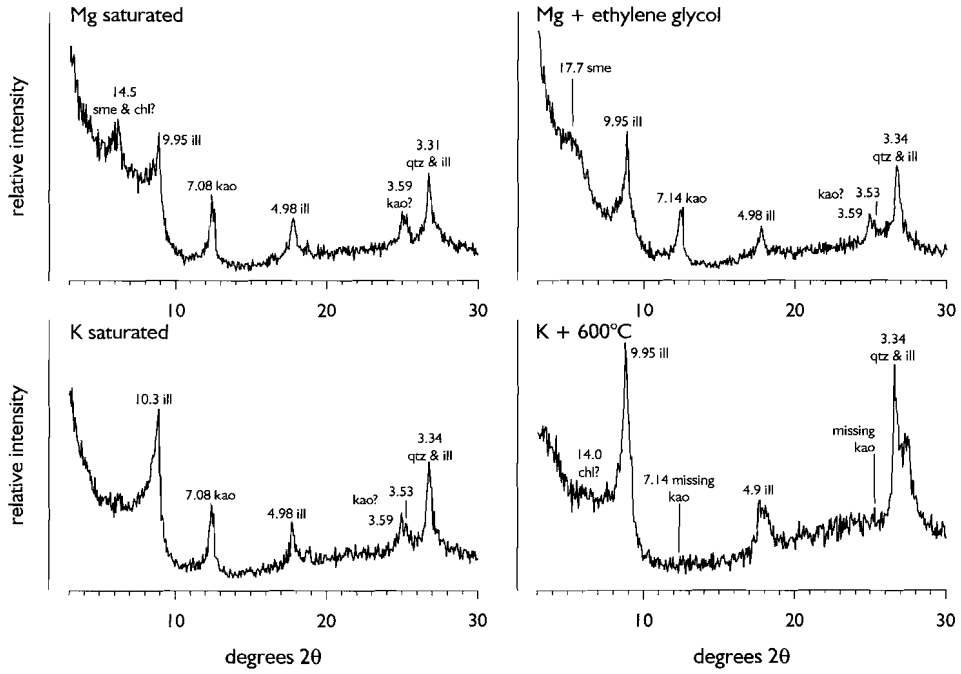

Figure 2.5 X–ray diffractograms of the clay size fraction of BMR with designation of the different peaks to various minerals and the spacing in 10^{-10} m; sme=smectite, chl=chlorite, ill=illite, kao=kaolinite and qtz=quartz.

observation but also showed that the two sludges differ in the relative amounts of the minerals present (Table 2.3). The main clay mineral in the BMR sludge is illite with minor amounts of smectite, kaolinite and some chlorite, whereas, equal amounts of smectite and illite were found in the BK sludge, together with some kaolinite and chlorite. Both sludges contain traces of quartz in the clay size fraction.

Additional information about the mineralogy of the clay size fraction of the sludges was obtained from the infrared analysis. The regions in the infrared containing the most valuable information for the identification of the clay minerals in the samples are the areas in which stretching, 3800–3200 cm^{-1}, and bending, 950–700 cm^{-1}, vibrations of the OH groups occur (Figure 2.6). The vibration frequencies of the OH–groups in these regions are of adsorbed water and structural OH–groups. As a reference the spectra of kaolinite and SWy–2 are also shown (Figure 2.6). Additionally, observed peak wavenumbers and previously assigned vibrations found in the literature are tabulated (Table 2.4). Most absorbences in the infrared spectra of the harbour

Table 2.4 Observed OH stretching and bending vibration frequencies of kaolinite (kao), SWy–2 and the clay fraction of the two harbour sludges. Previous band assignments for water and structural OH of kaolinite and smectite (sme) are also listed.

mineral	vibration	wavenumber				
		cm^{-1}				
		literature value	kao	SWy–2	BMR	BK
kao	inner surface + broken edges OH	3695–3700[1,2)]	3694		3698	3698
kao	OH groups located on the	3670[2)]	3668		sh	sh
	octahedral sheet between layers	3655[2)]	3652		sh	sh
kao	inner surface OH	3622[2)]	3619		3622	3621
sme	AlAl–OH[1)], firmly bound H_2O[3)]	3620[1)], 3610[3)]		3620		
sme	H_2O loosely bound	3415[3)]		3415	3433	3442
kao	AlAl–OH	940[2)]	938			
kao	AlAl–OH	918[2)]	912			
sme	AlAl–OH	915–918[1,3)]		918	912	912
sme	$AlFe^{III}$–OH	880–887[1,3,4)]		886	sh	sh
sme	AlMg–OH	835–845[1,3,4)]		846	839	835
kao	Si–O vibration mode	8794[2)]				
sme	$MgFe^{III}$–OH	795[1)]		798		798

[1)] Srasra *et al.*, 1994 [2)] Bantignies *et al.*, 1995; 1997 [3)] Bishop *et al.*, 1994 [4)] Borchart, 1987

sh stands for shoulder and is used when a shoulder against a larger band was observed at or near the reported wavenumber.

sludge samples can be assigned to the contribution of kaolinite and montmorillonite. The contribution of illite could not be accounted for. The spectrum for illite in the OH stretch region is rather dull with a broad peak centred around 3630 cm^{-1} (see Bantignies *et al.*, 1997). The intensity of the kaolinite peak at 3698 cm^{-1} in BK and BMR indicates that both sludges contain crystalline kaolinite. The shape of the broad

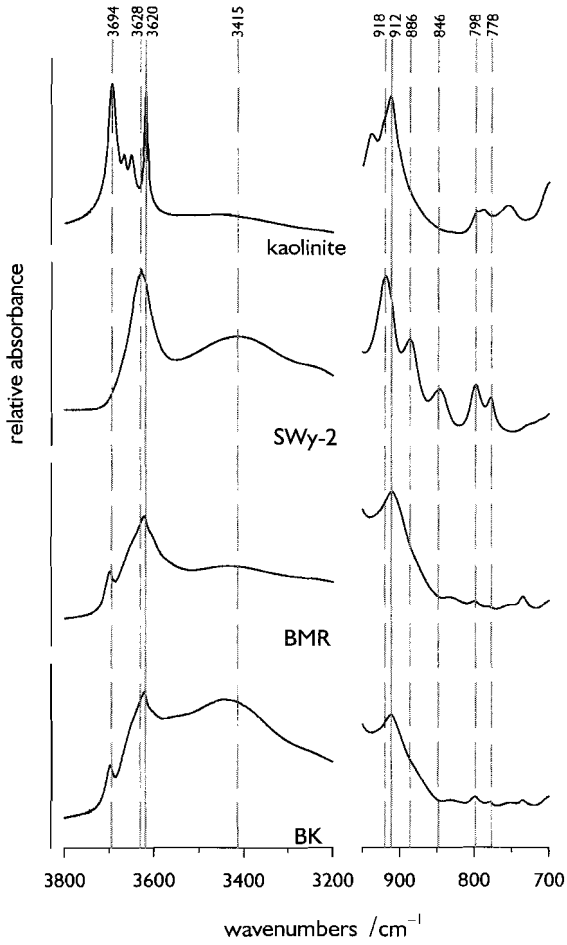

Figure 2.6 Infrared spectra showing the OH vibration frequencies of kaolinite, SWy–2 and the clay fraction of the two harbour sludges. The region between 3800–3200 cm^{-1} is associated with the stretch vibrations of adsorbed H_2O and structural OH groups, the bending vibrations occur between 950–700 cm^{-1}. The position of the major peaks of kaolinite and montmorillonite are indicated with wavenumber.

peak near 3620 cm^{-1} suggests that it is composed of an overlap of peaks from kaolinite and montmorillonite.

Although XRD analysis only indicated the presence of a smectite, the FTIR results clearly indicate that the smectite present is a dioctahedral smectite, either montmorillonite or beidellite. The AlAl–OH stretch near 3620 cm^{-1} and the bending frequency observed near 915 cm^{-1} in the spectra of the harbour sludges are considered to be characteristic of a dioctahedral smectite (Borchart, 1987; Srasra *et al.*, 1994). Additionally, bands are observed between 835–845 cm^{-1} which are assigned to the AlMg–OH bending frequency of montmorillonite. Beidellite has two stretching frequencies of AlAl–OH at 3660 and 3630 cm^{-1} and the bending frequency at 935 cm^{-1}, and no AlMg–OH bands around 840 cm^{-1} (Borchart, 1987). Therefore, it is concluded that the smectite present is montmorillonite.

The kaolinite band of AlAl–OH near 940 cm^{-1} is not found in the spectra of the sludges but lies probably below the broad peak at 912 cm^{-1}. Another peak, the Si–O–Si vibration at 794 cm^{-1}, characteristic for kaolinite (Bantignies *et al.*, 1995), is clearly visible in the spectrum of kaolinite but not observed in the sludges. This indicates small amounts of kaolinite present in the samples.

3 A novel experimental design for measuring chemical osmosis

3.1 INTRODUCTION

For the determination of water and solute transport by a chemical gradient in natural materials of high clay content, permeameters can be used with either a rigid wall or a flexible wall. In a rigid wall permeameter a soil sample is fitted in a rigid metal or plastic cylinder, whereas in a flexible wall permeameter the sample is fitted in a rubber 'sleeve' which is pressed against the sample by a surrounding pressurised liquid. Permeameters are widely used in soil physics and civil engineering to obtain soil transport properties like hydraulic conductivity (Daniel *et al.*, 1984; Boynton & Daniel, 1985; Mitchell, 1993).

In this chapter a short review is given of a number of experimental designs found in the literature which were used as a reference for the development of the equipment used in this study. Subsequently, the design criteria are formulated followed by a description of the experimental procedures and tests. Finally, the performance during several tests is discussed.

3.2 PERMEAMETER DESIGNS IN THE LITERATURE

Rigid wall permeameters

The simplest method to study chemical osmosis is a U–tube (Figure 1.3, p. 10) in which two solutions, each in a different 'leg' of the tube, are separated by a semipermeable membrane. Modified designs based on the U–tube were the first to be used in the study of semipermeability of natural materials.

In the classical paper by Young & Low (1965) an experimental design was described in which a slice of shale was sandwiched between two water reservoirs each containing a solution of different chemical composition (Figure 3.1). The induced water flux was measured using a standpipe connected to the salt water reservoir.

Designs in which hydraulic pressure differences across the sample were eliminated and the solutions in the reservoirs were homogenised were first described by Kemper and co–workers (Figure 3.1 – Kemper, 1961; Kemper & Rollins, 1966; Letey *et al.*, 1969; Kemper & Quirk; 1972).

Another type of permeameter was introduced by Olsen (1969; 1972) in which the sample was consolidated *in situ* by applying a vertical overburden pressure to determine the influence of porosity and compaction pressure on the salt sieving properties of clay membranes. Comparable designs were described by a number of authors studying the semipermeability of clays using reverse osmosis (e.g. Kharaka & Berry, 1973; Kharaka & Smalley, 1976; Fritz & Marine, 1983; Benzel & Graf, 1984; Demir, 1988; Whitworth & Fritz, 1994). Recently, Yeung *et al.* (1992) described an experimental device containing a series of rigid wall permeameters for the determination of diffusion coefficients and hydraulic and electro–osmotic permeabilities in compacted clays under conditions typically encountered in landfill liners.

The detection of water transport in all these designs was generally done using calibrated standpipes or differential pressure transducers and on the basis of conductometric changes in the reservoirs. The thickness of the samples studied varied between tenths of a millimetre to several centimetres.

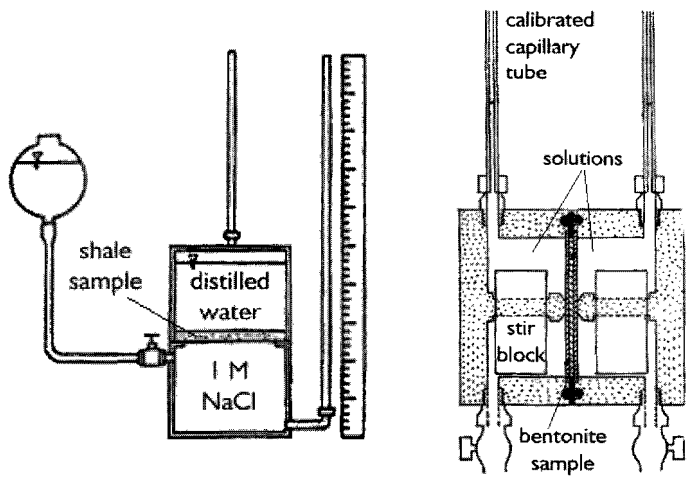

Figure 3.1 Experimental designs based on a rigid wall permeameter design; **left** as described by Young & Low (1965) for their experiments on the semipermeability of the shale from the Viking Formation (Lower Creteceous, Canada) and **right** by Kemper and co–workers for their experiments on bentonite (after Kemper & Rollins, 1966).

The main disadvantage of a rigid wall permeameters is the possibility of leakage or boundary flow between the soil sample and the wall of the permeameter (McNeal & Reeve, 1964; Hill & King, 1982). It occurs in clay rich samples as a result of the swell/shrink behaviour of the clay when in contact with solutions of different chemical composition. Boundary flow is a major source of errors in laboratory hydraulic conductivity measurements when using rigid wall permeameters (McNeal & Reeve, 1964). Consequently, a compacted clay sample is useless as a semipermeable membrane (Keijzer *et al.*, 1994). A second disadvantage of the rigid wall design is the friction it provides to soils that are subjected to volume increase while being in the permeameter —e.g. swelling clays— resulting in deformation of the sample.

Flexible wall permeameters

Flexible wall permeameters are currently the most widely used device for the determination of hydraulic conductivities of soil samples, including clay rich samples (Tavenas *et al.*, 1983a; 1983b; Daniel *et al.*, 1984; Benson & Trast, 1995). However, experimental equipment using a flexible permeameter for the investigation of semipermeable properties of clayey material is so far only described by Olsen and co–workers (Figure 3.2 – Olsen *et al.*, 1988a; 1988b; 1989). A flexible wall permeameter can also be used in the determination of related phenomena such as diffusion osmosis (Olsen *et al.*, 1989; 1990; Yearsley, 1989). Olsen's equipment is derived from a design used for the determination of the hydraulic conductivity using the flow–pump method (Olsen *et al.*, 1985; 1988b; Aiban & Znidarcic, 1989). As with designs based on a rigid wall permeameters, detection of osmotic phenomena is mainly done by pressure transducers and electrical conductivity measurements.

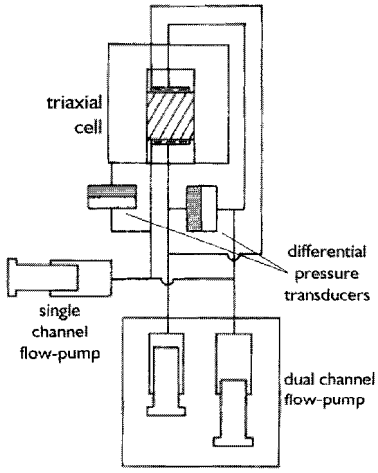

Figure 3.2
Schematic representation of the experimental design around a flexible wall permeameter used to study the chemical causes of ground water movement by Olsen and co–workers (after Olsen *et al.*, 1989).

3.3 EXPERIMENTAL DESIGN

Design criteria

An earlier design for semipermeability measurement by the author, based on a rigid wall permeameter proved to be susceptible to side wall leakage (Keijzer *et al.*, 1994). Therefore, a new design should eliminate the effects of the swell/shrink behaviour of the sample, and thus minimise the possibility of side wall leakage. The semipermeability of the sample should be tested under near surface conditions as encountered in the, mostly unconsolidated, subsoil of the Netherlands. The semipermeability should be tested directly, i.e. induced water fluxes and hydraulic pressures should be measured as they evolve. To minimise experimental time the design should be rigid; a small volume of water transported by the applied chemical gradient should result in a large induced hydraulic pressure. As the samples of interest are contaminated sediments, the advective transport of uncharged solutes should also be measured directly in the experimental design. This results in the following specific design criteria:

1. One dimensional water transport under well defined gradients, either solely hydraulic or chemical, can be induced across a sample.
2. Boundary flow resulting from swell/shrink of the sample by chemical non–equilibrium with the solutions in the reservoirs, or from poor filling of the permeameter should be avoided.
3. The design must be capable of withstanding pressures of maximum 1 MPa, corresponding to a hydrostatic pressure at approximately 100 m (water) depth, without deformation or leakage of the reservoirs.
4. The sample can be saturated by a solution of known concentration.
5. The solutions in the two reservoirs separated by the sample can be maintained at different concentrations and pressures.
6. Reservoirs must be as small and as rigid as possible. The solutions within the reservoirs must be of homogeneous chemical composition.
7. The volume flow rates into and out of the reservoirs as induced by the applied gradient must be measured directly.
8. The reservoirs must be as corrosion free and chemically inert as possible; the use of materials to which organic contaminants might adsorb must be minimised.
9. The occurrence of a streaming potential during the experiments should be avoided.
10. The temperature during experiments must be kept constant.

Experimental design

Based on the criteria an experimental design was built consisting of a flexible wall permeameter connected to two solution reservoirs (Figure 3.3, Photo 3.1). In the flexible wall permeameter a sample of 50 mm diameter and a maximum thickness of 100 mm can be fitted. The permeameter is located in a cylindrical cell, made of polyoxymethylene (POM – 141 mm outer diameter, o.d., and 115 mm internal diameter, i.d.) fitted between two stainless steel plates. The top and bottom plates can be bolted together with three stainless steel, all–thread rods placed at an angle of 120°. The apparatus is placed in a temperature controlled bench top chamber at 25 ± 0.2°C, using a custom made heating and ventilation system, equipped with a Pt100 sensor and a West® 6100 temperature regulator (TMC Instruments, Zeist, NL).

Samples are placed on a pedestal on the bottom plate between two porous stones and 15 µm nylon filters. A stainless steel cap, or top cap, is mounted on top of the assembly. A rubber 'sleeve' (length 200 mm, thickness 0.4 mm – ELE Intertest, Etten–Leur, NL) is placed over the sample, the porous stones, the top cap and pedestal. O–rings are placed over the rubber 'sleeve' on cap and pedestal to provide a seal (Figure 3.4, Photo 3.2). Prior to usage the porous stones were wrapped in teflon tape to prevent rupturing of the rubber 'sleeve' by the sharp edges of the stones. The top cap is connected to the bottom plate by two stainless steel capillary tubes (1 mm o.d., 0.5 mm i.d.). The POM cell can be filled, normally with de–aired tap water, and drained through a separate influent port in the bottom plate by a system referred to as the pressure and de–airing system (Figure 3.5, Photo 3.3). A maximum pressure of 1 MPa can be applied by this system to the cell liquid and is measured using a pressure transducer (0–1 MPa, MicroSwitch® 242PC150G – Dépex, De Bilt, NL) fitted between the cell and the pressure and de–airing system. However, safety considerations limit the cell pressure to 700 kPa. The pressurised water in the cell ensures a good contact between the rubber 'sleeve' and the sample. It prevents boundary flow when the dimensions of the sample change due to shrinkage in response to chemical non–equilibrium with the solutions in the reservoirs.

The bottom–end of the sample is connected to the reservoir containing a low concentration solution, referred to as the fresh water reservoir. The top–end of the sample is connected to the reservoir containing a saline solution, referred to as the salt water reservoir. All connections between the reservoirs and sample exit the cell through the bottom plate and are fitted with stainless steel Serto® regulating valves (Teesing, Rijswijk, NL). The reservoirs (Photo 3.4) consist of stainless steel tubing (6 mm o.d., 4 mm i.d.) with a volume of 13 cm^3 for the fresh water reservoir and 14 cm^3 for the salt water reservoir. Each reservoir contains an Ismatech Reglo–ZS® magnetically

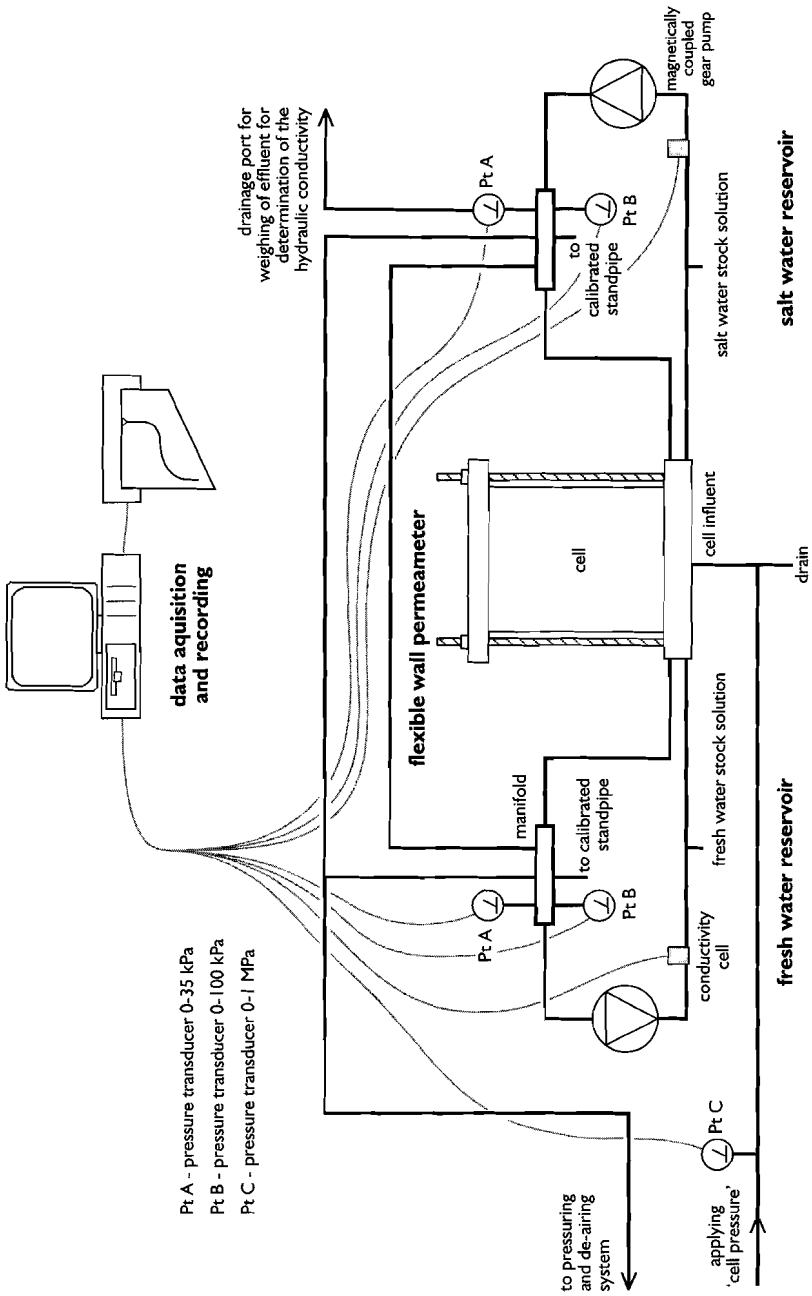

Figure 3.3 Schematic representation of the part of the experimental design placed within the temperature controlled bench top chamber (see also Photo 3.1).

coupled gear pump (Dépex, De Bilt, NL) fitted with a graphite gear. Default displacement of the pumps is approximately 30 $cm^3 \cdot h^{-1}$. A stainless steel manifold connects each reservoir to calibrated glass standpipes (6 mm o.d., 4 mm i.d.) and the pressuring and de–airing system. The glass standpipes are fitted with a water lock to prevent evaporation of the solutions in the reservoir during the experiments. The manifold also connects two pressure transducers (Dépex, De Bilt, NL), one with an operating range between 0–35 kPa (MicroSwitch® 236PC05GW), and the other between 0–100 kPa (MicroSwitch® 242PC15M) with the reservoir. Each reservoir contains a custom made electrical conductivity (Ec) cell fitted into a stainless steel T–tubing. The cell constant for each cell has to be determined prior to each experiment. The conductivity is recorded using a Tacussel® CD180 conductivity meter operating at 16 kHz. All pressure transducers are calibrated prior to each run.

The salt water reservoir is equipped with an extra drainage port connected to an air–tight tube in which the displaced water volume can be collected during the hydraulic conductivity measurements (Photo 3.5).

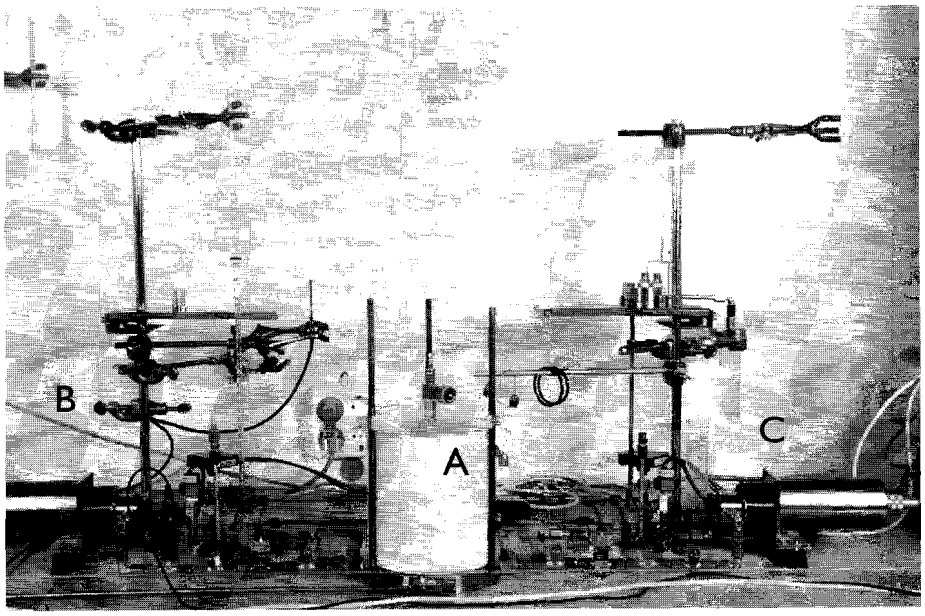

Photo 3.1 Photograph showing an overview of the part of the experimental design within the bench top temperature chamber. Clearly visible are **A** the cell in which the flexible wall permeameter is located, **B** the fresh water reservoir, and **C** the salt water reservoir.

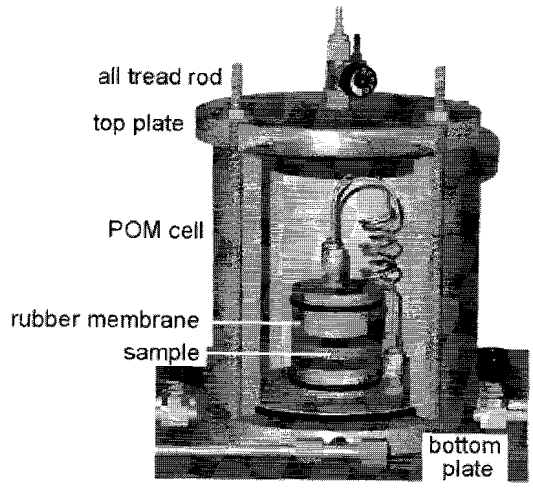

Figure 3.4
Schematic drawing of the flexible wall permeameter within the cell showing the position of the sample between the porous stones and filters. The cell can be filled with de–aired water and pressurised enabling an optimal contact between the flexible, rubber 'sleeve' wall and the sample (see also Photo 3.2).

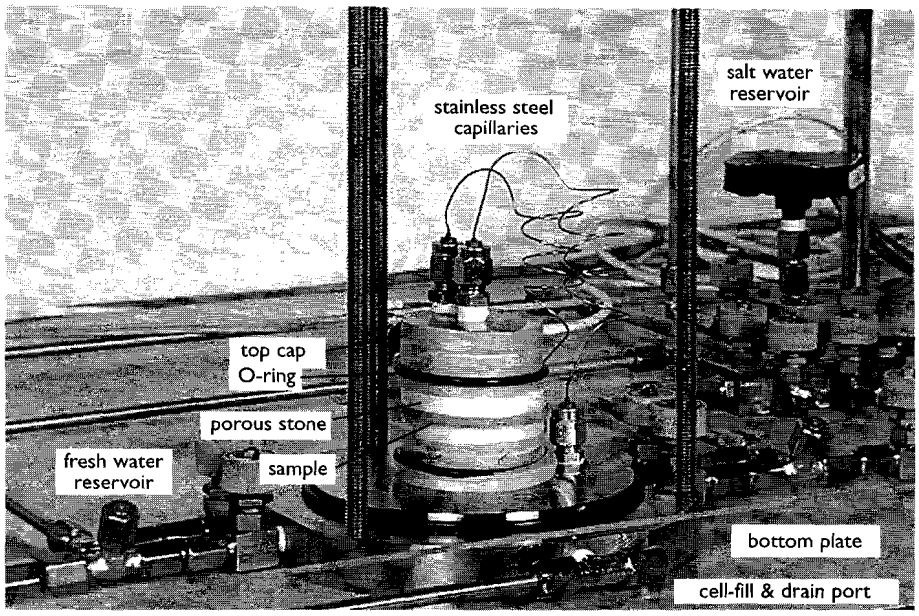

Photo 3.2 Photograph showing the flexible wall permeameter. The sample is fitted between porous stones and placed on the bottom plate. After the top cap is fitted the rubber 'sleeve' is placed over the sample and cap and held in place with an O–ring. The top end of the sample is connected to the salt water reservoir by stainless steel capillaries, the bottom end is connected with the fresh water reservoir through the bottom plate.

Data aquisition

All signals from the temperature sensor, pressure transducers and conductivity cells are logged on an IBM® compatible computer operating under MS–DOS v6.2, equipped with a AXIOM® AX5412 A/D–converter (16 channels single ended, 12 bits 100kHz) in combination with the AXIOM® RTG–DAS data acquisition software (AMT, Breda, NL). Simultaneously, eight channels (differential) are recorded typically at a five minute interval. Data processing is done by transferring the ASCII log file to a spreadsheet. It is also possible to continuously monitor and log analog signals using a dual channel Kipp® BD41 recorder.

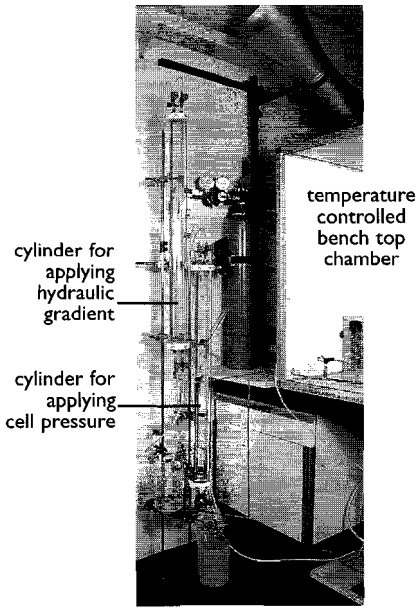

Photo 3.3
Photograph of the pressure and de–airing unit of the experimental design.

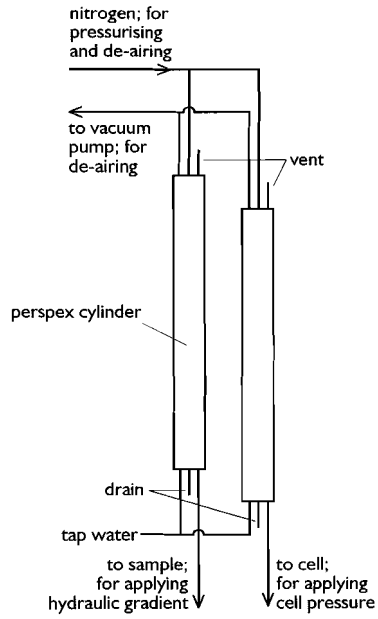

Figure 3.5
Schematic representation of the pressure and de–airing unit for applying the cell pressure and de–airing the reservoirs.

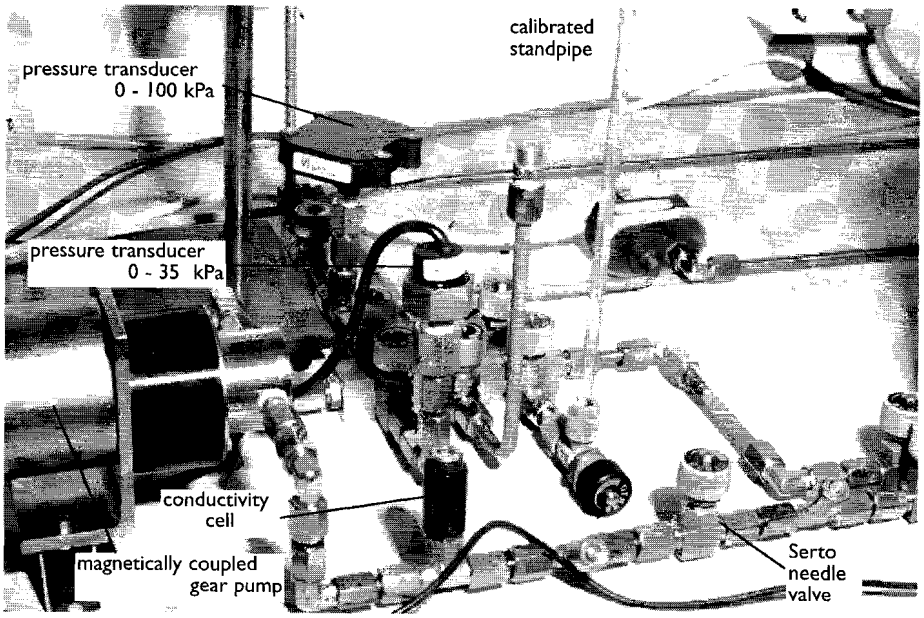

Photo 3.4 Detail of the experimental design showing the fresh water reservoir.

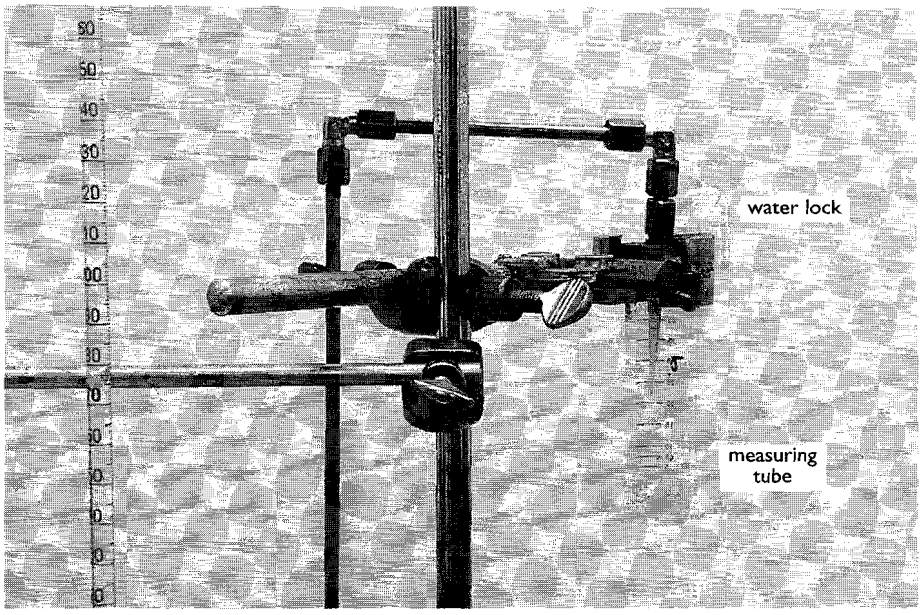

Photo 3.5 Detail of the experimental design showing the tube for gravimetrical measurement of the displaced water volume by an applied hydraulic gradient, in order to obtain the hydraulic conductivity value of the sample.

3.4 GENERAL EXPERIMENTAL PROCEDURES

Sample preparation

After compaction (see Chapters 4 & 5) samples are mounted in the cell between the porous stones and the filters, after which the latex membrane is placed over the sample (Photo 3.2). The sample can be saturated with de–aired tap water or a NaCl solution depending on the experiment. This is done by filling the fresh water reservoir with the required solution and applying a small hydraulic gradient for several days until a steady flow of water is observed into the salt water reservoir. During saturation no suction or so–called 'back pressure' is applied to the sample. The desired cell pressure for the specific experiment, however, is already applied during saturation. The porous stone and filter are soaked in the saturation solution prior to assembly to remove trapped air. After saturation both reservoirs including the tubing to and from the sample are flushed to remove bubbles.

Hydraulic conductivity

Prior to each chemical osmosis experiment the hydraulic conductivity of the sample is measured using a falling head method. The sample is subjected to a hydraulic gradient by filling the standpipe in the fresh water reservoir, creating a gradient typically in excess of 100 $cm \cdot cm^{-1}$. The water flow is measured gravimetrically at regular time intervals at the special drainage port in the salt water reservoir (Photo 3.5). The large gradient is needed to conduct the hydraulic conductivity test within an acceptable period of time. Detailed descriptions of different types of hydraulic conductivity tests, including the falling head method, with their advantages and disadvantages are given elsewhere (McIntyre *et al.* 1979; Benson & Daniel, 1990).

Chemical osmosis

Under identical conditions as applied in the hydraulic conductivity test the sample is subjected to a chemical gradient. The fresh water reservoir is filled with a low concentration NaCl solution and the salt water reservoir with a more saline solution (see Chapters 4 & 5). The solutions are de–aired prior to the filling of the reservoirs and kept at 25°C.

Two methods are used to follow water transport as a result of the applied chemical gradient. Firstly, with both reservoirs open to the atmosphere, the flow of water is measured using the calibrated standpipes. Evaporation of the solution in the reservoir is prevented by a water lock. This type of experiment is referred to as an

'open reservoir experiment'. Secondly, with the fresh water reservoir open and the salt water reservoir closed to the atmosphere, the differential pressure is monitored using the pressure transducers. This type of experiment is referred to as a 'closed reservoir experiment'. Diffusion or convection of salt across the sample in both types of experiments is monitored by the electrical conductivity in the reservoirs.

3.5 TESTING THE INSTRUMENTATION

Calibration

Calibration of the pressure transducers was done by determining the blank signal at atmospheric pressure and the subsequent increase with typically four to five data points within the measuring range of the transducers.

The calibration of the Ec–cell was done with a standard 0.01 mol·L^{-1} KCl solution in the fresh water reservoir and with a 0.1 mol·L^{-1} KCl solution for the salt water reservoir. These solutions have a known electrical conductivity at 25°C from which a cell constant can be derived.

Test samples

To test the experimental instrumentation and determine blank signals and stability of the signals several test were done without any samples fitted in the cell. Additionally, several test were run with two non–clay samples.

Stainless steel cylinder

A stainless steel cylinder (diameter 50 mm, height 10 mm) was used to detect any leakages from the water in the cell to the reservoirs. It was also used to test whether the reservoirs could be kept at constant pressures when the cell pressure changes. It also gives insight in the stability of the signals under different conditions. During the tests with the stainless steel cylinder the reservoirs were filled with de–aired tap water.

Reverse osmose membrane

The other test sample was a flat sheet Desal–11™ 'brackish water' thin–film semipermeable membrane (30x30 cm – Osmonics Desal, Wöschnau/Aarau, CH), and was used to determine the operation and performance of the experimental device during an osmosis experiment. The Desal–11™ Reverse Osmose (RO) membrane is used in the desalination of brackish water through a reverse osmosis system (Table 3.1).

The RO membrane was prepared as described by the test sheet supplied by Osmonics Desal whenever possible. From the RO membrane sheet a smaller sample was cut with a diameter of 50 mm and wetted out as prescribed by soaking in methanol (Baker, Deventer, NL) for 30 seconds. The prescribed short pre–flush with water at 2.4 MPa was skipped due to the lack of the desired equipment to do so. The RO membrane was then fitted into the cell with the side functioning as a semipermeable membrane facing the fresh water solution and the supporting side facing the salt water solution. In the RO membrane test a 0.01 mol·L^{-1} NaCl solution was used in the fresh water reservoir and a 0.10 mol·L^{-1} NaCl solution in the salt water reservoir. The theoretical, maximum pressure difference to be expected at this concentration difference, based on Eq. 1.4 (p. 9) is 421.5 kPa at 25°C.

Table 3.1 Membrane specifications for the Desal–11 ™ 'brackish water' reverse osmosis membrane.

material	probably cellulose acetate
applications	brackish water desalination, reactive silica removal
membrane rating	99.5 % average NaCl rejection, based on 1 g·L^{-1} NaCl solution feed at 1.4 MPa at 25°C
thickness	0.14 mm
pH range	optimum rejection at pH 6.5–7.5
operating temperature	up to 50°C

Table 3.2 Signal and signal error for applied cell pressures using the pressuring and de–airing system for cell pressures up to 500 kPa.

applied pressure	measured pressure	error
kPa	kPa	%
100	87.1 ± 2.1	2.4
200	185.1 ± 1.7	0.9
300	278.6 ± 1.4	0.5
400	377.5 ± 1.5	0.4
500	482.0 ± 1.9	0.4

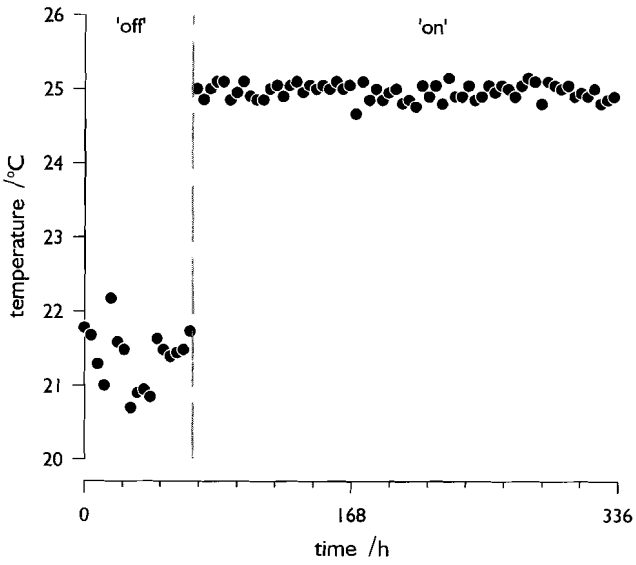

Figure 3.6 Typical temperature signal and stability in the bench top chamber with the temperature control switched off and on.

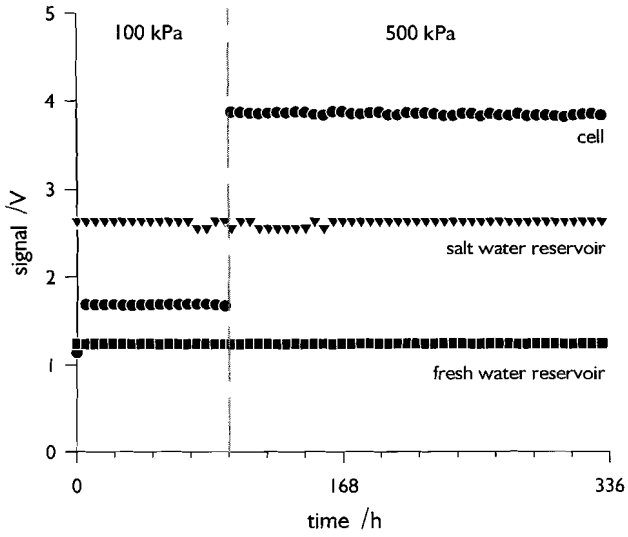

Figure 3.7 Response and stability of the signals of the pressure transducers measuring the pressure in the cell and the two solution reservoirs when switching from a cell pressure of 100 kPa to 500 kPa.

SWy bentonite

To test the method and configuration used for the hydraulic conductivity measurement a compacted source clay SWy–2 sample was fitted in the cell. Approximately 20 gram of the clay was consolidated under 20.3 MPa in a stainless steel mould before fitting in the cell. This resulted in a sample with a thickness of about 1 cm. A cell pressure of 100 kPa was applied and the sample was saturated with de–aired tap water in the absence of a back pressure. After saturation the sample was subjected to a hydraulic gradient of approximately 100 $cm \cdot cm^{-1}$ and the flow of water was measured gravimetrically at regular intervals.

3.6 TEST RESULTS AND DISCUSSION

Stability and reproducibility of the signals

The temperature of the bench top chamber can be raised within a hour from ambient laboratory temperatures to 25.0 ± 0.2°C and kept constant for any desired period of time (Figure 3.6). However, as the heating and ventilation system is unable to cool the air in the chamber the temperature should be kept approximately 5°C above the ambient laboratorium temperature.

The cell pressure can be kept constant with an maximum error of 2.5 % (Table 3.2) as long as the temperature remains constant. If the temperature is not controlled the fluctuations in the laboratory temperature can result in volume changes of the cell liquid and cell wall and thus pressure changes. This is an undesirable effect as the pressure applied to the liquid in the cell has to be maintained at a constant value to ensure contact between the rubber 'sleeve' and the sample. Large fluctuations in the cell pressure can result in volume and porosity changes of the sample, or loose contact between the rubber 'sleeve' and sample resulting in boundary flow.

The temperature changes must also be kept to a minimum as the reservoirs are constructed to be as rigid as possible making them highly susceptibility to small changes. Fluctuations in the temperature in the laboratory down to 0.5°C could be accurately measured by the pressure transducers fitted in the reservoirs. Finally, isothermal conditions were necessary to eliminate thermo–osmosis, i.e. water transport driven by a temperature gradient.

Table 3.2 also shows that there is an approximate 10 % difference between applied cell pressure and actual cell pressure measured with the pressure transducer. This results from the inaccuracy of the scale of the pressure regulator fitted in the pressure and de–airing system (Photo 3.5).

Typical calibration curves with regression coefficients for the different types of transducers are given in Table 3.3. Linearity in the measuring range of the transducers is good, and reproducibility between calibration sessions was good.

The experiment with the stainless steel cylinder showed that the signals from the pressure transducers in the reservoir are stable when the cell pressure is increased (Figure 3.7). These signals showed no increase when the cell pressure was increased from 100 up to 500 kPa under isothermal conditions. It is thus possible to maintain the two reservoirs on different elevated pressures without being influenced by fluctuations in the cell pressure.

The cell constants for the electrical conductivity cells were typically between 0.7 and 1.0 cm^{-1} at 25°C. However, it was observed that the signal of the Ec cell increased with increasing pressure in the reservoir. This means that the cell constant of the electrical conductivity cell changes as the pressure in the reservoir increases. This can be attributed to the design of the Ec–cell (Figure 3.8). The teflon plug in which the Pt–wire is fitted can deform under the pressure in the reservoir. This results in a change of cell configuration and thus a change in the cell constant. The most profound

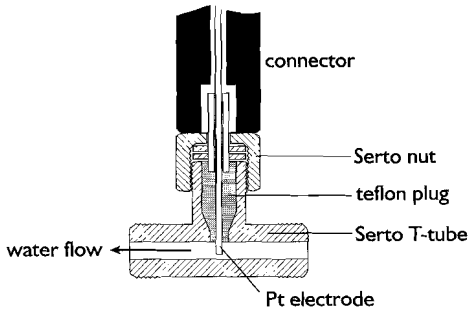

Figure 3.8
Schematic cross section through an electrical conductivity cell.

Table 3.3 Typical regression equations and regression coefficients (r) for the different types of pressure transducers used in the experimental design.

transducer type	pressure range kPa	regression equation[1)]	r
236PC05GW	0–35	$(p/kPa) = 601.2(U/V) + 4.1$	0.998
242PC15M	0–100	$(p/kPa) = 16.1(U/V) - 17.3$	0.998
242PC150G	0–1000	$(p/kPa) = 179.2(U/V) - 214.3$	0.996

1) U in the equations is the response of the pressure transducer in volts

changes in the cell are taking place between atmospheric pressure and 100 kPa; above 100 kPa the cell configuration changes less dramatically. To circumvent this problem the Ec–cell was calibrated prior to every experiment and the values obtained during experiments were corrected. Consequently, a more rigid design of the Ec–cell was incorporated into the design. Cation and anion concentrations at the start and end of the experiments were measured using ICP–AES for the cation and Ion Chromatography (IC – QID Dionex equipped with an Ionpac AS4A column) for the anion concentration.

Testing with a reverse osmosis membrane

Testing the design with a reverse osmosis membrane in place of a soil sample proved succesful (Figure 3.9), although the measured pressure did not reach the theoretical value. Using the definition of the reflection coefficient (Eq. 1.11, p. 13) and taking the mean differential pressure during the last two days of the experiment a reflection coefficient of the RO membrane of 0.10 can be calculated, thus, the membrane is 10 % effective. According to the membrane specifications it should exhibit an ideality above 99 % (Table 3.1). However, the pretreatment of the membrane could not be done as prescribed by the supplier due to the lack of the desired RO installation. The membrane was therefore only treated with methanol to remove the agent used to preserve the membrane. It therefore probably kept some of its hydrophobic properties reducing its ideality. According to the test sheet provided by Osmonics Desal an incomplete pretreatment can result in poor performance. It also states that the membrane type is susceptible to ageing which also negatively influences its ideality. After obtaining the RO sheets from Osmonic Desal they were stored for approximately six months before usage, consequently reducing their ideality.

Hydraulic conductivity measurement

The specifications of the compacted SWy–2 sample are listed in Table 3.4 together with the experimental parameters of the hydraulic conductivity test. The hydraulic conductivity, K_h in $m \cdot s^{-1}$, is determined using Darcy's law:

$$J_w = K_h A \frac{\Delta p}{x} \tag{3.1}$$

in which J_w is the measured water flux in $m^3 \cdot s^{-1}$, A is the cross section of the sample in m^2, Δp the applied hydraulic pressure difference in m H_2O across the sample with

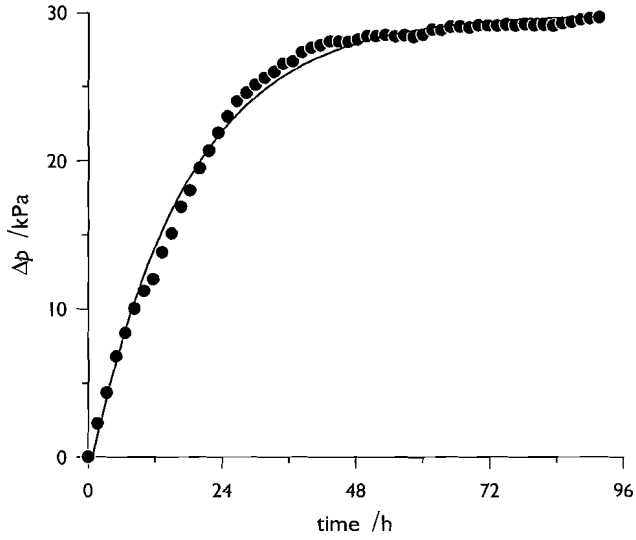

Figure 3.9 The development of the differential pressure as the result of a chemical osmosis experiment on a 0.14 mm thick Desal–11 ™ 'brackish water' semipermeable membrane.

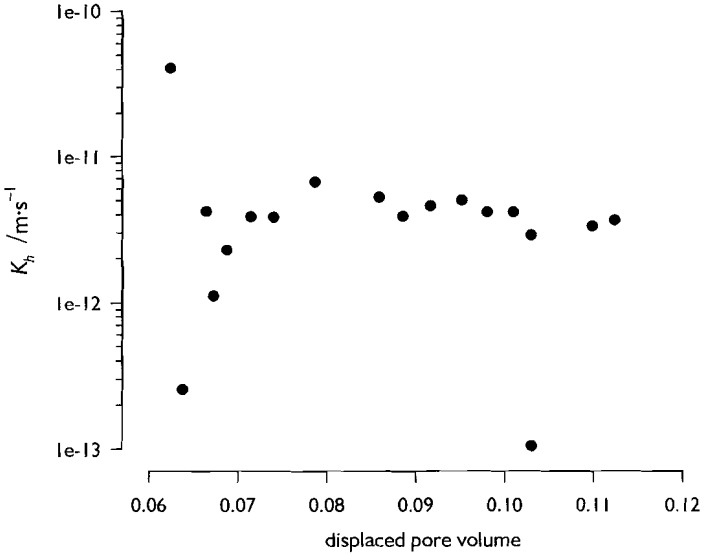

Figure 3.10 Development of the hydraulic conductivity, K_h, for a sample of compacted SWy–2 bentonite in a falling head experiment plotted against the displaced pore volume.

thickness x in m. The average hydraulic conductivity for this sample of SWy–2 was determined to be $(3.9 \pm 1.3) \cdot 10^{-12}$ m·s^{-1} based on fifteen individual measurements during the falling head test (Figure 3.10). The first three points were discarded as they represent a non–steady–state period under the applied hydraulic gradient.

This experiment showed that the low hydraulic conductivities of samples with high clay content can be measured in the developed permeameter. The period it takes to determine K_h with sufficient accuracy with the falling head method is in excess of four weeks, even with the large hydraulic gradient applied.

The time needed for complete saturation of this 1.3 cm thick sample and determination of its hydraulic conductivity was about two months. Based on this and two similar experiments it was decided that the sample height should be reduced in order to perform a complete experiment including preparation, saturation, determination of hydraulic conductivity and chemical osmosis within a period of three months.

Streaming potential

As indicated in Table 1.1 (p. 8) an applied hydraulic head can induce an electric current (a streaming current) in the sample. In a non–shorted permeameter a streaming potential will develop that will counteract the water flow (Mitchell, 1993). The streaming current is more profound in fine grained soils with hydraulic conductivities $<10^{-9}$ m·s^{-1}, in which the percentage error can be as high as 100 % (Yeung, 1990; 1994). In the experimental design presented in this chapter the streaming potential could not be measured due to the chosen design. However, we conclude that the

Table 3.4 Measured sample properties and experimental parameters for the determination of the hydraulic conductivity of the SWy–2 sample.

net dry weight	19.3	g
sample height	1.3	cm
sample diameter	50.0	cm
pore volume	25.3	cm^3
porosity	0.71	
hydraulic gradient[1)]	73	cm·cm^{-1}
hydraulic conductivity[2)]	$(3.9 \pm 1.3) \cdot 10^{-12}$	m·s^{-1}

1) average gradient for the falling head method

2) number of observations: 15

streaming potential is negligible as a result of the design. The top and bottom end of the sample are connected through the stainless steel reservoirs without the reservoirs being open to each other. Thus, the system is short circuited through the stainless steel reservoirs and therefore no streaming potential will develop across the sample.

3.7 CONCLUDING REMARKS

The developed experimental instrumentation for measuring the semipermeability of a given sample proved to be capable of measuring hydraulically driven water transport across a clay sample, and osmotically driven water transport across a commercially available reverse osmosis membrane. Solutions in the reservoirs, kept at different concentrations and pressure, were not susceptible to changes in the cell pressure. The experimental design, due to its rigid design, proved to be highly susceptible to temperature changes but the designed temperature controlled bench top chamber reduced the negative effect satisfactorily. The occurrence of a streaming potential during the experiments cannot be measured but is presumed, as a result of the chosen permeameter materials, to be negligible.

Whether other criteria were met and whether the experimental design performed as desired will be discussed in later chapters.

4 Chemical osmosis in bentonite

4.1 INTRODUCTION

Solutions concerning the disposal of waste and the containment of pollutants focus around the application of low permeable clay barriers to prevent undesirable transport. However, as clays are capable of acting as a semipermeable membrane the application of clays can not be done without the knowledge of, or insight in the semi-permeable properties of these clays. Therefore, the ability of a commercially available Wyoming bentonite as a semipermeable membrane under near surface condi-tions is evaluated in this chapter. Experiments were conducted on loosely compacted samples with a porosity >0.6, and more highly compacted samples with a porosity of approximately 0.5. Semipermeability of the bentonite was assessed by measuring the water flux by chemical osmosis and determining the reflection coefficient, σ, of the samples. The values for σ were compared to those available in the literature and with values obtained from the models presented in Chapter 1. Taking bentonite as a reference material, these experiments provide useful information on the operation of our experimental apparatus for measuring chemical osmosis in other clayey samples.

4.2 EXPERIMENTAL CONDITIONS

General

All experiments were conducted with Ankerpoort Colclay A90 bentonite (AWy). A full description of bulk properties of this bentonite was given in Chapter 2. The bentonite was used without pretreatment. In studies elsewhere the clay was repeatedly washed, with a NaCl–solution, and sedimentated to disperse the clay minerals and occupy the exchange complex with a monovalent cation making it theoretically a more ideal membrane.

A clay membrane with a thickness of approximately 2 mm was obtained by weighing 5.0 g of air–dried bentonite into a stainless steel mold with an internal diameter of 50 mm. The clay was then subjected to a compaction pressure gradually increasing to 20.3 MPa, and kept at that pressure for 30 minutes. The compaction was done to obtain an easy to handle sample, and to reduce the initial porosity of the sample. After compaction the sample was mounted in the cell between the porous stones and filters, after which the latex membrane was placed over the sample and the sample was saturated with de–aired tap water. The porous stone and filter at the bottom end of the sample were soaked in the saturation solution prior to assembly to remove air. The stone and filter at the top end of the sample were not saturated with solution to enable the escape of trapped air within the sample during saturation. After saturation all tubing to and from the sample were flushed. The hydraulic conductivity of the sample was measured on the saturated sample prior to the chemical osmotic experiment by using a falling head permeability test (Chapter 3). Under identical conditions the sample was subjected to an osmotic pressure gradient.

Bentonites with high porosity

The bentonite samples with high porosity, AWy–A and AWy–B, were saturated with de–aired tap water of atmospheric pressure, under an approximate 100 kPa pressure applied to the water in the cell. The low cell pressure was chosen to mimic near surface conditions. After determination of the hydraulic conductivity the fresh water reservoir was filled with a 0.1 $mol \cdot L^{-1}$ and the salt water reservoir with a 0.6 $mol \cdot L^{-1}$ NaCl solution. According to Eq. 1.4 (p. 9) this corresponds to an osmotic pressure difference of 2.37 MPa or 241.2 m H_2O at 25°C. The concentrations were chosen to represent the possible concentration difference between a fresh and salt water aquifer. The properties of the samples and the experimental conditions are listed in Table 4.1.

Compacted bentonites

The more compacted samples, AWy–C and AWy–D, were also saturated with de–aired tap water at atmospheric pressure, and a pressure of approximately 500 kPa was applied to the water in the cell. This cell pressure exceeds the swelling pressure of the bentonite as it caused volume reduction during the experiments. After the hydraulic conductivity experiment, the fresh water reservoir was filled with a 0.01 $mol \cdot L^{-1}$ and the salt water reservoir with a 0.1 $mol \cdot L^{-1}$ NaCl solution, corresponding to an osmotic pressure difference of 421.5 kPa or 43.0 m H_2O at 25°C (Eq. 1.4).

The chemical gradient was lowered to reduce negative effects of a high concentration gradient has on the stability of the clay. The specific properties and the experimental conditions for AWy–C and AWy–D are also listed in Table 4.1.

4.3 MODEL PREDICTIONS OF THE REFLECTION COEFFICIENT

The theoretical reflection coefficient of the samples was estimated using the FMMM, the Kemper–Bresler and Groenevelt–Bolt model (Chapter 1).

In Figure 4.1 σ is plotted as a function of the porosity for AWy at the experimental mean concentrations of 0.35 and 0.055 mol·L^{-1} NaCl according to the FMMM, and compared to a monomineral montmorillonite and illite. It illustrates the rise in membrane ideality as the concentration is lowered. All curves in Figure 4.1 are calculated based on the AWy properties (Table 2.1, p. 28) and experimental conditions (Table 4.1) using Eq. 1.12 (p. 14). For the frictional coefficient R_{wm} in Eq. 1.12 values were taken which decreased linearly between 0.1 and 0 in the porosity range between 0 and 0.4. All other necessary values for the frictional coefficients and formulae are discussed in § 1.4. The porosity of a sample during the experiment being known, σ can be easily derived from these curves (Table 4.2).

To obtain values for σ using the model by Groenevelt and Bolt the reflection coefficient is plotted against the reduced mobile double layer thickness, $\kappa_0 d_l$, for the $\kappa_0\delta$–value of the given sample, using Eq. 1.20 (p. 19 – Figure 4.2). The value for $\kappa_0 d_l$ can be calculated from the properties of the bentonite listed in Table 2.1 and the

Table 4.1 Measured properties and experimental conditions for the chemical osmosis experiments on AWy.

	AWy–A	AWy–B	AWy–C	AWy–D	
sample thickness	2.32 ± 0.13	3.39 ± 0.14	2.32 ± 0.08	2.29 ± 0.04	10^{-3} m
sample diameter	52.5 ± 1.3	53.9 ± 1.3	50.1 ± 1.3	51.0 ± 0.5	10^{-3} m
porosity after saturation	0.64	0.67	0.56	0.55	
hydraulic conductivity	7.6 ± 0.9	2.9 ± 0.9	1.2 ± 0.7	7.6 ± 4.5	10^{-12} m·s^{-1}
low concentration	0.1	0.1	0.01	0.01	mol·L^{-1} NaCl
high concentration	0.6	0.6	0.1	0.1	mol·L^{-1} NaCl
average eq. concentration	0.35	0.35	0.055	0.055	mol·L^{-1}
osmotic pressure	2 367	2 367	421	421	kPa
cell pressure	89.2 ± 2.2	91.9 ± 0.7	481.6 ± 3.9	482.1 ± 1.9	kPa
temperature	25.0 ± 0.2	25.0 ± 0.2	25.0 ± 0.2	25.0 ± 0.2	°C

experimental conditions listed in Table 4.1. All necessary additional values needed for Eq. 1.20, like δ, t_s and t_d can be calculated with the formulae provided in § 1.6. Eq. 1.20 converges at n>60 for the summation terms. Subsequently, knowing $\kappa_0 d_l$ of the samples σ can be derived from the curves.

The reflection coefficient can also be determined using Bresler's Fig. 1 (Bresler, 1973) by plotting σ as a function of the product of water film thickness between the particles and the square root of the equilibrium solution concentration. This was done by Neuzil (2000) for his *in situ* experiments on the Pierre shale and for the AWy–A and AWy–B samples in Keijzer *et al.* (1999). However, the obtained values should not be used as the error included is huge, especially at the lower end of the σ scale.

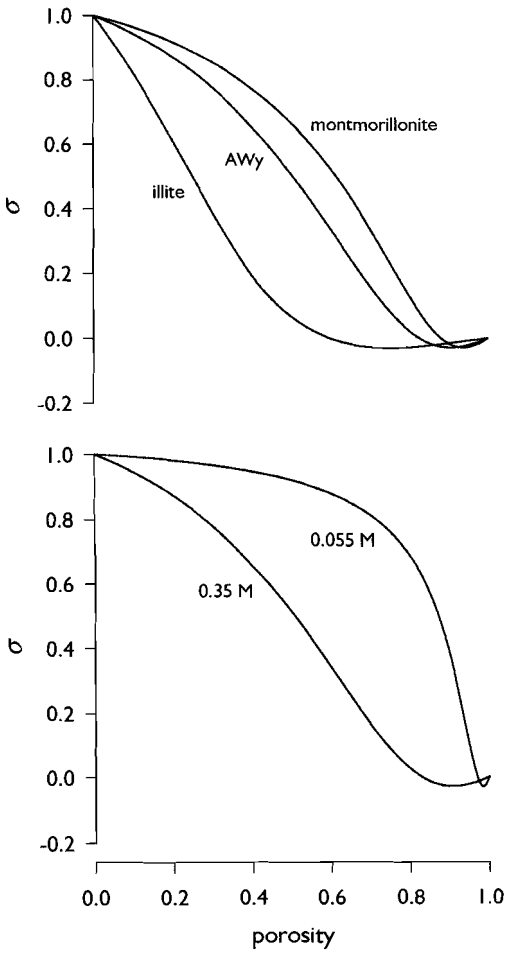

Figure 4.1
The reflection coefficient, σ, of AWy as a function of the porosity according to the FMMM; **top** the ideality of AWy compared with a typical montmorillonite with CEC of 100 $cmol_c \cdot kg^{-1}$, and an illite with CEC of 20 $cmol_c \cdot kg^{-1}$, using a mean salt concentration of 0.35 $mol \cdot L^{-1}$ NaCl, and **bottom** the ideality of AWy at the two mean average concentrations applied in the experiments.

Therefore, σ is calculated for all AWy samples after determining the water film thickness b by:

$$b = \frac{n}{\rho_b A_s} \tag{4.1}$$

where n is the porosity, ρ_b is the bulk density in $g \cdot m^{-3}$ and A_s the specific surface area in $m^2 \cdot g^{-1}$ of the sample. The value for y in Eq. 1.17 or 1.18 at distance b is obtained from the DDL (Mitchell, 1993):

$$e^{y/2} = \frac{e^{z/2} + 1 + (e^{z/2} - 1)e^{-\kappa_0 b}}{e^{z/2} + 1 - (e^{z/2} - 1)e^{-\kappa_0 b}} \tag{4.2}$$

where:

$$z/2 = \operatorname{arcsinh}\left(\frac{\chi}{\sqrt{8 n_0 \varepsilon_0 \varepsilon_r R T}}\right) \tag{4.3}$$

Here χ is the double layer charge in $C \cdot m^{-2}$, n_0 is the concentration of ions in the equilibrium solution in ions$\cdot m^{-3}$, ε_0 is the permittivity of the vacuum ($8.85419 \cdot 10^{-12}$ $C \cdot V^{-1} \cdot m^{-1}$), ε_r is the dielectric constant of water (78.54 at 298.15 K), R is the gas constant (8.31451 $J \cdot K^{-1} \cdot mol^{-1}$), and T is the absolute temperature. The value of κ_0 is the Debye–Hückel reciprocal thickness which can be found using Eq. 1.21 (p. 19). The reflection coefficient can be plotted either as a function of $b\sqrt{c_0}$ (Bresler, 1973) or against the equilibrium concentration c_0 for a given value of b (Figure 4.3). All obtained theoretical values for σ are listed in Table 4.2.

4.4 RESULTS

Immediately after compaction all samples had a porosity of approximately 0.35 that increased during the saturation period, resulting in a porosity between 0.5 and 0.7 (Table 4.1) depending on the cell pressure applied. The compaction pressure used on the dry material did not have a negative influence on the bulk properties, like the CEC and A_s, of the bentonite. The porosities after saturation of AWy–A and B are higher than for naturally occurring clays, those of AWy–C and D are similar to that of

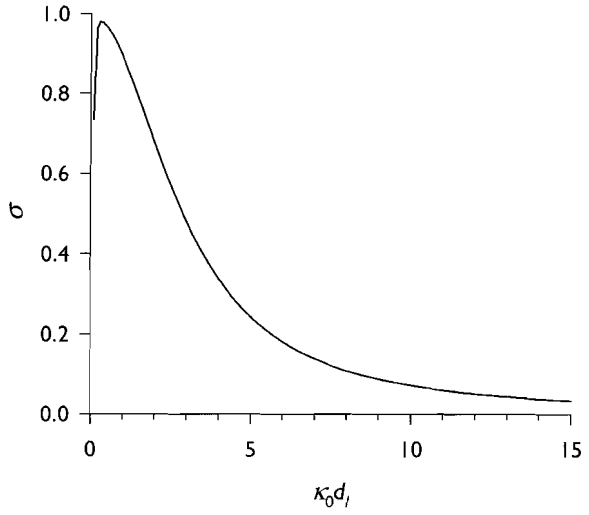

Figure 4.2 The reflection coefficient, σ, of AWy–C as a function of the normalised mobile water layer, $\kappa_0 d_l$, according to Eq. 1.20.

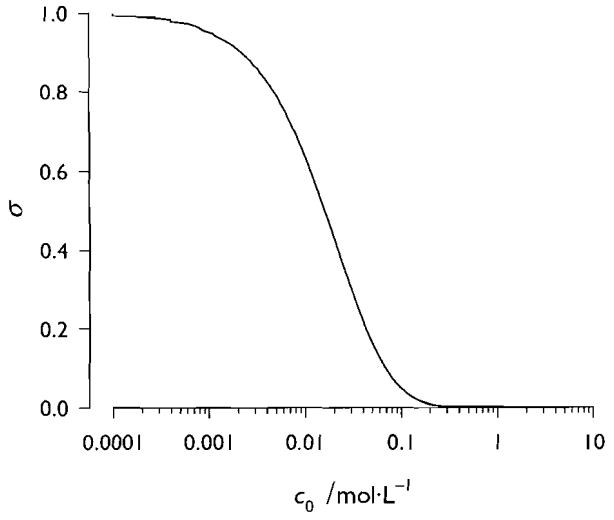

Figure 4.3 The reflection coefficient, σ, of AWy–C as a function of the concentration of the equilibrium solution according to Kemper (1972) and Bresler (1973) at a waterfilm thickness b of $8.2 \cdot 10^{-10}$ m.

natural unconsolidated clays under near surface conditions, typically around 0.5. Porosities under these conditions are not as low as can be expected under geological conditions where they are generally 0.3 or lower.

The hydraulic conductivity measured on the samples is between 10^{-11} and 10^{-12} $m \cdot s^{-1}$ and is comparable with reported values for compacted clayey soils (Benson & Trast, 1995).

Chemical osmosis

As a result of the applied chemical gradient, a water flux from the fresh water reservoir into the salt water reservoir was observed in sample AWy–A (Figure 4.4). The hydraulic pressure development across the sample and the change in electrical conductivity of the fresh water reservoir during the entire experiment are shown in Figure 4.5. The development of the hydraulic pressure difference (Δp) between the two reservoirs is defined as $\Delta p = p_{fresh} - p_{salt}$. This definition yields negative values for Δp as water flows from the fresh to the salt water reservoir. The first 48 hours, during which the experiment was run with open reservoirs (Chapter 3), a water flux (J_w) of 0.019 ± 0.004 $cm^3 \cdot h^{-1}$ from the fresh to the salt water was measured (Figure 4.5). We assume this flux to be the result of chemical osmosis. After the period with open reservoirs they were closed and the hydraulic pressure difference was monitored using only the pressure transducers in the reservoirs. Note the sudden decrease in Δp at that point (Figure 4.5). A reversal of the water flow took place after 67 hours.

Table 4.2 Theoretical values for the reflection coefficients for the experiments on AWy at the experimental porosity values.

		AWy–A	AWy–B	AWy–C	AWy–D
theoretical σ according to	FMMM	0.270	0.212	0.899	0.901
	Groenevelt–Bolt	0.0089	0.0066	0.117	0.124
	Kemper–Bresler	>0.0001	>0.0001	0.0019	0.0023

Table 4.3 Observed reflection coefficients for the experiments on AWy.

	AWy–A	AWy–B	AWy–C	AWy–D	
observed J_w	0.019 ± 0.004	0.016 ± 0.005	0.0048 ± 0.0021	nd	$cm^3 \cdot h^{-1}$
σ based on J_w	0.003 ± 0.001	0.0006 ± 0.0002	0.030 ± 0.013	nd	
observed Δp	–4.7	–0.7	–6.27 ± 0.55	nd	kPa
σ based on Δp	0.002	0.0002	0.015 ± 0.001	nd	

nd not detected

The reflection coefficient can be calculated from the experimental data in two different ways. Firstly, by applying an analogue of Darcy's law modified by σ (Barbour & Fredlund, 1989; Keijzer *et al.*, 1999):

$$J_w = \sigma K_h A \frac{\Delta\pi_o}{x} \tag{4.4}$$

in which J_w is the measured water flux in $m^3 \cdot s^{-1}$, K_h is the hydraulic conductivity in $m \cdot s^{-1}$, A is the cross sectional area of the sample in m^2 and $\Delta\pi_o$ is the pressure difference in m H_2O across the sample with thickness x in m. Using Eq. 4.4, a value for the reflection coefficient of 0.003 ± 0.001 is obtained for the period with open reservoirs (Table 4.3). Secondly, by applying Eq. 1.11 (p. 13) and using the maximum observed Δp with closed reservoirs which for AWy–A was reached after 67 hours in the experiment at –4.7 kPa, yielding a similar value for σ (Table 4.3). The two methods are apparently consistent.

Sample AWy–B was subjected to an identical chemical gradient as AWy–A, however, the experiment was run with open reservoirs only. This resulted in an elevated hydraulic pressure in the salt water reservoir as the result of osmotically driven water transport (Figure 4.6). The Δp development during the first 48 hours is also shown on an enlarged scale. From the measured water flux of 0.016 ± 0.005 $cm^3 \cdot h^{-1}$ in this period a σ of 0.0006 ± 0.0002 is derived for this sample (Table 4.3). After 48 hours the rate of decrease of Δp dropped until the differential pressure reached a value of –0.7 kPa after 310 hours, resulting in a σ of 0.0002. Both the rate of change of hydraulic pressure and the absolute value of Δp are lower than for sample AWy–A. This can solely be attributed to the experimental method used.

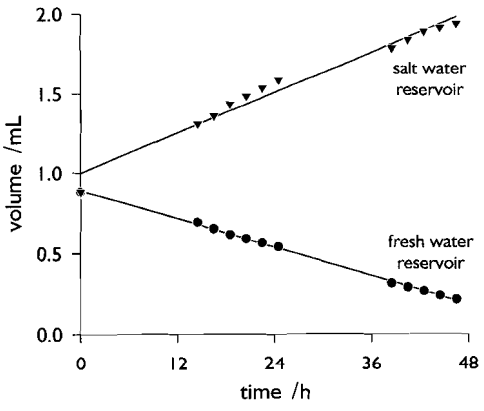

Figure 4.4
Observed volume changes in the calibrated standpipes of the fresh and salt water reservoir, showing the transport of water from the fresh to the salt water side of the AWy–A sample as the result of the applied chemical gradient.

As expected, the more compacted AWy–C bentonite also showed semipermeable properties when it was subjected to the chemical gradient (Figure 4.7). This experiment was run with closed reservoirs only. During the first few days the pressure across the bentonite sample decreased rapidly until reaching a minimum value between five and ten days, after this period Δp slowly decreased. Using the average measured water flux during the first 48 hours of the experiment and applying Eq. 4.4, a σ of

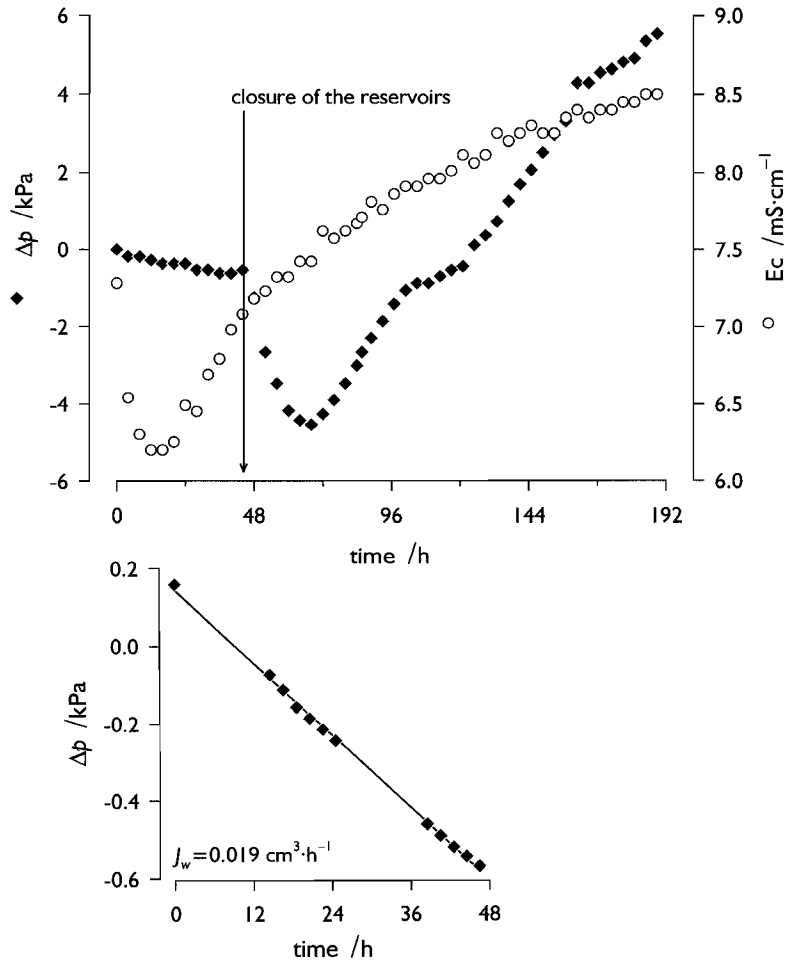

Figure 4.5 Development of the hydraulic pressure difference, $\Delta p = p_{fresh} - p_{salt}$, between the reservoirs and the electrical conductivity, Ec, in the fresh water reservoir for the AWy–A sample. The first 48 hours of the experiment is shown in the enlargement, where also the measured water flux (J_w) is given.

0.030 ± 0.013 is obtained (Table 4.3). Use of the formal definition of the reflection coefficient (Eq. 1.11) yields a similar value (Table 4.3).

Water transport was also observed in the experiment on the AWy–D bentonite (Figure 4.8) this was, however, not due to the applied chemical gradient. No semipermeability was observed in this particular sample.

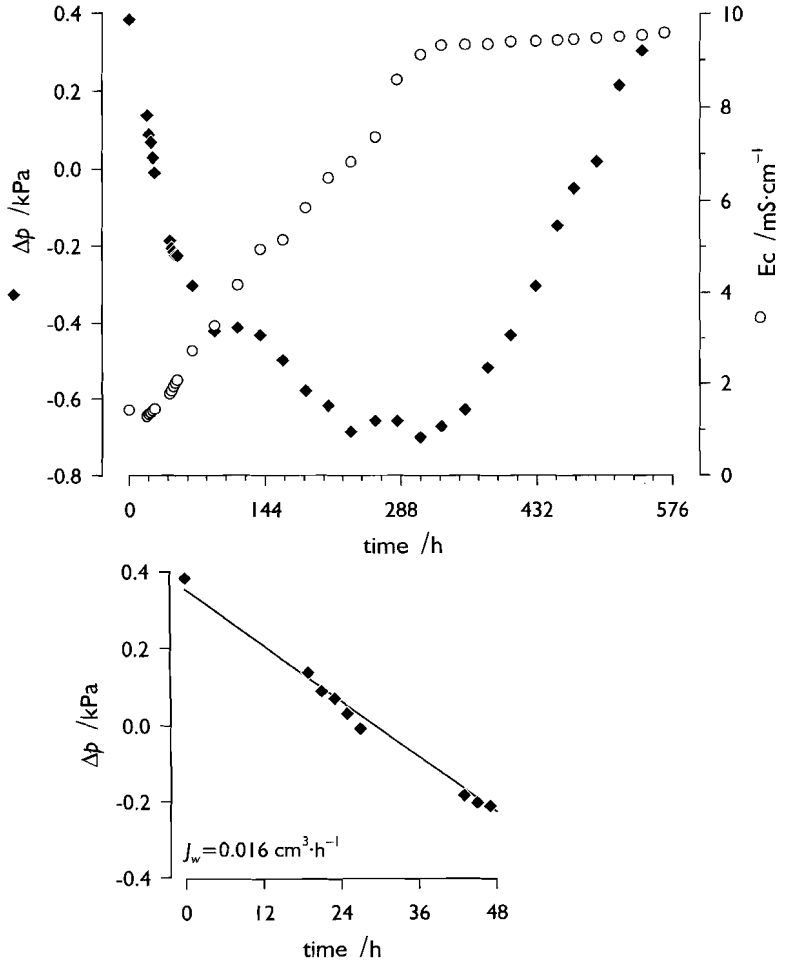

Figure 4.6 Development of the hydraulic pressure difference $\Delta p = p_{fresh} - p_{salt}$, between the reservoirs and the electrical conductivity, Ec, in the fresh water reservoir for the AWy–B sample. The first 48 hours of the experiment is shown in the enlargement, where also the measured water flux (J_w) is given. This experiment was run with open reservoirs.

4.5 DISCUSSION

Loosely compacted bentonites: AWy–A and AWy–B

The overall trend for both the AWy–A and AWy–B experiment is the same: initially Δp decreases linearly due to steady–state water transport from the fresh to the salt water reservoir as a result of the applied chemical gradient (Figures 4.5 & 4.6). After approximately 50 hours the rate of change of Δp drops. After reaching a minimum value it increases because of the reversal of the water flow and the hydraulic pressure in the fresh water reservoir increases. Because the clay membrane is not ideal, diffusion of ions is not completely restricted. For that reason the chemical gradient across the membrane will slowly decrease. Consequently, Δp will slowly diminish, but the rate at which this occurs in these experiments is faster than the rates observed by other authors in their experiments (Kemper, 1961; Elrick *et al.*, 1976).

The sudden drop in Δp in both experiments is not a result of collapse of the double layers caused by the increased equilibrium concentrations within the clay membrane, or of other failure of the samples as semipermeable membrane like the occurrence of side wall leakage. If this were so, Δp would change until it equalled zero (Figure 4.9). In that situation the salt gradient would diminish rapidly resulting in a fast increase in electrical conductivity (Ec) in the fresh water reservoir. In both experiments the Δp changed into high positive values and the observed Ec did not increase rapidly. Also, in both experiments the rate of increase in Ec became slower in the fresh water reservoir during the last stage of the experiment. In Figure 4.9 a schematic representation of the observed changes in Δp and Ec for the experiments and their interpretation is given, together with the expected signal if the sample would fail as a semipermeable membrane.

The changes in Δp and Ec in the fresh water reservoir are consistent with what is described by Olsen *et al.* (1990) as diffusion osmosis. Diffusion osmosis describes the transport of water in response to the diffusion of dissolved solutes. Olsen *et al.* (1990) described it as follows "*... solute diffusion in response to a concentration gradient imposes drag on, or momentum transfer to, the pore fluid and thus tends to move the pore fluid in the direction of decreasing solute concentration.*" According to Olsen *et al.* (1990) this behaviour was also observed but not recognised by other authors, for instance by Kemper and Quirk (1972), Elrick *et al.* (1976), Veder (1979), and Yearsley (1989). Diffusion osmosis should be more dominant in loosely compacted clayey material of low cation exchange capacity (Olsen *et al.*, 1990). Because the bentonite samples had no pretreatment before usage they perform as low exchange capacity clays. Therefore, σ's in Table 4.3 were calculated using the low N_2–BET value for the

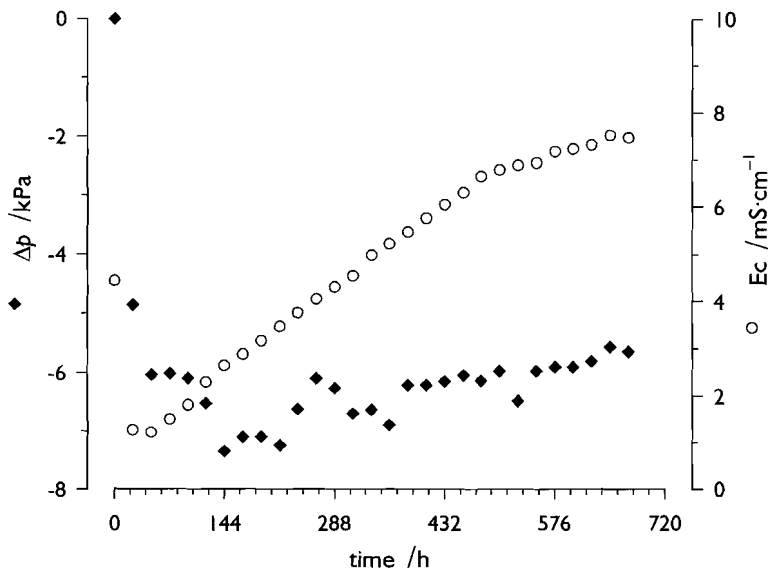

Figure 4.7 The development of a differential hydraulic pressure $\Delta p = p_{fresh} - p_{salt}$, as a result of chemical osmosis, and the electrical conductivity, Ec, in the fresh water reservoir for the AWy–C bentonite. The entire experiment was run with closed reservoirs.

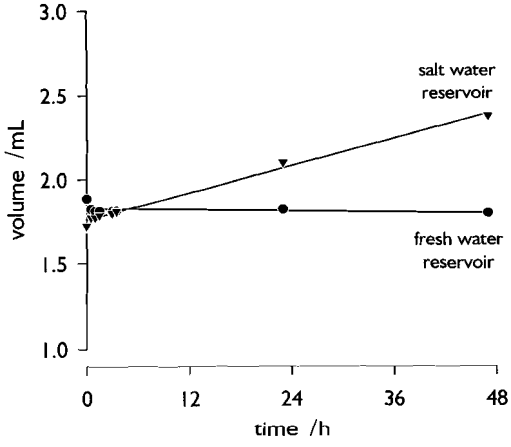

Figure 4.8
Water transport in the AWy–D experiment; there is transport of water into both reservoirs which is not consistent with chemical osmosis.

surface area. If σ is plotted as a function of the distance from the clay platelet for the conditions in the AWy–A and AWy–B experiment using the Kemper–Bresler model (Figure 4.10), one observes that the salt sieving effect at a distance from the particle surface above 40 to $50 \cdot 10^{-10}$ m is negligible. The waterfilm thickness in AWy–A calculated using Eq. 4.1, is $142 \cdot 10^{-10}$ m and for AWy–B $164 \cdot 10^{-10}$ m, therefore a large part of the water film does not contribute to the salt sieving effect. Consequently, the reflection coefficient for these samples is negligible (Table 4.3). Another requirement for a clay to exhibit diffusion osmosis, a high porosity of the sample (Olsen *et al.*, 1990), was also met.

Highly compacted bentonites: AWy–C and AWy–D

The development of the AWy–C experiment (Figure 4.7) can also be explained by the non–ideality of bentonite as a semipermeable membrane. In the first ten days water is mainly transported by chemical osmosis causing Δp to decrease. During the same period diffusion of ions across the sample also occurs because the clay as a non–ideal membrane is not capable of completely restricting the diffusion of salt. As a result the salt concentration in the fresh water reservoir increases (Figure 4.7), decreasing the osmotic gradient and thus reducing the osmotic water flux. The diffusion also causes shrinkage of the double layer of the clay platelets, enhancing flocculation and making the clay more permeable. The second period in the experiment, after day ten, is characterised by the slow dissipation of the induced pressure difference by water transport as a result of the hydraulic gradient. Because the porosity as well as the equilibrium concentration are lower than in the AWy–A and AWy–B experiment, diffusion osmosis did not occur in this sample.

The water transport observed in AWy–D (Figure 4.7) is neither the result of chemical osmosis nor of diffusion osmosis. The volume increase in the salt water reservoir does not coincide with a similar decrease in the fresh water reservoir indicating that water is flowing from the fresh to the salt water side, as was observed for AWy–A (Figure 4.4). The observed volume increase in the salt water reservoir can be attributed to leakage either in the rubber 'sleeve' in which the sample is fitted in the experimental apparatus, or at the point were the stainless steel capillaries are fitted into the Serto® connectors on the top cap (Photo 3.2, p. 44). This connection is welded but showed small fractures upon inspection, presumably caused by repeated use. The presence of these fractures can result in leakage of water from the cell into the reservoirs causing the hydraulic head in the reservoirs to increase.

In all experiments the Ec in the fresh water reservoir at the beginning of the experiment is unexpectedly high and then drops sharply. After several hours the Ec

slowly starts rising. This high initial value and the subsequent drop can be explained by the experimental procedures followed. After measuring the hydraulic conductivity the reservoirs were filled with the NaCl solution. It took about two days before both reservoirs were de–aired, filled with the NaCl solution and homogenised. The reservoirs were not filled simultaneously but one by one. With both reservoirs filled generally an extra hour was required to return to and stabilise the bench top chamber at 25.0 ± 0.2°C. Solute diffusion already occurred during the filling of the reservoirs, increasing the salt concentration in the porous stone at the fresh water side. At time o the reservoirs were opened and measurement of chemically induced water transport

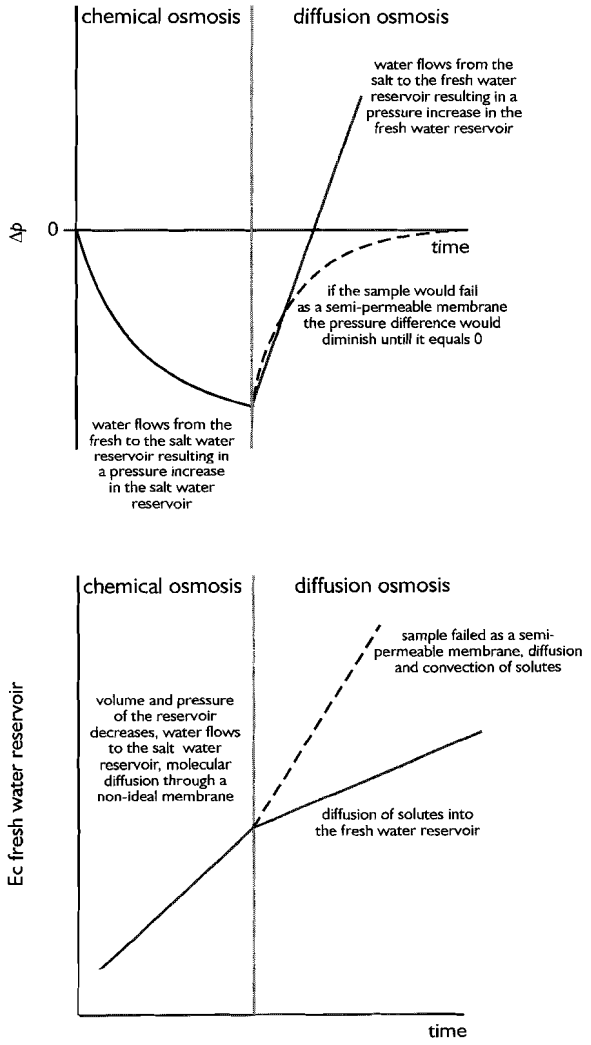

Figure 4.9
Schematic representation of the observed (——) changes in Δp and the electrical conductivity in the fresh water reservoir for the experiments and their interpretation, and the expected signal (– – – –) if the sample would fail as a semipermeable membrane (after Keijzer *et al.*, 1999).

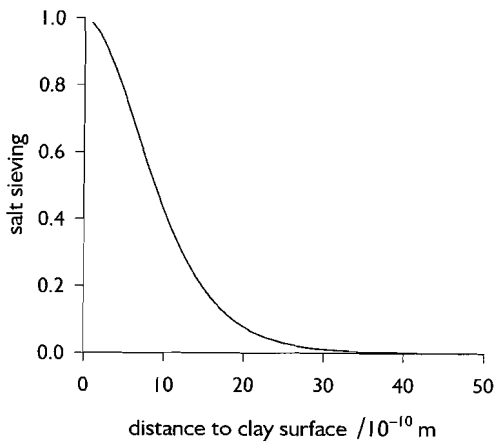

Figure 4.10
Salt sieving as a function of the distance from a clay surface according to the Kemper–Bresler model. The curve is calculated for the AWy bentonite at an equilibrium solution of 0.35 mol·L^{-1} NaCl.

started. Concurrently, the pumps started flushing the reservoir solutions through the porous stones homogenising the now more saline solution in the porous stones with the bulk solution. Therefore, the first measurements yield high values as the saltier solution from the porous stones flowed through the conductivity cell. The initial high value dissipates through homogenisation. The slow rise afterwards is the result of diffusion.

Comparison between modeled and experimentally obtained reflection coefficients

The experimental values for σ obtained by the two different methods are in good agreement (Table 4.3). The experimental values are, however, considerable lower than the theoretical values for σ as predicted by the models (Table 4.2). The Groenevelt–Bolt model yields the best agreement with the experimental values, whereas the FMMM predicts higher, and the Kemper–Bresler model lower values of σ. To decide whether this trend is limited to our samples or generally applicable to the semipermeability of bentonites a literature review was conducted (Table 4.4).

In the older literature on (reverse) osmosis it was customary to express the semipermeability as the filtration efficiency E (%), derived from the Teorell–Meyer–Siever model (TMS – e.g. Kharaka & Berry, 1973):

$$E = \frac{c_i - c_e}{c_i} 100 \tag{4.5}$$

where c_i is the concentration of the solution at the high pressure input side, and c_e is

the concentration at the low pressure effluent side at steady–state. However, to enable comparison between the older, reported E–values and the reflection coefficient a σ for these studies, based on the published data, was calculated using:

$$\sigma = \frac{c_i - c_e}{c_i + c_e} \tag{4.6}$$

Fritz and Marine (1983) derived Eq. 4.6 assuming a very small value for ω in compacted clay membranes and observed good agreement between calculated and experimantally derived values. Reflection coefficients obtained by Eq. 4.6 are lower than those obtained using Eq. 4.5. Already Kharaka and Berry (1973) observed that Eq. 4.5 tends to overestimate the semipermeability of the samples under investigation. They concluded that the TMS is useful in indicating the trends but is inadequate for the prediction of the semipermeability of natural systems. Additionally, for all the studies listed in Table 4.4 the reflection coefficient was also calculated using Eq 1.12 (p. 14) and listed as σ_{FMMM}. Values of σ were also calculated using the Kemper–Bresler (Eq. 1.18, p. 17) and Groenevelt–Bolt models (Eq. 1.20, p. 19) and incorporated in Table 4.4 as σ_{KB} and σ_{GB} respectively.

Most authors mention the CEC and the porosity of their samples, but the value of the surface area (A_s) is often omitted. The A_s was estimated based on literature values to be either 85 or 750 $m^2 \cdot g^{-1}$ (Mitchell, 1993) based on the information of the author about the pretreatment of the sample. Samples with minor pretreatment were given the low, or primary A_s–value, whereas samples with extensive pretreatment were given the higher, secondary A_s–value. Experiments were omitted when two out of the four crucial parameters to predict the σ–values —CEC, A_s, porosity or c_0— were missing.

From Table 4.4 it is clear that none of the models predicts the σ for all the observed reflection coefficients correctly. Generally, all models overestimate the semipermeability with respect to the measured values at small equilibrium concentrations. This is clearly shown for the experiments by McKelvey and Milne (1964) with porosities of 39 % and 41 %, and for the samples of Kemper and Rollins (1966) and Kemper and Quirk (1972) with very high porosities. In this respect the porosity is of minor importance whenever c_0 is low. The opposite can also be seen, the models overestimate σ when the sample has a low porosity at high values of c_0. For example, both the FMMM and Groenevelt–Bolt model overestimate σ for the samples of Benzel and Graf (1984) at 31 % porosity. None of the models performs better than the other in the range of moderate porosities (40–60 %) and moderate concentrations (0.1–1 $mol \cdot L^{-1}$). A comparison of σ for the AWy bentonite as a function of the

equilibrium concentration and porosity for all three models is given in Figure 4.11. From this figure and Table 4.4 it can be tentatively concluded that at the higher porosities the FMMM and Groenevelt–Bolt model overestimate σ, whereas the Kemper–Bresler model underestimates the reflection coefficient. This observation is consistent with the measurements on the AWy bentonites.

There are some other observations which draw attention. Of the experimental, data those by Hanshaw and Coplen (1973) and Fritz and Marine (1983) are closely matched by all models. There are also a few studies in which the experimental σ is higher than all model–derived values, for instance the studies by Kemper (1961), Benzel and Graf (1984) and Haydon and Graf (1986). For the Kemper (1961) study the values of σ were derived from his Figure 2 where pressure buildup is plotted against the experimental time. Deriving σ–values from this figure can result in a large error. For the discrepancy in the study of Graf and co–workers, no readily available explanation could be found. The most prominent difference between data and model predictions is seen in the study by Kemper (Kemper & Rollins, 1966; Kemper & Quirk, 1972). All three models overestimate the measured reflection coefficient, even the Kemper–Bresler model. The large variation in predicted σ–values and the differences between studies suggest that there are two major reasons why calculated values deviate from experimental values. Firstly, the assumptions made in the different models do not hold, or are only partially valid for the experiments. Secondly, there are experimental factors affecting the value of σ.

Model assumptions

The FMMM was supported on a laboratory scale by hyperfiltration experiments on bentonite, and on a field scale by using the model in predicting anomalous hydraulic heads in the Dunbarton Triassic Basin, US (Marine & Fritz, 1981). The authors found a good correspondence between the experimental and theoretical σ's even for porosities of the bentonite around 0.5. However, there is a fundamental difference between a hyperfiltration experiment and the direct measurement of the water transport as used in this study. In a typical hyperfiltration experiment the saline solution is forced through the clay membrane against the osmotic gradient (Figure 1.3, p. 10) and the force to be overcome is the osmotic pressure difference between the two solutions. Subsequently, the ideality of the sample is derived. In a hyperfiltration experiment the sample is generally confined in a rigid wall permeameter and subjected to a vertical overburden pressure to ensure good contact with the wall. The hyperfiltration experiment is relatively fast which made it popular in research of osmotic phenomena (see Table 4.4, studies marked with RO). However, since in hyperfiltration σ is determined in a relatively short contact time between the sample

Table 4.4 Reflection coefficients calculated using the FMMM (σ_{FMMM}), Kemper–Bresler (σ_{KB}) and Groenevelt–Bolt (σ_{GB}) model for published experimental work (continued on next page, legend see p. 76)

study		CEC	A_s	n	c_0	measured σ	σ_{FMMM}	σ_{KB}	σ_{GB}
		$cmol_c \cdot kg^{-1}$	$m^2 \cdot g^{-1}$	%	$mol \cdot L^{-1}$ NaCl				
Kemper (1961)	O	94	750[1)]	39	2.65	0.37	0.06	0.19	0.26
					2.65	0.25	0.06	0.19	0.26
McKelvey & Milne (1964)[A]	RO	88	750[1)]	34	1.295	0.27	0.43	0.41	–[2)]
				34	1.715	0.46	0.32	0.34	0.41
				34	2.405	0.46	0.21	0.25	0.30
				39	0.101	0.54	0.93	0.90	–
				41	0.092	0.79	0.94	0.90	–
Kemper & Rollins (1966)	O	80	720	80	0.002	0.98	0.99	0.97	–
					0.006	0.77	0.97	0.91	–
					0.020	0.42	0.90	0.74	0.86
					0.060	0.10	0.71	0.44	0.66
					0.200	0.01	0.26	0.11	0.34
	O	80	720	84	0.002	0.76	0.99	0.96	–
					0.006	0.54	0.96	0.86	–
					0.020	0.28	0.87	0.62	0.79
					0.060	0.07	0.63	0.29	0.55
					0.200	0.01	0.15	0.04	0.24
	O	80	720	91	0.002	0.66	0.98	0.86	–
					0.006	0.36	0.93	0.62	0.80
					0.020	0.13	0.76	0.26	0.54
					0.060	0.01	0.37	0.04	0.27
					0.200	0.01	0.003	0.001	0.08

study		CEC	A_s	n	c_0	measured σ	σ_{FMMM}	σ_{KB}	σ_{GB}
		$cmol_c \cdot kg^{-1}$	$m^2 \cdot g^{-1}$	%	$mol \cdot L^{-1}$ NaCl				
Kemper & Quirk (1972)	O	80	720	84	0.002	0.75	0.99	0.96	–
					0.006	0.50	0.96	0.86	–
					0.020	0.25	0.87	0.62	0.79
					0.060	0.03	0.63	0.29	0.55
					0.200	0.003	0.15	0.04	0.24
Kemper & Quirk (1972)	O	80	720	91	0.002	0.20	0.98	0.86	–
					0.006	0.08	0.93	0.62	0.80
					0.020	0.01	0.76	0.26	0.54
					0.060	0.001	0.37	0.04	0.27
Hanshaw & Coplen (1973)[A,B]	RO	60	750[1)]	36	0.001	0.98	0.99	0.99	–
				36	0.007	0.98	0.99	0.99	–
				36	0.046	0.92	0.96	0.93	–
				36	0.111	0.99	0.90	0.86	–
Fritz & Marine (1983)	RO	98	750[1)]	41	0.111	0.84	0.92	0.89	–
				41	0.467	0.79	0.68	0.64	–
				41	1.343	0.30	0.28	0.34	0.46
				59	0.080	0.87	0.88	0.81	–
				59	0.239	0.61	0.66	0.56	0.72
				59	0.981	0.04	0.11	0.15	0.33
Benzel & Graf (1984)[A]	RO	128	750[1)]	31[3)]	0.416	0.52	0.87	0.41	–
				31[3)]	0.546	0.46	0.82	0.33	–
				55[4)]	0.746	0.27	0.40	0.02	0.53
				71[4)]	0.771	0.21	0.11	0.06	0.26

(continued on next page, legend see p. 76)

Table 4.4 continued

study		CEC	A_s	n	c_0	measured σ	σ_{FMMM}	σ_{KB}	σ_{GB}
		$cmol_c \cdot kg^{-1}$	$m^2 \cdot g^{-1}$	%	$mol \cdot L^{-1}$ NaCl				
Haydon & Graf (1986)[A]	RO	128	750[1)]	71[5)]	4.410	0.14	–0.02	>0.001	0.03
Demir (1988)	RO	128	750[1)]	68	0.544	0.17	0.30	0.17	0.40
this study	O	68	47	56	0.055	0.03	0.90	0.002	0.12
				64	0.350	0.003	0.27	>0.001	0.01
				67	0.350	>0.001	0.21	>0.001	0.01

RO reverse osmosis, hyperfiltration experiment

O direct measurement

A expressed according the definition given by Fritz and Marine (1983), Eq. 4.6

B reports the same experiments and results as Hanshaw (1962)

1) estimated value, see text

2) model not applicable as the value of $\kappa_0 d_f < 1$

3) samples with orientated fabric

4) samples with random fabric

5) experiment conducted at 20°C

and the salt solution, salt diffusion is minimised. During the longer contact time in the present experiments diffusion of salt occurs through the matrix of the sample (Figures 4.5, 4.6 & 4.7), causing the clay to flocculate, making it more permeable for the salt as the salt sieving effect is reduced. As the experiment progresses, the diffusion front extends further into the clay reducing the overall σ of the sample. Thus σ will decrease during the experiment. As most of the work on membrane behaviour in the past is done with hyperfiltration or reverse osmosis experiments, change in the semipermeability of the samples is avoided and therefore not incorporated in the theoretical framework for the prediction of σ. That the reflection coefficient is not an intrinsic value for a given sample or geological membrane was first recognised by Whitworth and Fritz (1994).

The models are based on additional assumptions that do not apply to the experimental conditions. A completely dispersed monomineral sample is assumed, with an exchange complex completely occupied by one monovalent cation. Some of these assumptions are clearly stated in the derivation of the model framework, others are less clearly defined or assumed to be logical. The FMMM assumes a monomineral semipermeable clay membrane completely occupied by sodium. This assumption follows implicitly from the frictional coefficients, which are only calculated for the $NaCl+H_2O$ system (e.g. Fritz, 1986). The influence of other cations on double layer thickness, and thus on the salt sieving capabilities of the samples are neglected. Because no pretreatment was given to our AWy–samples, its CEC was substantially occupied by Ca^{2+} during the experiments, which reduces the double layer thickness and makes the samples less ideal.

Complete dispersion of the clay particles did not exist in our experiments. Because complete dispersion is usually absent, Mitchell (1993, p. 259) considers the assumption by Bresler (1973) that the water film is evenly distributed over the full surface area invalid, and argues that the σ's derived from Breslers Figure 1 should be treated as upper bounds. Bolt (1982b, p. 406), on the other hand, argues that particularly for larger values of $\kappa_0 d_l$, the Kemper–Bresler model underestimates the salt sieving effect. The difference between the Kemper–Bresler and Groenvelt–Bolt models is obvious for samples with moderate and high porosities (Figure 4.11). Recalculation of the value for σ using the total A_s confirms that complete dispersion in our samples is absent. According to Bolt (1982b) the specific surface area needed to calculate the $\kappa_0\delta$ should be the total A_s as determined by the EGME–method (Churchman *et al.*, 1991; Feller *et al.*, 1992). When using the total A_s for the samples (Table 2.1, p. 28) the model results in a σ for AWy–A of 0.43, for AWy–B of 0.37, for Awy–C of 0.90 and finally for AWy–D of 0.91. Values which correspond more closely with values calculated with the FMMM (Table 4.2). The Kemper–Bresler

model, which also assumes complete dispersion, yields σ–values of 0.20, 0.22, 0.83 and 0.82 respectively for the AWy samples when using the total A_s. The values calculated with the Kemper–Bresler and Groenevelt–Bolt model in Table 4.2 were, however, found using the external A_s, which was determined with the N_2–BET method (Aylmore *et al.*, 1970). The external A_s is the surface area of assemblies of surfaces such as aggregates of stacked clay and other silicate minerals, whereas the total A_s includes also the internal surfaces between the clay platelets (Aylmore *et al.*, 1970; Churchman & Burke, 1991; Churchman *et al.*, 1991). The external A_s is a more realistic value to use because our samples were not thoroughly dispersed prior to use and most certainly contained small aggregates of clay minerals. The absence of complete dispersion of the clays in some of the studies listed in Table 4.4 may also be responsible for the observed differences between the measured and theoretical σ–values.

Experimental factors

As was observed in Table 4.4, the data provided by Kemper (Kemper & Rollins, 1966; Kemper & Quirk, 1972) are overestimated by all three models, even by the

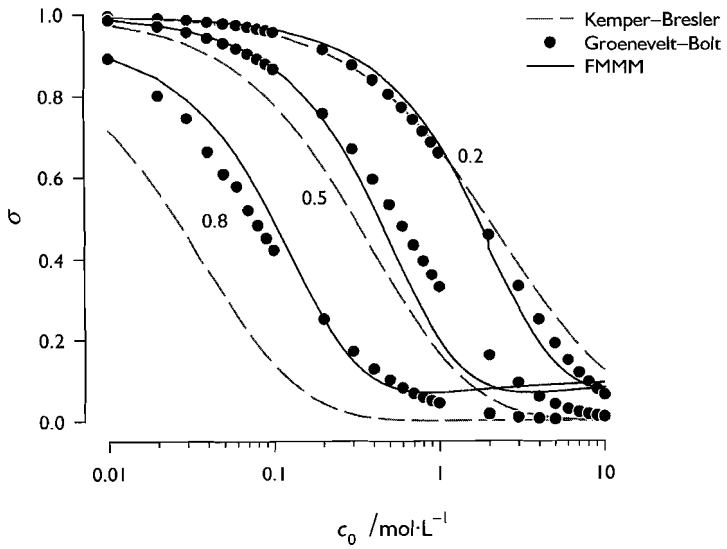

Figure 4.11 The reflection coefficient as a function of the equilibrium concentration for different porosities according the FMMM, the Kemper–Bresler and Groenevelt–Bolt models. Curves were calculated for AWy at porosities of 0.2, 0.5 and 0.8 with a CEC of 68 $cmol_c \cdot kg^{-1}$ and an A_s of 556 $m^2 \cdot g^{-1}$.

Kemper–Bresler model. Kemper and Rollins (1966) argued that their experimental values were lower than their theoretical values as a result of the design of the apparatus used (see Figure 3.1, p. 38). According to the authors the salt concentration in the porous stainless steel plate, which enclosed the sample at the fresh water side, was higher than the bulk solution because of diffusion. This caused a smaller concentration gradient than the one derived from the concentrations in the bulk solution. This type of problem is probably common to experimental apparatus that directly measure chemical osmosis. Our set up is not susceptible to this problem as a result of the chosen configuration of the pedestal and method employed for flushing the filter stone (Figure 4.12). Instead of the conventional concentric grooves with interconnecting grooves between the in- and outflow channel, we used only one concentric groove without interconnections. Moreover, the circulation was changed using the channel in the centre of the pedestal as the inlet of the solution. These changes improve circulation within the porous stone and prevent short circuiting between the in- and outflow. It also prevents the buildup of two separate water phases in the porous stone. One expects that through diffusion a saltier solution would accumulate in the porous stone at the fresh water side, whereas at the salt water side a stagnant fresh water film would form as a result of the osmotically driven water transport (Figure 4.12). Because the sample resides in a pressurised water chamber it is impossible to measure the salt concentration directly at the interface between the sample and the solution reservoirs. Therefore, the conductivity cells were mounted in the reservoirs and it was assumed that the concentration in the reservoir equals the concentration at the sample/reservoir interface. We relied on the instantaneous and thorough mixing of the water that exits the sample and the solution already present in the reservoirs. The formation of a fresh water film at the salt water side and that of a salt water film at the fresh water side are unfavourable as they reduce the concentration gradient across the sample. This results in a discrepancy between experimental and model–derived σ's because the latter are calculated on the basis of concentrations in the bulk solution.

The formation of water films of different composition does not occur in reverse osmosis experiment. In these experiments, however, it is crucial that the effluent concentration reaches a steady–state before calculating a filtration efficiency or reflection coefficient. Demir (1988) reports a period of more than 50 days before the concentration of the downstream solution in his hyperfiltration experiment reaches steady–state. The reflection coefficient drops from 0.57 at the beginning of the experiment to 0.17 at steady–state. From most of the publications listed in Table 4.4 it is impossible to determine whether the experiments did reach steady–state. The large difference between the theoretical and experimental values might suggest that in most of the experimental work steady–state may not have been achieved.

4.6 DIFFUSION AND CATION EXCHANGE

In addition to chemical osmosis, NaCl–diffusion and cation exchange take place in our non–ideal samples. Gillham *et al.* (1984) indicated that diffusion is the dominant transport mechanism whenever the water flux is in the order of 10^{-10} m·s^{-1}. The measured water fluxes for the AWy–A and B bentonite are close to this threshold whereas the AWy–C has a flux well below this value, thus making diffusion dominant over salt convection.

The diffusion of a solute (J_s) in response to a concentration gradient is given by Fick's first law:

$$J_s = -D_0 \frac{dC}{dx} \tag{4.7}$$

where D_0 is the diffusion coefficient of the solute in the free solution and dC/dx is the concentration gradient across the sample. However, Eq. 4.7 has to be corrected for the tortuous pathway of the diffusing solute in natural samples by the

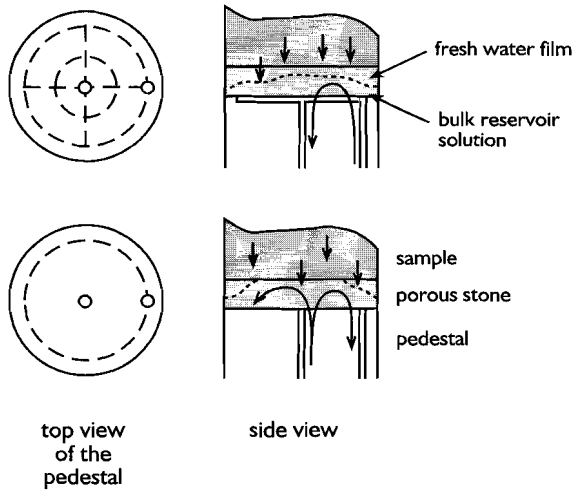

Figure 4.12 Experimental configuration at the sample/permeameter interface for the salt water reservoir; **top** conventional configuration of the pedestal with concentric grooves and the method of flushing which can result in a stagnant fresh water film in the porous stone, and **bottom** type of pedestal and flushing used in our experimental set–up to minimise the possibility of a stagnant fresh water film in the porous stone.

tortuosity factor τ (Chapter 1, p. 13) and for the volumetric water content θ (e.g. Shackelford & Daniel, 1991):

$$J_s = -\frac{D_0}{\tau}\theta\frac{dC}{dx} \tag{4.8}$$

There are additional effects which are not included in Eq. 4.8 that reduce the diffusion rate. Kemper *et al.* (1964) incorporated a factor α' to account for the increasing viscosity of the water directly adjacent to the surface of the clay particles. In addition, a factor γ was introduced by Kemper and Van Schaik (1966) to account for the anion exclusion properties which are exhibited by shales and clay rich materials. Adding these to Eq. 4.8 yields:

$$J_s = -\frac{D_0}{\tau}\theta\alpha'\gamma\frac{dC}{dx} \tag{4.9}$$

Because it is impossible to separate or independently measure the effects of viscosity, tortuosity and anion exclusion on diffusion, Shackelford and Daniel (1991) defined an apparent tortuosity factor τ_a:

$$\tau_a = \frac{1}{\tau}\theta\alpha'\gamma \tag{4.10}$$

In experimental studies the measured diffusion coefficients include all these effects and it is therefore convenient to define an apparent or effective diffusion coefficient, D^* in $m^2 \cdot s^{-1}$, which includes these effects and is related to the diffusion coefficient in free solution according to:

$$D^* = D_0\tau_a \tag{4.11}$$

Introducing the effective diffusion coefficient in Eq. 4.7 results in the often used version of Fick's first law:

$$J_s = -D^*\frac{dC}{dx} \tag{4.12}$$

From measured electrical conductivity values D^* can be calculated after converting the Ec to concentrations by the Marion–Babcock equation, which for a NaCl solution is (Sposito, 1989):

$$\log C = 1.159 + 1.009 \log \mathrm{Ec} \tag{4.13}$$

where C is the concentration in mmol·L^{-1} and Ec is the electrical conductivity in mS·cm^{-1}. Eq. 4.13 yields calculated concentrations close to the measured values in the fresh water reservoir before and after the osmosis experiment. Assuming steady–state for diffusion over the period in which chemical osmosis was observed, Fick's first law

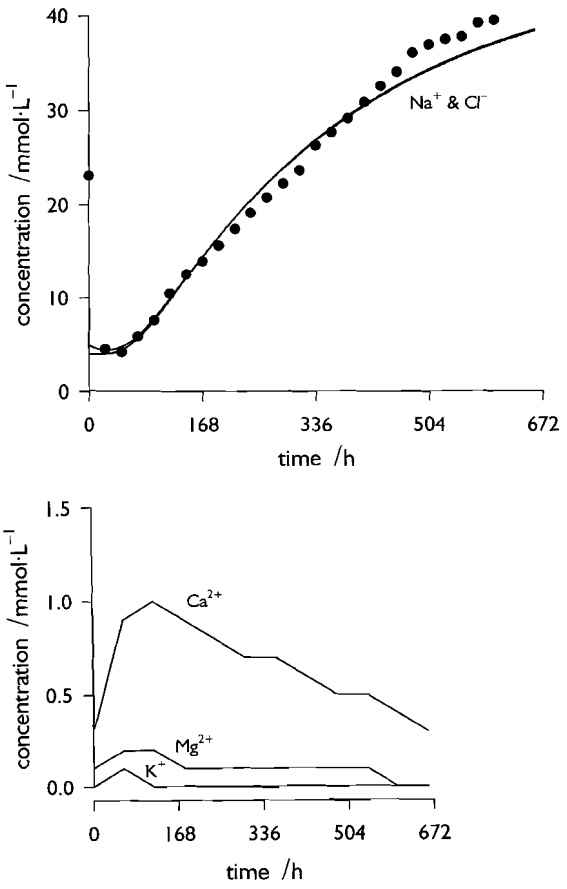

Figure 4.13 Observed concentration profile based on the electrical conductivity (•) and the modeled curve (———) in the fresh water reservoir; **top** for Na^+ and Cl^- using a diffusion coefficient of $1.9 \cdot 10^{-12}$ m^2·s^{-1} with cation exchange and no advective water transport, and **bottom** for the other cations present at the exchange complex.

can be rewritten as (Choi & Oscarson, 1996):

$$D^{\star} = -J_s \Big/ \frac{dC}{dx} = -\frac{\Delta Q_s}{A\,\Delta t} \Big/ \frac{\Delta C}{\Delta x} \tag{4.14}$$

where ΔQ_s is the amount of solute diffusing in $mol \cdot s^{-1}$ through the sample in an increment of time (Δt) in s, A is the cross sectional area of the sample in m^2, ΔC is the concentration difference between the ends of the sample in $mol \cdot L^{-1}$ and Δx is the thickness of the sample in m. The use of Eq. 4.14 implicitly assumes a linear diffusant concentration distribution through the sample. The use of Eq. 4.14 for the AWy samples for the period in which chemical osmosis was observed yields values for $D^{\star}_{NaCl}$ between $0.25 \cdot 10^{-12}$ and $0.65 \cdot 10^{-12}$ $m^2 \cdot s^{-1}$. These values are considerably lower than $D^{\star}_{NaCl}$–values reported in the literature (typically $0.15 \cdot 10^{-9}$ $m^2 \cdot s^{-1}$ – e.g. Li & Gregory, 1974; Shackelford, 1991). These low values are the result of the integral tortuosity factor (Eq. 4.10), the retardation of diffusion by cation exchange, the osmotic counterflow and the absence of linearity of the concentration distribution.

Modelling diffusion with cation exchange

In order to exclude the steady–state assumption, and to explicitly specify cation exchange, the diffusion can be assessed by modelling the observed concentration with a transient transport model, neglecting convective fluxes. This was only done for the experiment on the AWy–C bentonite. The diffusion was modelled using PHREEQC version 2 (Parkhurst, 1995). The program is not capable of modelling a double reservoir type diffusion experiment with finite column length and variable concentrations in both reservoirs. Therefore, a semi–infinite 1–D column was modelled in PHREEQC with a constant concentration of 90 $mmol \cdot L^{-1}$ NaCl at the top end of the column. The concentration of the solution at a distance equal to the thickness of the sample was computed. The modeled and observed data curves were manually fitted by adjusting the diffusion coefficient (Figure 4.13); resulting in a value of $1.9 \cdot 10^{-12}$ $m^2 \cdot s^{-1}$ for $D^{\star}$. A value of $0.25 \cdot 10^{-12}$ $m^2 \cdot s^{-1}$ was derived using Fick's first law (Eq. 4.14). The difference between the two values can be explained by the retardation caused by cation exchange. The modelled amount of Ca^{2+} coming from the sample as the result of the exchange process is small, as it is for the other cation concentrations (Figure 4.13). These Ca^{2+} values are close to the total concentration of 0.8 $mmol \cdot L^{-1}$ measured for Ca^{2+} at the end of the osmosis experiment. The other cations were not detected in the solutions.

4.7 CONCLUDING REMARKS

Chemical osmosis was observed in three Wyoming bentonite samples when subjected to a salt concentration gradient. In the less compacted samples which were subjected to the highest concentration gradient chemical osmosis gave rise to diffusion osmosis. Diffusion osmosis is transport of water by drag in response to diffusion of solutes. In the more compacted bentonite with a relatively low concentration gradient this phenomenon was not observed.

For all experiments the measured values of the reflection coefficient were considerably lower than those calculated with three different theoretical models: the Fritz Marine Membrane Model (Fritz, 1986), a model postulated by Kemper (1972) and Bresler (1973) and a model by Groenevelt and Bolt (Bolt, 1982b). A literature survey on the semipermeability of bentonites revealed that differences between experimental and theoretical values is not limited to this study. Two major causes for the difference are given: firstly, the model assumptions do not hold for the samples investigated, and secondly the concentrations measured in the bulk reservoirs during the experiment may deviate from those at the sample interface. The limitations of the models are discussed and it is concluded that several model assumptions, like a complete dispersion of the clay and the occupation of the exchange complex by a monovalent cation, do not hold for our samples and experimental conditions. To assess the influence chemical osmosis has on diffusion and cation exchange for the compact bentonite a semi-infinite 1–D column was modelled using PHREEQC. The observed data could be fitted using a diffusion coefficient of NaCl between 10^{-12} and 10^{-13} $m^2 \cdot s^{-1}$. This low value results from the combined effect of increased tortuosity due to semipermeability of the bentonite, retardation by cation exchange and osmotic counterflow.

The experiments on the AWy–A and AWy–B samples were published as: Keijzer ThJS, Kleingeld PJ & Loch JPG (1999). Chemical osmosis in compacted clayey material and the prediction of water transport. *Engineering Geology* **53**, p. 151–159. The experiment on the AWy–C sample was presented together with the experiments on the harbour sludge as: Loch JPG & Keijzer ThJS (1999), Chemical osmosis in dredging sludge, at the 91th Annual Meeting of the Soil Science Society of America, Salt Lake City, USA, p. 339. A more extended manuscript is submitted for publication in the *Journal of the Soil Science Society of America*.

5 Chemical osmosis in unconsolidated harbour sludge

5.1 INTRODUCTION

The ability of the harbour sludge from the *Beerkanaal* (BK) and the *Beneden Merwede* (BMR) to act as a semipermeable membrane was assessed by the same method as used for bentonite (Chapter 4). The values for σ were compared with those for other natural clayey materials available in the literature and with values calculated with the previously discussed models. These experiments also give insight in the potential of a sludge in depot to act as a semipermeable membrane and in the relative importance of osmotic and hydraulic water transport.

5.2 EXPERIMENTAL CONDITIONS

Prior to the experiments the larger shell fragments were removed from the air–dried harbour sludge and the sample was gently crushed in a mortar to remove large aggregates. In order to obtain an easy to handle sample and to reduce the initial porosity, 5.0 g of sample was weighed into a stainless steel mold with an internal diameter of 50 mm. The sludge was then subjected to a compaction pressure gradually increasing to 20.3 MPa, and kept at that pressure for 30 minutes, resulting in a sample with an approximate thickness of 2 mm. Subsequently, the sample was mounted in the cell between the porous stones and filters, after which a rubber 'sleeve' was placed over the sample and it was saturated with de–aired tap water. The porous stone and filter at the bottom end of the sample were water saturated prior to assembly to remove air. The stone and filter at the top end of the sample were not water saturated to enable the escape of trapped air from the sample during saturation. After saturation all tubing to and from the sample was flushed. The hydraulic conductivity of the sample was measured at saturation prior to the osmotic experiment using a falling head permeability test (Chapter 3). Under identical conditions the sample was subjected to

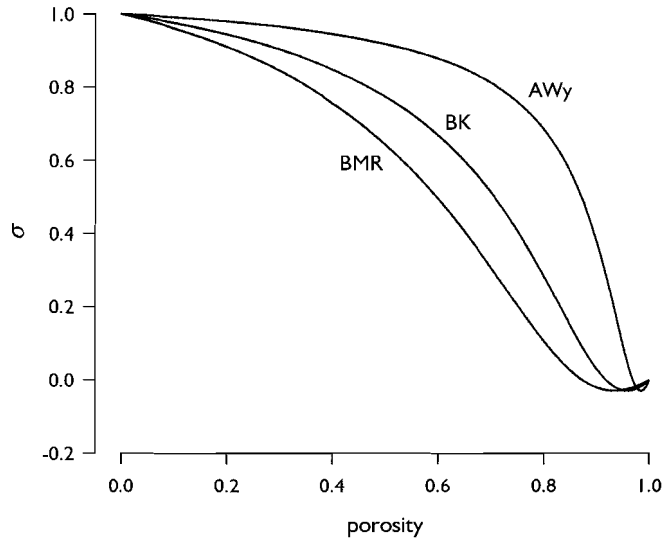

Figure 5.1 The reflection coefficient, σ, as a function of the porosity according to the FMMM for the harbour sludges; the curve for the AWy–C bentonite is given for comparison. All curves were calculated for a mean NaCl concentration of 0.055 mol·L^{-1}.

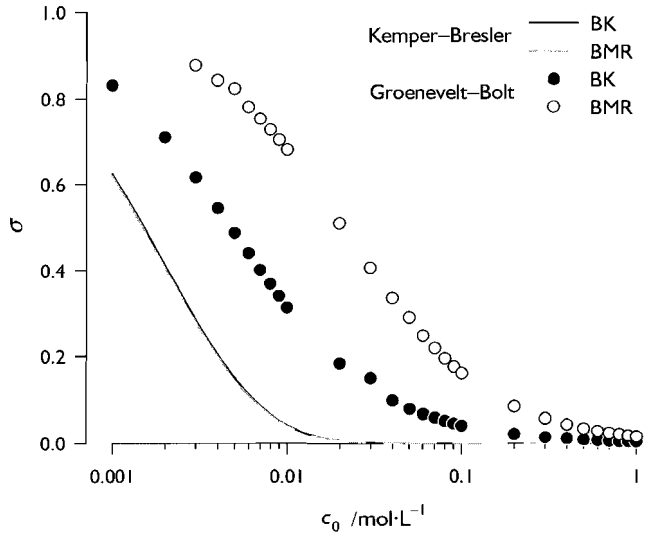

Figure 5.2 The reflection coefficient, σ, for the BK and BMR sludges as a function of the equilibrium concentration, c_0, according the Kemper–Bresler and Groenevelt–Bolt model. For the BK sludge a porosity of 0.51, a CEC of 24.2 cmol$_c$·kg^{-1} and an A_s of 30 m^2·g^{-1} was taken. For BMR these values were 0.34, 14.9 and 32 respectively.

a chemical gradient. The fresh water reservoir was filled with a 0.01 $mol \cdot L^{-1}$ NaCl solution and the salt water reservoir with a 0.1 $mol \cdot L^{-1}$ NaCl solution, corresponding to an osmotic pressure difference of 421.5 kPa or 43.0 m H_2O at 25°C (Eq. 1.4, p. 9). The chemical osmosis experiments were repeated once on the same compacted sample. Between the two experiments the samples were resaturated with de-aired tap water.

5.3 MODEL PREDICTIONS OF THE REFLECTION COEFFICIENT

The theoretical reflection coefficient of the samples was estimated using the FMMM, the Kemper–Bresler and Groenevelt–Bolt models as described in Chapter 4.

In Figure 5.1 the reflection coefficient is plotted according to the FMMM as a function of the porosity for both sludges at the experimental mean concentration of 0.055 $mol \cdot L^{-1}$ NaCl and compared to AWy–C bentonite. The curves in Figure 5.1 were calculated using the BK and BMR properties (Table 2.2, p. 28) and experimental conditions (Table 5.1) using Eq. 1.12 (p. 14). As in the case of the bentonites, the value for the frictional coefficient R_{WIII} was adjusted over the porosity range to reflect the increase in frictional resistance as the porosity of the membrane decreases. Because the porosities of the sludges during the experiment are known, σ can be derived from the curves (Table 5.2).

Table 5.1 Measured properties and conditions for the harbour sludge samples.

	BK–A	BK–B	BMR–A	BMR–B	
sample thickness	2.29 ± 0.10	2.29 ± 0.10	1.58 ± 0.04	1.58 ± 0.04	10^{-3} m
sample diameter	50.0 ± 0.2	50.0 ± 0.2	49.8 ± 0.2	49.8 ± 0.2	10^{-3} m
porosity after saturation	0.51	0.51	0.34	0.34	
hydraulic conductivity	5.2 ± 1.6	5.2 ± 1.6	21 ± 4	21 ± 4	10^{-12} m·s^{-1}
low concentration	0.01	0.01	0.01	0.01	mol·L^{-1} NaCl
high concentration	0.1	0.1	0.1	0.1	mol·L^{-1} NaCl
average equilibrium concentration	0.055	0.055	0.055	0.055	mol·L^{-1}
osmotic pressure	421	421	421	421	kPa
osmotic gradient	$14.8 \cdot 10^3$	$14.8 \cdot 10^3$	$27.2 \cdot 10^3$	$27.2 \cdot 10^3$	
cell pressure	491.1 ± 4.3	490.0 ± 3.8	479.3 ± 3.8	477.6 ± 4.0	kPa
temperature	25.0 ± 0.2	25.0 ± 0.2	25.0 ± 0.2	25.0 ± 0.2	°C

To obtain values for σ from the model by Groenevelt–Bolt, σ is plotted against the reduced mobile double layer thickness, $\kappa_0 d_l$, for the $\kappa_0\delta$ –value of the given sample using Eq. 1.20 (p. 19) and the formulae provided in Chapter 1. Additionally, a reflection coefficient was determined from the Kemper–Bresler model using the scheme described in Chapter 4. The reflection coefficients were plotted against the equilibrium concentration c_0 for the Groenevelt–Bolt and Kemper–Bresler models (Figure 5.2). All obtained theoretical values for σ are listed in Table 5.2.

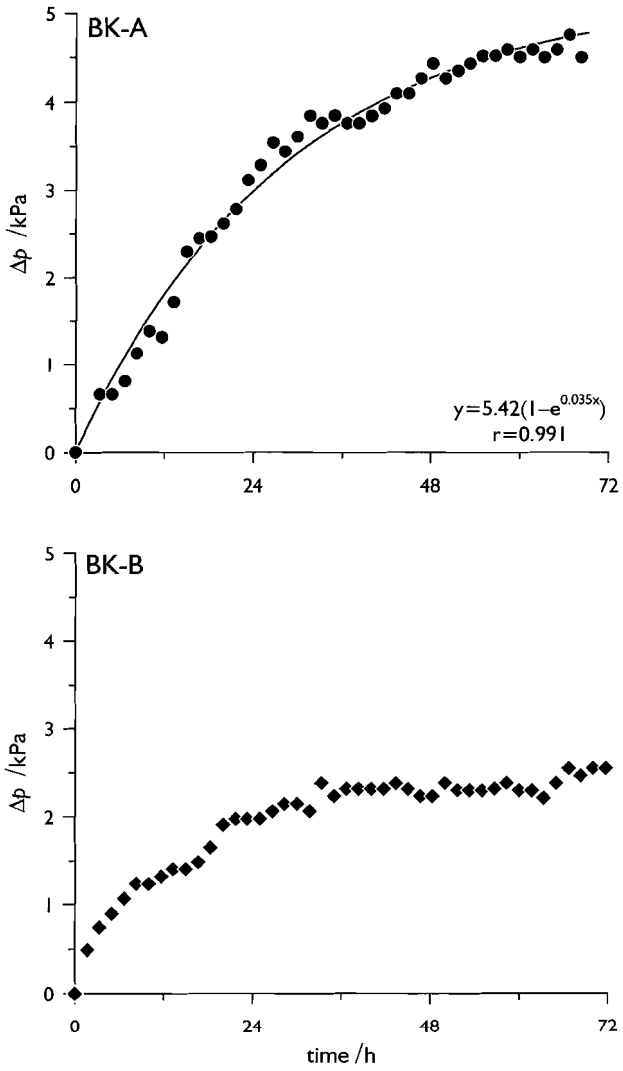

Figure 5.3
The development of a differential pressure, defined as $\Delta p = p_{salt} - p_{fresh}$, as a result of chemical osmosis with closed reservoir; **top** for the BK–A sample where also the best fit is shown, and **bottom** for the BK–B sample.

5.4 RESULTS

Sample preparation and hydraulic conductivity

After saturation the BK sample had a porosity close to 0.5, whereas the porosity obtained for the BMR sample was low, 0.34 (Table 5.1). The porosity of the BK sample is comparable with that of naturally occurring clays under near surface conditions, which lies typically around 0.5.

The hydraulic conductivity (Table 5.1) measured for both harbour sludges is between 10^{-11} and 10^{-12} $m \cdot s^{-1}$ and is representative for compacted soils with a high clay content (Benson & Trast, 1995). It is probably significantly lower than that of sludge in depot in its consolidation phase.

Chemical osmosis

In the two experiments conducted on the BK sludge an increase in differential pressure defined as $\Delta p = p_{salt} - p_{fresh}$, between the two reservoirs was observed (Figure 5.3). The Δp as defined yields positive values as water flows from the fresh water reservoir into the salt water reservoir by osmosis (Figure 5.4). The experimental reflection coefficient for these experiments in duplicate can be calculated from the experimental data in two different ways as was discussed in Chapter 4. Values are given in Table 5.3.

In the BMR–A experiment no water transport was observed. In the BMR–B water transport was observed but it is not consistent with osmotically induced water transport (Figure 5.5).

5.5 DISCUSSION

Chemical osmosis

The development of the differential pressure during the two experiments on the BK (Figure 5.3) is almost instantaneous. Figure 5.3 also shows that the experimental duration of 72 h was too short for the BK–A sample to reach equilibrium. The experiment had to be terminated prematurely because after 72 h the water level in the standpipe in the fresh water reservoir dropped below the readout. The BK–B, on the other hand, reached equilibrium within 72 h. The development of the pressure after 72 h was not monitored but is expected to be similar as schematically given in

Table 5.2 Theoretical reflection coefficients for the two harbour sludges. The σ for the A and B sample of the sludge are the same because the experiments were run using the same sample.

		BK	BMR
theoretical σ according to	FMMM	0.756	0.812
	Groenevelt–Bolt	0.064	0.225
	Kemper–Bresler	0.0001	0.032

Table 5.3 Observed reflection coefficients for the harbour sludge samples. The σ based on the differential pressure is calculated with the maximum Δp-value obtained with the regression line for BK–A, and the average Δp between 48 and 72 hours for BK–B.

	BK–A	BK–B	BMR–A	BMR–B	
observed J_w	0.050 ± 0.021	0.022 ± 0.009	nd	nd	kPa
σ based on J_w	0.030 ± 0.013	0.008 ± 0.003	–	–	
observed Δp	5.24 ± 0.10	2.36 ± 0.11	nd	nd	$cm^3 \cdot h^{-1}$
σ based on Δp	0.022 ± 0.001	0.010 ± 0.001	–	–	

nd not detected

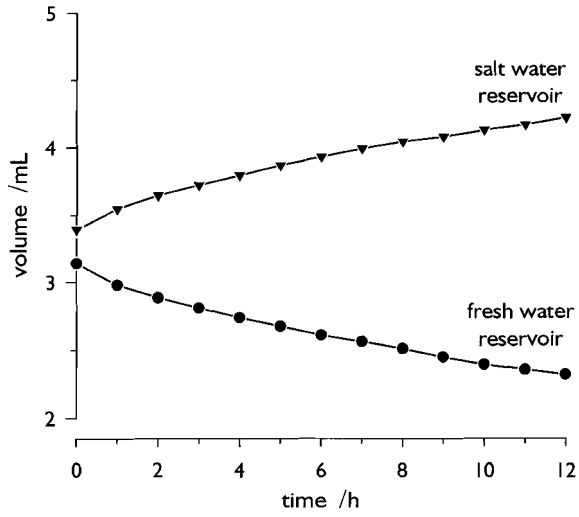

Figure 5.4
Observed volume changes in the calibrated standpipes of the fresh and salt water reservoir, showing the transport of water from the fresh to the salt water side of the BK–B sample as the result of the applied chemical gradient.

Figure 1.4 (p. 11). Because the BK–A sample did not reach equilibrium the value for the reflection coefficient calculated using Δp between 48 an 72 h in Table 5.3 is an underestimation of its semipermeability. Using an exponential best fit with the form $y = a(1-e^{-bx})$ a maximum value of 5.24 kPa is found ($r = 0.991$ – Figure 5.3). This value results in a σ of 0.022 which corresponds closely with the value derived from the observed water flux during the experiments (Table 5.3). In general, as in the AWy experiments the values for σ obtained by the two different methods yield values which are in good agreement. They are, however, again considerably lower than the theoretical values for σ as predicted by the models, except the values predicted with the Kemper–Bresler model.

The most striking contrast between theory and practice is found for the BMR sludge which did not show any semipermeable properties experimentally but for which high values of σ were predicted. The water transport observed in the BMR–B experiment (Figure 5.5) could be the result of chemical osmosis but as it differs from observed water transport in other experiments, for example in BK–B (Figure 5.4), it is not ascribed to chemical osmosis. That the experiments on BMR did not show chemical osmosis despite the low porosity can be attributed to the low clay content. Compared to the BK sample the sludge from the *Beneden Merwede*–river has a clay size fraction of 26% (Table 2.2). This amount was probably insufficient to result in a even distribution of clay throughout the sample, therefore, the more permeable or sandier parts of the sample may have facilitated short–circuiting of the water transport. A membrane can only be semipermeable when it is homogeneous in porosity. Additionally, the mix of clay minerals present in BMR is less likely to exhibit semipermeable properties due to the smaller amounts of smectite and larger fraction of illite (Table 2.3, p. 29).

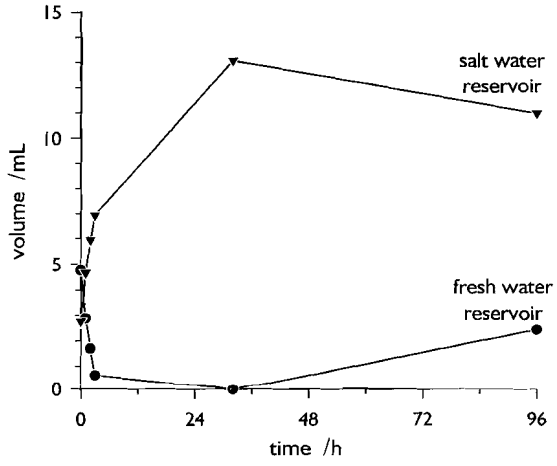

Figure 5.5
Observed volume changes in the calibrated standpipes of the fresh and salt water reservoir for the experiment on the BMR-B sample.

Table 5.4 Reflection coefficients calculated using the FMMM (σ_{FMMM}), Kemper-Bresler (σ_{KB}) and Groenevelt-Bolt (σ_{GB}) model for published experimental work on natural clayey material. Table continued on opposite page

study	sample		CEC	A_s	n
			$cmol_c \cdot kg^{-1}$	$m^2 \cdot g^{-1}$	%
Kemper (1961)	Pierre Shale, fine fraction	O	30.5	39.7[1)]	24
	Pierre Shale	O	18.0	39.7[1)]	21
Yearsley (1989)	Salton Sea, siltstone no. 2	O	10.0[2)]	65.0[2)]	6
	Salton Sea, sandstone no. 3	O	10.0	65.0	20
	Salton Sea, shale no. 4	O	10.0	65.0	3
	Salton Sea, shale no. 6	O	10.0	65.0	3
	Salton Sea, shale no. 6	O	10.0	65.0	3
Cey (1999)	Bearpaw Form. clay, 88 m	O	30.0[5)]	63.5[6)]	41
	Bearpaw Form. clay, 123 m	O	30.0	63.5	37
	Bearpaw Form. clay, 123 m	O	30.0	63.5	37
	Bearpaw Form. clay, 123 m	O	30.0	63.5	37
Neuzil (2000)	Pierre Shale, HC1	F	18.0[8)]	39.7	34
	Pierre Shale, HC2	F	18.0	39.7	34
this study	harbour sludge, BK	O	24.2	30.0	51
	harbour sludge, BMR	O	14.9	32.0	34

nd not detected.

O direct measurement.

F field experiment.

1) based on the data of the Pierre shale by Neuzil (2000).

2) based on the observation that illite and chlorite are the predominant clay minerals (Yearsley, 1989), lowest CEC and A_s–values used based on Mitchell (1993), p. 38–39.

3) derived from the data supplied total dissolved solutes in wt%, assuming NaCl as only solute

4) model not applicable as $\kappa_0 d_f < 1$.

5) derived from the data supplied in $g \cdot L^{-1}$, assuming NaCl as the only solute.

6) based on the data of the Pierre shale by Kemper (1961).

7) average of reported values.

8) based on Mitchell (1993), p. 38–39 and the reported mineralogy of the samples.

Table 5.4 continued

c_0 / mol·L^{-1} NaCl	measured σ	σ_{FMMM}	σ_{KB}	σ_{GB}	study
2.65	0.007	0.03	>0.001	0.02	Kemper (1961)
2.65	>0.001	0.02	>0.001	0.03	
0.13[3)]	≫0.001	0.92	0.88	–[4)]	Yearsley (1989)
3.25[3)]	>0.001	0.02	>0.001	0.03	
2.31[3)]	≫0.001	0.45	0.45	–	
1.05[3)]	≫0.001	0.72	0.65	–	
2.22[3)]	≫0.001	0.47	0.46	–	
0.096	0.27[7)]	0.79	0.22	0.31	Cey (1999)
0.21	0.031[7)]	0.63	0.079	0.21	
0.42	0.009[7)]	0.36	0.003	0.11	
0.84	0.004[7)]	0.10	>0.001	0.06	
0.086[7)]	0.093[7)]	0.76	0.03	0.26	Neuzil (2000)
0.082[7)]	0.069[7)]	0.78	0.04	0.27	
0.055	0.017[7)]	0.77	>0.001	0.06	this study
0.055	nd	0.81	0.03	0.23	

Semipermeability of natural clayey materials

For the harbour sludge BK semipermeability was expressed in the previous paragraph as a reflection coefficient. Measured values were observed to be lower than those derived from theoretical models. Shortcomings of these models were discussed in Chapter 4 and some of the model assumptions are certainly not applicable to the samples. Neither BK nor BMR are monomineral membranes as the clay size fraction consists of several clay minerals which include smectite, illite and kaolinite (Table 2.3). Additionally, the assumption of complete dispersion is invalid as the samples were not pretreated for that purpose: none of the organic material or carbonates were removed, and divalent cations were not removed from the exchange complex. Applying the total A_s (Table 2.2, p. 28) for the case of complete dispersion in the Kemper–Bresler and Groenevelt–Bolt models yields higher reflection coefficients that correspond more closely to those obtained with the FMMM. The values listed in Table 5.2 were calculated using the lower A_s from N_2–BET corresponding with the outer surface of mineral aggregates. Therefore, the difference between the observed and calculated values for σ are the result of model assumptions which are not applicable to the harbour sludge samples.

Nevertheless, the ability of the BK sludge to act as a non-ideal semipermeable membrane is an indication that natural sediments of high clay content can be subjected to osmotic water transport. This can have profound implications on the transport of contaminants from harbour sludge stored in depots like *De Slufter*.

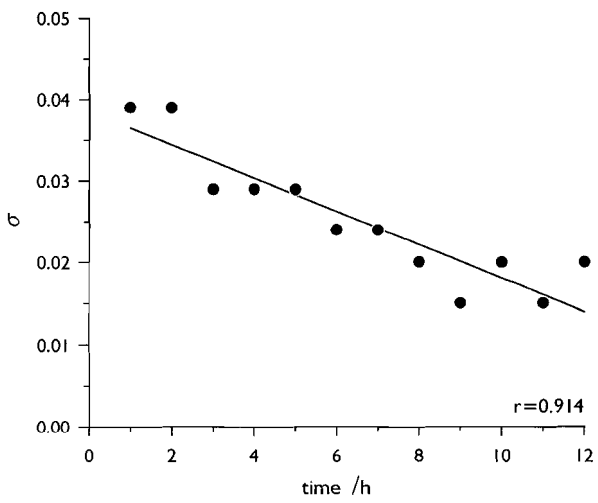

Figure 5.6
Deterioration of the reflection coefficient with the progression of time in the BK–B experiment.

The observed σ should be used with caution because it is not an intrinsic value of the material. It is dependent on several bulk properties as discussed in Chapter 1 which do change in time. Because natural clay layers are non–ideal membranes, diffusion renders the material more and more non–ideal, which is governed by the solute filtration coefficient ω. Whitworth and Fritz (1994) termed ω the 'death' coefficient as it determines the length of time that a natural clayey material can operate as a semipermeable membrane. Based on the water flux measured during the first twelve hours the deterioration of σ for the BK–B sample can be followed (Figure 5.6). The sample starts out with a value for σ which is twice the average value listed in Table 5.3. The σ of a sample drops because the membrane is not capable of completely restricting the diffusion of the salt. Consequently, the thickness of the double layer is reduced and the clay will flocculate, resulting in a reduction of double layer overlap and therefore a decrease in ideality.

There are few studies conducted in which natural materials with a high clay content other than monomineral materials were subjected to a chemical gradient, and those reported are all conducted on shales. Kemper (1961) demonstrated that the clay fraction of the Cretaceous Pierre Shale (USA) was a better semipermeable membrane than the shale itself. He separated the clay size fraction, which mainly consisted of montmorillonite and illite, by repeated sedimentation and washed it with a NaCl solution. In doing so he increased the ideality of the material. Based on his Figure 2 (Kemper, 1961) and the data provided, an experimental σ of approximately 0.007 can be derived, whereas the complete shale yielded a value of less than 0.001 (Table 5.4). Similar direct experiments of chemical osmosis on unprepared shales were published by Young and Low (1965) on the Lower Cretaceous Viking Formation shales (Canada) yielding similar low values, between 0.001 and 0.004, for the experimental σ. However, since the CEC and surface area are not reported for the sample, model predictions of σ for this material cannot be made. It is expected that the difference between the measured and calculated values are of the same magnitude as for the Kemper (1961) study in Table 5.4. Yearsley (1989) studied samples from different depths from a core taken near the Salton Sea (CA, USA) and found coupled flow phenomena in several experiments, consistent with chemical osmosis. The observed induced hydraulic heads were small compared to the applied chemical gradients and reported σ derived from the data provided have extremely small values (Table 5.4). All models overestimate σ because of the extremly low porosities of the samples and the high equilibrium concentration used. Generally, the differences between measured and calculated values increase when the equilibrium concentration in the experiment is small. This can be seen for the field experiment by Neuzil (2000) and the samples reported in this thesis. None of the models is capable of accurately predicting the

semipermeability of complex natural clay rich materials. The values obtained from the relatively simple and straightforward DDL model by Kemper–Bresler describes osmotic behaviour most succesfully. This was also observed in laboratory experiments on cores from a clay in the Bearpaw Formation (Canada – Cey, 1999) and for an *in situ* experiment on the Pierre Shale (USA – Neuzil, 2000).

5.6 CONCLUDING REMARKS

For the first time semipermeability was measured on contaminated, unconsolidated sediments with a high clay content. For the harbour sludge samples from the *Beerkanaal* with a clay content of approximately 56 % semipermeabilty was observed in two successive experiments. No semipermeability was observed for a sludge from the *Beneden Merwede* –river with a lower clay content (approximately 26 %). As with the experiments on bentonites, the measured reflection coefficients were considerably lower than those calculated by the available models. The model by Kemper–Bresler yields values nearest to those observed in our experimental work. A review on published data on shales supports this observation.

The experiments on the harbour sludge samples and on the previous described AWy–C bentonite was presented as: Loch JPG & Keijzer ThJS, Chemical osmosis in dredging sludge, at the 91th Annual Meeting of the Soil Science Society of America, Salt Lake City, USA, p. 339. A more extended manuscript is submitted for publication in the *Journal of the Soil Science Society of America*.

6 Desorption behaviour of polycyclic aromatic hydrocarbons in harbour sludge

6.1 INTRODUCTION

The experimental set–up described in Chapter 3 was designed to facilitate the measurement of organic contaminants, like polycyclic aromatic hydrocarbons (PAH), in the reservoir solutions. During chemical osmosis in the harbour sludge nonionic hydrophobic contaminants can desorb from the sample and be transported into the reservoirs. Therefore, materials to which PAH are known to adsorb were avoided in the experimental set–up. In order to test if this requirement was met, the development of the concentration of a phenanthrene (Phe) solution within a reservoir was monitored. A stainless steel cylinder was fitted into the cell to mimic a sample. A reservoir was filled with a Phe solution, which was circulated through the reservoir for a week with the same displacement as used in a chemical osmosis experiment. During that period it was observed that the Phe concentration decreased linearly, probably owing to sorption onto small teflon O–rings used in the Serto® needle valves. Therefore, measurements of PAH in the solution reservoirs as a result of desorption during chemical osmosis was not feasible. As an alternative desorption of PAH was studied in a more traditional column elution experiment.

In this chapter the results obtained in these column experiments are reported and discussed. The experiments were carried out on saturated samples of *Beerkanaal* and *Beneden Merwede* sludges under low convective regimes. The PAH chosen for this study were: phenanthrene (Phe), anthracene (Ant), fluoranthene (Flu), benzo[b]fluoranthene (BbF), benzo[k]fluoranthene (BkF), benzo[a]pyrene (BaP), benzo[ghi]perylene (BgP) and indeno[1,2,3 cd]pyrene (InP).

PAH sorption in natural materials

In the lower Rhine delta, the Netherlands, large quantities of sediments are deposited in the major waterways and harbours. A large part of these sediments is contaminated with organic and inorganic pollutants (Stigliani *et al.*, 1993; Van Zoest

& Van Eck, 1993). Consequently, depending on the level of contaminants dredged sediments are stored permanently in sludge depositories. A major depot, *De Slufter*, near the Port of Rotterdam (Figure 2.1) is currently receiving about 3 Mm^3 of contaminated harbour sludge each year.

It is often assumed that in consolidated fine–grained sediments the mobility of pollutants is negligible. The mobility of a compound is controlled by its water solubility which can be described in terms of the distribution coefficient, K_d, defined as the ratio of the concentrations in the solid and liquid phase at equilibrium. For most of the hydrophobic organic compounds, like PAH, the distribution coefficient is high and positively correlated with the organic matter in the soils and sediments (e.g. Loch, 1996). In experimental studies on sorption and transport, PAH are either dissolved in the percolating solution (Brusseau *et al.*, 1991a; Liu & Amy, 1993) or present as a separate, contaminated solid phase within the column (Grathwohl *et al.*, 1993). For contaminated aquifer material Grathwohl *et al.* (1994) showed that distribution coefficients derived from column experiments were higher than those obtained from short term laboratory experiments in which equilibrium was assumed. The desorption data could be fitted with a non–steady state, diffusion limited model. Liu & Amy (1993) showed that deviation from equilibrium depended on the flow rate applied and that it typically resulted in asymmetrical breakthrough curves and extended tailing (Brusseau *et al.*, 1991a, 1991b; Grathwohl *et al.*, 1993; Liu & Amy, 1993).

For the assessment of transport of PAH from contaminated sediments K_d–values are commonly obtained from sorption equilibrium batch experiments. However, in a harbour sludge depot convective solute transport occurs in the sludge layer during the consolidating stage. Depending on the hydraulic and chemical conditions water transport can be driven by hydraulic and/or osmotic gradients. Under convective transport conditions sorption equilibrium may be absent and desorption of contaminants like PAH may be underestimated. In order to assess the long term fate of PAH in a harbour sludge depot it is necessary to measure partitioning under conditions of low advective water flow.

6.2 MATERIALS AND METHODS

Chemicals

Chemicals used in this study were either obtained from J.T. Baker (Deventer, NL) or Merck (Darmstadt, GE), and were of HPLC or Supra Pure grade. PAH stock solutions were prepared from J.T. Baker custom PAH mixture JTB0005a lot J–1025.

Water, used for dilution and preparation of stock solutions, was prepared with a Milli–Q filtration unit.

HPLC

All PAH analyses were carried out using a high performance liquid chromatograph (HPLC – Hewlett Packard model 1050) equipped with a fluorescence detector (Hewlett Packard 1046A) on a ChromSpher 5PAH reverse–phase column (Chrompack, Bergen op Zoom, NL) using a water:acetonitril gradient. Calibration curves of all PAH under investigation were determined prior to each sample run. A standard PAH solution from the National Institute of Standards and Technology (NIST 1947c) was used to assess the reproducibility of retention times and detection signals.

Sample description and total PAH determination

Harbour sludge samples were retrieved from the *Beerkanaal* (BK) and the *Beneden Merwede*–river (BMR) in the port of Rotterdam, the Netherlands (Figure 2.1, p. 26) during the autumn of 1993. A thorough description of the mineralogy of the clay size fraction, and the bulk sample properties were presented in Chapter 2.

Before the start of the column experiments the individual PAH content of the samples was determined after an eight hour soxhlet extraction with a 1:3 aceton:hexane mixture. The extract was cleaned on a Al_2O_3/Na_2SO_4–column at a flow rate of 2 $mL \cdot min^{-1}$ using 12 mL hexane as eluent. Before their use Al_2O_3 (ICN, Eschwege, GE) was dried during 18 hours at 180°C, after which 10 wt% water was added, and Na_2SO_4 was dried for 3 hours at 500°C. Two mL of acetonitril were added to the eluate, and subsequently concentrated to approximately 1 mL under a gentle N_2 flow and analysed by HPLC. In order to determine the efficiency of the extraction method and the recovery of the individual compounds, a PAH contaminated standard (NIST 1941a) was also analysed.

Batch experiment

The sludge samples were stored for over three years under dark, anaerobic conditions at 4°C. It is assumed that during this period an equilibrium partitioning was reached between the solid and aqueous phase. Consequently, the equilibrium distribution coefficient, K_d^{eq}, can be determined by measuring the concentrations in both phases.

One hundred grams of wet sediment was centrifuged at 24000 rpm and 4°C for 20 minutes using an ultra–centrifuge (MSE Europe 24M). According to Puchelt & Bergfeldt (1992) ultra–centrifugation yields the pore water directly subjected to convective transport. Water trapped in dead–end pores or present as a water film on grains is not retrieved by this method. The supernatant after centrifugation was aspirated over a previously conditioned Bakerbond C_{18}/NH_2 PAH solid–phase extraction (SPE) column. The PAH are adsorbed onto the SPE–column and elution of the compounds from the SPE–column was done by aspirating 3 mL hexane at a flow rate of 1 $mL \cdot min^{-1}$ after a soaking period of 20 minutes. This procedure was repeated three times. Finally, two mL acetonitril was added to the SPE–eluate and the sample was concentrated under a gentle N_2 flow to approximately 1 mL and analysed by HPLC. The method to retrieve the PAH from the aqueous solution is based on the Bakerbond Application Note ENV103 and yields the water soluble and DOM–bound fraction of the PAH. The DOM suspended in the solution is trapped on the SPE–column, and during the soaking and elution stage the PAH are dissolved into the hexane and recovered. The PAH concentrations measured in the aqueous solution are therefore assumed to represent the total PAH content eluted from the sediment, including the DOM–bound fraction. The PAH content of the solid phase was determined using the method described for the total PAH determination.

Table 6.1 Detection limits and average recoveries, with their standard deviation, from aqueous solution for the different PAH using Bakerbond SPE extraction columns and HPLC with fluorescence detection. Recoveries were determined on three individually spiked solutions in the presence of 10 $mg \cdot kg^{-1}$ DOM and without DOM.

compound	HPLC detection limit	recovery without DOM	recovery with DOM[A]
	$\mu g \cdot L^{-1}$	%	%
Phe	0.002	119.0 ± 3.6	116.9 ± 3.5
Ant	0.0001	97.2 ± 2.6	93.8 ± 2.6
Flu	0.001	100.6 ± 0.8	93.8 ± 0.7
BbF	0.001	78.2 ± 0.3	74.1 ± 0.3
BkF	0.0001	61.3 ± 0.8	72.8 ± 1.0
BaP	0.002	94.0 ± 2.0	103.0 ± 2.2
BgP	0.049	71.7 ± 1.2	55.6 ± 0.9
InP	0.107	94.0 ± 0.7	50.6 ± 0.4

A synthetic DOM (Aldrich, Zwijndrecht NL)

Column experiments

Glass columns (internal diameter 7 cm, height 30 cm) were packed with a 700 g slurry of harbour sludge and sand. The sand was heated beforehand to 900°C to remove carbonate and organic matter. For the BMR a 1:1 sludge–sand mixture was used; for the BK sludge a 1:3 mixture was used. Because of the high clay content of the BK sample a higher sand content was used to increase the hydraulic conductivity. For each sludge sample two columns were packed which are referred to as BMR–I, BMR–II, BK–III and BK–IV.

The columns were fitted with a coarse glass frit and a 0.7 µm glassfiber filter to prevent the removal of fine solid material during elution. The column experiments were conducted at 4°C and under dark, anaerobic conditions to minimise breakdown of PAH. A constant hydraulic head was maintained at the top of the columns using a 0.01 M NaCl solution, resulting in a hydraulic gradient of approximately 1. The freely draining eluate was collected over a one or two week period for about four months. BMR–I was sampled during a period of nine months. The eluate was collected in N_2 filled, airtight 250 mL flasks to which 3 mL of a 600 $\mu g \cdot L^{-1}$ benzethonium chloride (Hyamine™) solution was added to prevent adsorption of the PAH onto the glass walls (Kicinski, 1992). The PAH content in the eluate was determined using the method described for the supernatant of the batch experiments. Detection limits and recoveries for the individual PAH in aqueous solution with and without DOM are listed in Table 6.1. DOM concentrations were calculated from measured dissolved organic carbon (Shimadzu TOC–500 Analyzer). The chloride concentration in the eluate was determined using ion chromatography (Dionex QIC Analyser).

Hydrodynamic parameter estimation

The diffusion–dispersion coefficient (D) of the columns was derived from the slope of the chloride breakthrough curve (BTC) assuming chloride to be a non–reactive, conservative tracer. The value of D was then used in a 1–D single solute transport model SOLUTE (Wilkens, 1995) together with the measured pore water velocities (Table 6.2) to gain insight in the presence of immobile water. Immobile or stagnant water presents a source/sink for the transported solute as it does not actively participate in the transport. The transfer between mobile and immobile water is assumed to be diffusion limited, therefore the presence of stagnant water in a column results in so–called transport non–equilibrium (Kookana *et al.*, 1993; Gaber *et al.*, 1995; Beigel & Di Pietro, 1999). The exchange between immobile and mobile water is generally represented by a first order mass transfer coefficient α (d^{-1}) e.g. Domenico and Schwartz (1990). The presence of immobile water in the columns can

have a profound effect on the desorption behaviour resulting in non-equilibrium behaviour whenever the sorption sites are located within the immobile water regions (Ball & Roberts, 1991; Gratwohl & Reinhard, 1993; Kookana *et al.*, 1993; Schuth & Gratwohl, 1994; Gaber *et al.*, 1995; Beigel & Di Pietro, 1999).

6.3 RESULTS AND DISCUSSION

Total PAH-content

The concentrations of the individual PAH compounds are given in Table 6.3. PAH concentrations in the BK sample are lower than in the BMR sample. The higher concentrations of the BMR site can be explained by its location near industrial sites, and the larger influence of river transported material and contaminants compared to the BK site. Based on the Dutch classification system† the BMR sludge falls within the concentration category which has to be stored in permanent harbour sludge depots like *De Slufter.* Based on the total sum of PAH this sludge exceeds the target value and therefore falls in class 2 which is unsuitable for disposal on land or in open water. Conversly, the BK sludge does not exceed environmental criteria and can be disposed of in open sea after dredging.

The total amount of PAH in the sludges, however, is low compared to concentrations found in sites like gas works.

Table 6.2 Physical properties and experimental parameters for the harbour sludge columns.

	height	velocity	water content	pore volume	bulk density
	cm	$cm \cdot d^{-1}$	$cm^3 \cdot cm^{-3}$	cm^3	$g \cdot cm^{-3}$
BMR-I	9.2	0.077	0.48	169	1.36
BMR-II	8.7	0.108	0.45	150	1.44
BK-III	8.4	0.430	0.42	134	1.53
BK-IV	8.6	0.374	0.44	143	1.47

† – the quality class of a sludge is based on comparison of the concentration of heavy metals and organic compounds with a number of limits. For each compound or group of compounds a target value is defined as the desired value (class 1), an upper value (class 2), a critical value (class 3) and an intervention value (class 4).

Equilibrium K_{OC}–values

The values of K_d^{eq} obtained for the compounds from the batch experiments were normalised on the organic carbon content of the samples (Table 2.2, p. 28) thus obtaining K_{OC}^{eq}–values (Table 6.3). Because of the high HPLC detection limits no values for K_{OC}^{eq} were obtained for BgP and InP (Table 6.1). In Table 6.3 also K_{OW}–values of the individual compounds, and K_{OC} data for sediments comparable to BMR and BK are presented as found in the literature.

In general, the obtained log K_{OC}^{eq} are higher than these literature values. For the less hydrophobic PAH, Phe, Ant and Flu, the difference with literature values is somewhat larger than for the more hydrophobic compounds BkF and BaP. For Phe, for instance, generally a value of approximately 4.30 is reported with a range of 0.10 log K units, whereas the values reported here are about 1.0 to 1.5 log units higher. For the more hydrophobic PAH the difference is on average 0.5 or less partly because the reported range for these compounds is larger than for the lighter PAH. The differences in log K_{OC}^{eq}–values are partly explained by the differences in the temperature at which they were determined. Most literature values were determined at 25°C whereas our values were obtained at 4°C. Adsorption of most nonionic hydrophobic compounds decreases with increasing temperature. The temperature effect can be assessed using (Schwarzenbach *et al.*, 1993):

$$\frac{K_{OC}(T_{high})}{K_{OC}(T_{low})} = e^{\left[\frac{\Delta H_s^e}{R}\left(\frac{1}{T_{high}} - \frac{1}{T_{low}}\right)\right]} \qquad (6.1)$$

giving the ratio of the distribution coefficients at the high, T_{high}, and the low, T_{low}, temperature in K. ΔH_s^e is the dissolution enthalpy of the compound in J·mol^{-1} and R is the gas constant (8.31451 J·K^{-1}·mol^{-1}). He *et al.* (1995) found for Flu close correspondence between experimental changes of the log K–values at different temperatures and predicted values by Eq. 6.1. An increase from 15°C to 25°C resulted in a decrease in adsorption of Flu of around 30 %. In order to eliminate the temperature effect the obtained log K_{OC}^{eq}–values at 4°C were converted to values at 25°C (Table 6.3). This could only be done for Phe, Flu and Ant, for the other compounds the required thermodynamic data could not be found. As expected, the log K_{OC}–values at 25°C are lower than at 4°C, but they are still 0.3 to 1 log K–value above literature values. This difference can be explained by the experimental method used to determine the K_{OC}^{eq}–value. Contrary to the literature values, our log K_{OC}^{eq}–values were not obtained after short contact times by addition of the PAH

Table 6.3 Concentration of the different PAH in the two sludges *Beneden Merwede*–river (BMR) and the *Beerkanaal* (BK), and their distribution coefficient normalised on the organic carbon, K_{OC}^{eq}, at 4°C and at 25°C as calculated using Eq. 6.1. The correction from K_d^{eq} to K_{OC}^{eq} was done using $K_{OC}=K_d/f_{OC}$ where f_{OC}=(%Organic Carbon/100) using a f_{OC} for BK of 0.0135 and for BMR of 0.0124. For comparison, literature values for K_{OC} of comparible sediments are listed together with the octanol/water distribution coefficient, K_{OW}, for the different compounds.

compound	PAH content mg·kg^{-1}		experimental log K_{OC}^{eq} at 4°C		experimental log K_{OC}^{eq} at 25°C using Eq. 6.1		log K_{OW} at 25°C [1,2)]	log K_{OC} at 25°C [1,2)]
	BMR	BK	BMR	BK	BMR	BK		
Phe	0.75 ± 0.10	0.15 ± 0.02	5.70	5.14	5.46	4.90	4.57	4.22 – 4.48
Ant	0.44 ± 0.04	0.05 ± 0.01	6.20	5.85	5.96	5.61	4.54	4.62
Flu	0.98 ± 0.09	0.17 ± 0.02	6.02	5.94	5.69	5.61	5.22	4.89 – 5.32[2)]
								4.65 – 4.82[4)]
BbF	0.69 ± 0.07	0.15 ± 0.02	6.31	6.36	nd	nd	6.32[3)]	5.70 – 5.74
BkF	0.36 ± 0.03	0.07 ± 0.01	6.37	6.33	nd	nd	6.00	5.47 – 6.04
BaP	0.61 ± 0.06	0.07 ± 0.02	6.40	6.16	nd	nd	6.04	5.53 – 5.99
BgP	0.38 ± 0.06	0.09 ± 0.01	na	na	na	na	6.50	6.20 – 6.26
InP	0.45 ± 0.09	0.11 ± 0.02	na	na	na	na	7.09[3)]	nr

na not analysed.

nd not determined due to a lack of sufficient data.

nr not reported, no literature values found

1) Mackay *et al.* (1992).

2) De Maagd *et al.* (1998).

3) Crunkilton & DeVita (1997).

4) He *et al.* (1995).

to the sediment samples in the laboratory (e.g. De Maagd, 1996). Short contact times result in weaker interaction between the PAH and the solid phase, resulting in an underestimation of the log K_{OC}^{eq}–value. This effect is probably stronger for the less hydrophobic compounds than for heavier, hydrophobic compounds as the lighter PAH are less strongly bound to the organic material in the sediments and more soluble in the aqueous phase. In the sludges contact time exceeded the three years storage time of the samples. It may therefore be assumed that the lighter PAH are more strongly bound to the solid phase, and have diffused further into the organic matter than can be achieved in the short laboratory contact times of the compounds in an uncontaminated soil or sediment. In the typical batch experiments commonly used to obtain these values, a sample is (vigorously) shaken causing dispersion of the solid phase and an increase in the fraction of DOM in the aqeous phase. This adds to the underestimation of the partition coefficients (Schrap & Opperhuizen, 1992). The method used in this study for concentration measurements of the PAH also enables the determination of the DOM–bound PAH in the solution. Recoveries in solutions with and without DOM were in close correspondence, with the exceptions of BgP and InP (Table 6.1). Thus, the log K_{OC}^{eq}–values obtained here by the centrifugation method are in our opinion more representative for the partitioning likely to be encountered in field sediments contaminated with PAH.

The log K_{OC}^{eq}–values for the brackish BK sample are somewhat lower than those obtained for the fresh water sample BMR. This trend is not consistent with the brackish nature of the BK sediment. Theoretically the distribution coefficient of a nonelectrolyte increases with increasing salinity as the solubility of the compound decreases due to the so–called salting out effect (Schwarzenbach *et al.*, 1993). However, this effect is small as Hegeman *et al.* (1995) experimentally determined. An an increase for Phe and BgP of less than 0.2 log units of the K_{OC} with salinity increasing from 0 to 35 ‰.

Relations between log K_{OC}^{eq} and log K_{OW}

Several authors have reported linear relationships between experimental log K_{OC}^{eq}–values and the corresponding log K_{OW}–values of the PAH compounds (Karickhoff *et al.*, 1979; Chiou *et al.*, 1983; De Maagd, 1996; Walter *et al.*, 2000). For the BMR and BK sludge similar relationships are presented in Figure 6.1. The regression equations obtained, for log K_{OC}^{eq} at 4°C, are:

$$\log K_{OC}^{eq}\,(\text{BMR}) = 0.26 \log K_{OW} + 4.73 \qquad r = 0.755$$
$$\log K_{OC}^{eq}\,(\text{BK}) = 0.29 \log K_{OW} + 3.34 \qquad r = 0.846$$

For both sediments the regression lines are less steep than reported elswhere (Karickhoff *et al.*, 1979; Chiou *et al.*, 1983; Walter *et al.*, 2000). De Maagd (1996) found slopes close to one for sediments from the *Ketelmeer* and *Oostvaardersplassen*, two large fresh water lakes in the Netherlands, with comparable organic carbon contents. The differences can be solely attributed to the high values of log K_{OC}^{eq} obtained in our experiments for the smaller, less hydrophobic compounds Phe, Ant and Flu. The overall trend of increasing log K_{OC}^{eq}–values with an increase in hydrophobicity as expressed by the log K_{OW} remains.

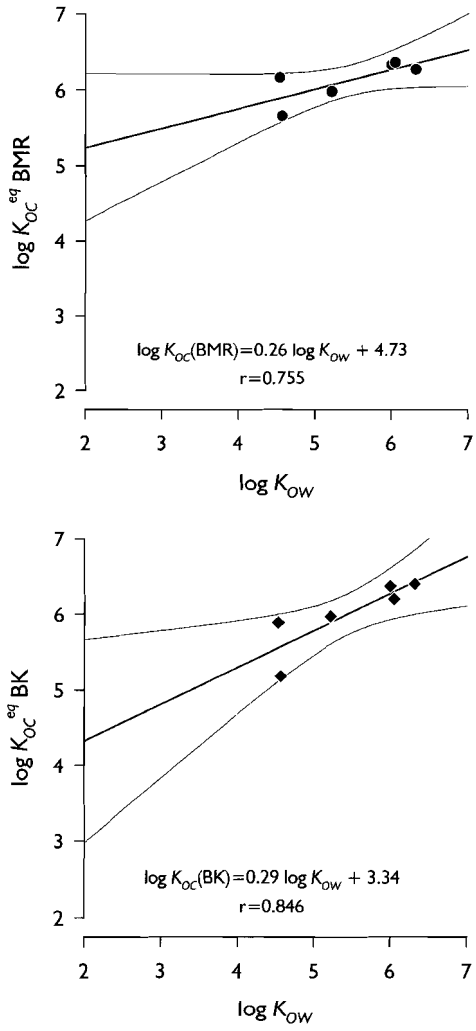

Figure 6.1
The relationships between the log K_{OW} and log K_{OC}^{eq} at 4°C for; **top** BMR sludge, and **bottom** the BK sludge. For the linear regression lines the relationship, regression coefficient and 95 % confidance interval is given.

Chloride breakthrough curves

From the measured breakthrough curves of chloride (Figure 6.2) the diffusion–dispersion coefficient (D) was derived using (Van Beek & Pal, 1978):

$$\frac{D}{v} = \lambda = \frac{L}{4\pi S^2} \tag{6.2}$$

where v is the pore water velocity in $m \cdot d^{-1}$, λ is the dispersion length in m, L the length of the column in m, and S the slope of the BTC at $C/C_0 = ½$. Values of D for each column are listed in Table 6.4. Using these values the presence of stagnant or immobile water was evaluated, resulting in a fit of the observed data (Figure 6.2). The fit of the breaktrough curve of BMR was good for 20 to 30 % of immobile water and α of 0.01 ± 0.005 d^{-1} (Table 6.4). Indeed the asymmetrical shape of the BTC (Figure 6.2) indicates the presence of a large portion of stagnant water and a relatively slow mass transfer between the two water regions. Because of the brackish nature of the sample the BTCs of the BK sludge represent elution curves (Figure 6.2). Therefore the BTCs for BK–III and BK–IV can be plotted as $1-(C/C_0)$ which enables the use of Eq. 6.2 to determine the slope of the BTC and the subsequent derivation of D. It was not possible to estimate the fraction of immobile water from the BTC of BK–III and BK–IV, but it can be argued that this fraction is negligible. The presence of immobile water will shift the curve more to the right, as Cl^-–elution will be retarded from the column with increasing amounts of stagnant water.

In addition to the difference in initial Cl^-–content of the columns the water regimes in the columns differ. The different regimes are reflected in the column Peclet number ($P_c = vL/D$ – Table 6.4). Peclet numbers smaller than one are indicative for diffusion–dispersion dominated transport, whereas values above ten are found for convection dominated transport (Dunnivant *et al.*, 1993; Totsche *et al.*, 1997). In the BMR columns a large portion of the water is immobile with a low pore

Table 6.4 Hydrodynamic properties of the columns derived from cloride breakthrough curves.

	D	immobile water	α	P_c	λ
	$cm^2 \cdot d^{-1}$	%	d^{-1}		cm^{-1}
BMR–I	0.288	~30	0.015	2.3	3.9
BMR–II	0.432	~20	0.010	2.2	3.9
BK–III	0.322	none	–	11.2	0.75
BK–IV	0.265	none	–	12.1	0.71

water velocity, whereas the flow regime in the BK columns is convection dominated supporting the assumption of zero immobile water content. The higher pore water velocities are the result of higher proportion of sand that was added to the sludge to increase the hydraulic conductivity of the columns.

Pore water velocities compared to osmotically induced velocities

The pore water velocities used in these column experiments were higher than observed in the experiments on chemical osmosis, especially in the BK columns. The induced pore water velocity during chemical osmosis was in the order of 0.02 $cm \cdot d^{-1}$ which is a factor 20 smaller than used in the BK column experiments (Table 6.2).

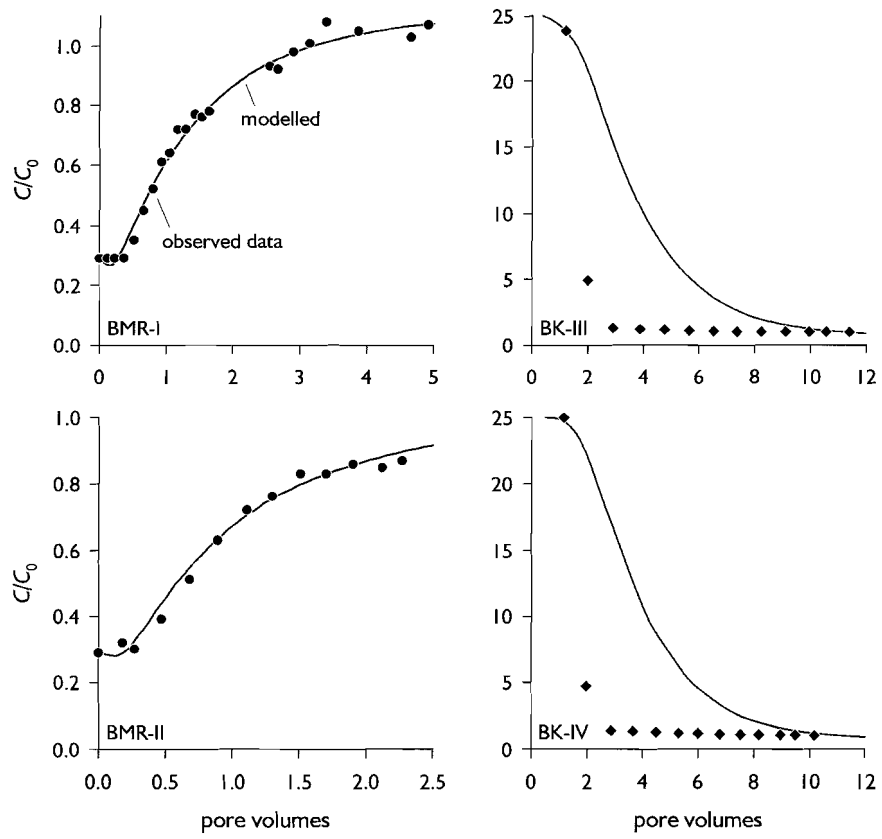

Figure 6.2 Observed chloride concentrations in the effluent and modelled breakthrough for chloride, **left** for the BMR columns, and **right** for the BK columns.

Desorption of PAH

For BMR–I and BMR–II the elution of the individual PAH from the sludge columns is shown in Figure 6.3. An exponential decrease for the Phe, Ant and Flu concentrations with time was observed in both columns. No significant decrease was found for the hydrophobic compounds BbF, Bkf and BaP during the first four months of the experiment. Thereafter, concentrations for BbF, BkF and BaP dropped below the detection limit. As a result of the relatively high detection limits for BgP and InP (Table 6.1) these compounds could not be detected in any of the eluates. The elution from the BK–III and BK–IV columns of all detected compounds, including the heavier ones, remained more or less constant during the experimental period (Figure 6.4). The concentrations are lower than those of the BMR columns most likely due to the lower initial concentrations in this sludge (Table 6.3). BgP and InP were not detected in the eluate of the BK columns.

The different elution patterns in the columns of the two sludges can be explained by a simple conceptual model (Figure 6.5). At the start of the column experiment the PAH concentration in the water and solid phase are in equilibrium. During percolation a part of the water is mobile, whereas another part remains stagnant. The concentration in the mobile water can only be replenished by diffusion of the PAH out of the immobile water region, thus, assuming the desorption of PAH to be diffusion controlled. In reality desorption most likely consists of two sequential diffusion steps; firstly, diffusion in the solid phase which is most likely the microporous organic matter present in the sediment, and secondly diffusion from the immobile to the mobile water region. Diffusion in the solid phase is generally thought to be a slow process as it is retarded by e.g. resorption on the organic material, interaction with the micropore walls and steric hindrance. Diffusion between the different water regions is relatively fast. As the pore water velocity in the column increases, the immobile water film adjacent to the solid phase decreases, reducing the diffusional distance. Therefore, the mobile water is in near–equilibrium with the immobile water because of the small distance to be covered by diffusion, and rapid replenishment of the leached solute. When the immobile water region is thicker as result of a lower pore water velocity the diffusional distance is larger, resulting in non–equilibrium desorption (Figure 6.5). The desorption data for the BK columns (Figure 6.4) show basically an equilibrium release of the PAH as only a negligible fraction of immobile water was present in these columns. The desorption data for the BMR columns show non–equilibrium desorption for Phe, Ant and Flu owing to the lower pore water velocity and the large fraction of immobile water. For the BMR columns this fraction was estimated to be between 20 and 30 % based on the BTC of chloride (Table 6.4). This large fraction is

not only caused by the lower pore water velocity but also by the smaller amount of sand added to the sludge than in the BK columns.

Closely related to this conceptual model is the description of non–equilibrium sorption assuming spherical particles (Wu & Gschwend, 1986; Ball & Roberts, 1991; Grathwohl & Reinhard, 1993; Grathwohl *et al.*, 1994). Diffusion controlled desorption from a solid sphere can be described by Fick's second law (e.g. Crank, 1975):

$$\frac{\partial C}{\partial t} = D^{app}\left(\frac{\partial^2 C}{\partial r^2} + \frac{2}{r}\frac{\partial C}{\partial t}\right) \tag{6.3}$$

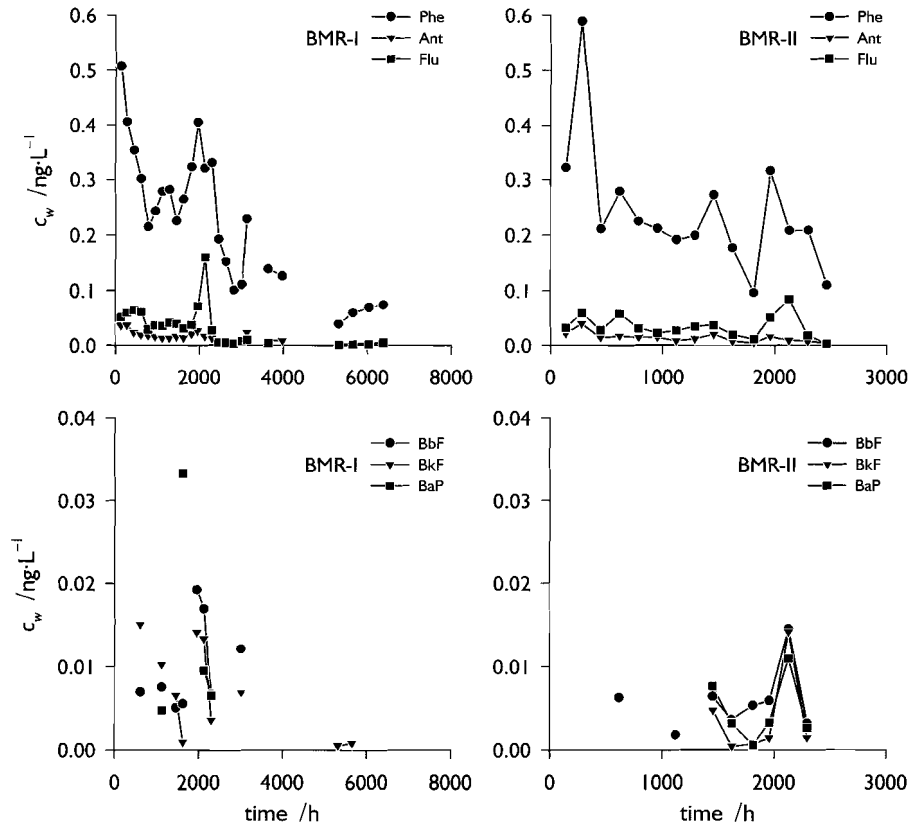

Figure 6.3 Observed PAH concentrations in the eluate, c_w, over time for **left** BMR–I, and **right** BMR–II. No lines are shown during periods in which the compound was not detected in the eluate or for which no data are available.

where D^{app} is the apparent diffusion coefficient in $m^2 \cdot s^{-1}$, C is the solute concentration in the solution in $g \cdot m^{-3}$, r the radial distance from the centre of the sphere in m, and t the time in s. The analytical solution of the desorption flux q ($\mu g \cdot g^{-1} \cdot s^{-1}$) from a spherical soil particle of radius r into bulk water, with sorption equilibrium at $t = 0$ and with the boundary condition of $C = 0$ for $t > 0$ in the bulk water (Grathwohl & Reinhard, 1993) is:

$$q = 6M_0 \frac{D^{app}}{r^2} \sum_{i=1}^{\infty} e^{\left(-i^2 \pi^2 D^{app} / r^2\right)} \tag{6.4}$$

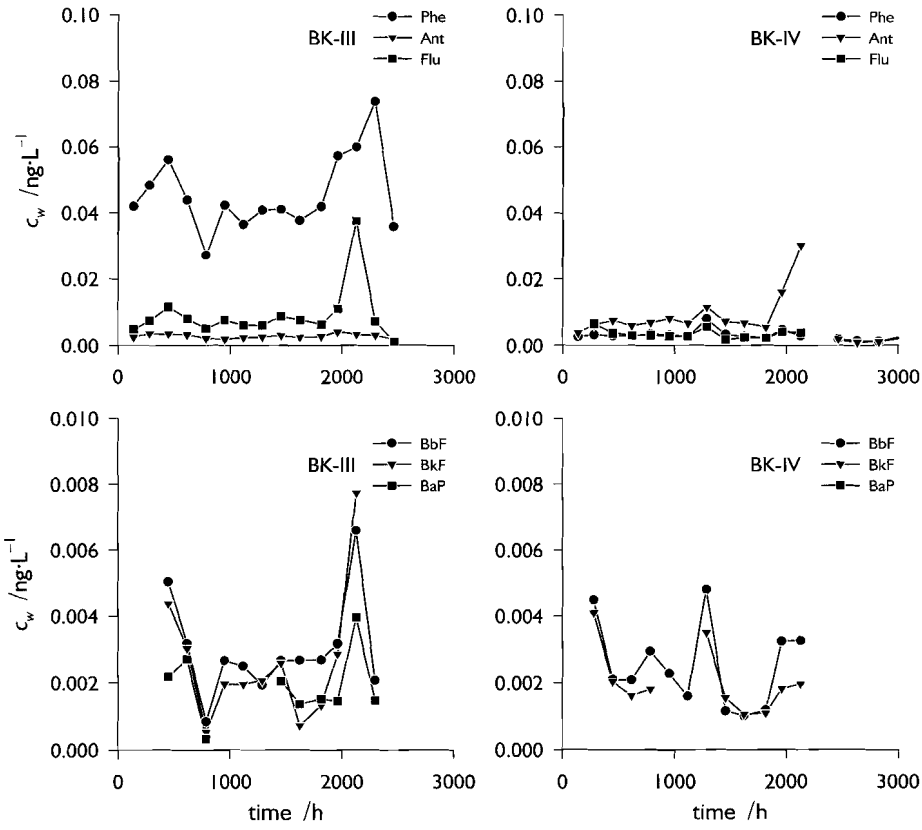

Figure 6.4 Observed PAH concentrations in the eluate, c_w, over time for **left** BK–III, and **right** BK–IV. No lines are shown during periods in which the compound was not detected in the eluate or for which no data are available.

where M_0 is the initial contaminant concentration in $\mu g \cdot g^{-1}$ which is assumed constant throughout the sphere at $t=0$. This analytical solution enables description of the desorption by adjusting D^{app}/r^2. Thus, the desorption rate decreases with increasing particle radius and therefore with the diffusional distance. The desorption flux of the smaller PAH, Phe Ant and Flu, in the BMR columns was described using Eq. 6.4 by fitting the measured fluxes, after proper adjustment of units (Figure 6.6). Using the modus of the grain size derived from the grain size distribution (Figure 2.3, p. 31) D^{app} was obtained by fitting (Table 6.5). The derived D^{app}–values are low compared

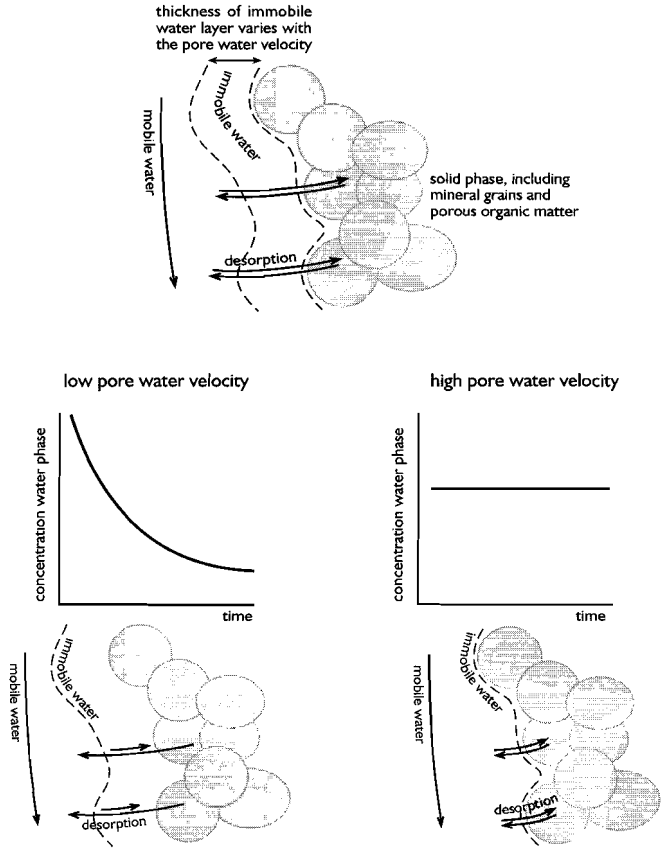

Figure 6.5 Conceptual model of the desorption of PAH during the column experiments. As desorption is governed by diffusion the path length increases as the pore water velocity in the column decreases. This results for low pore water velocities in a thick immobile water layer resulting in non–equilibrium sorption, whereas at higher pore water velocities the thinner immobile water layer enables the presence of equilibrium desorption.

to literature values (Grathwohl *et al.*, 1994). This can be attributed to a larger diffusional distance due to an immobile water layer adjacent to the sediment particles and aggregates. However, interaction with the pore walls and steric hindrance also determine D^{app}, factors which can vary largely between different soils and sediments (Cornelissen, 1999). Only Phe could be satisfactorily fitted with Eq. 6.4; the model is less succesful in describing the data of Ant and Flu. This is most likely the result of the low concentrations of the compounds in the aqueous solution at the end of the experiment resulting in a relatively large analytical error.

Table 6.5 Values for the apparent diffusion coefficient, D^{app}, for Phe, Flu and Ant in the BMR columns obtained by fitting the parameters of Eq. 6.4.

compound	D^{app}	
	$cm^2 \cdot d^{-1}$	
	BMR–I[1)]	BMR–II
Phe	$0.3 \cdot 10^{-12}$	$0.3 \cdot 10^{-12}$
Ant	$25 \cdot 10^{-15}$	$27 \cdot 10^{-15}$
Flu	$27 \cdot 10^{-15}$	$25 \cdot 10^{-15}$

1) for the nine month period

Table 6.6 Apparent distribution coefficients, log K_{OC}^{app}, for the individual PAH based on the measured concentrations in the column effluent at 4°C.

compound	log K_{OC}^{eq}	log K_{OC}^{app}		log K_{OC}^{eq}	log K_{OC}^{app}	
	BMR	BMR–I[1)]	BMR–II	BK	BK–III	BK–IV
Phe	5.70	5.56 ± 0.12	5.40 ± 0.16	5.14	5.26 ± 0.12	5.27 ± 0.18
Ant	6.20	6.63 ± 0.21	6.49 ± 0.28	5.85	6.08 ± 0.12	6.09 ± 0.15
Flu	6.02	6.64 ± 0.33	6.46 ± 0.36	5.94	6.23 ± 0.30	6.28 ± 0.28
BbF	6.31	nd	nd	6.36	6.60 ± 0.21	6.67 ± 0.12
BkF	6.37	nd	nd	6.33	6.39 ± 0.20	6.61 ± 0.17
BaP	6.40	nd	nd	6.16	6.47 ± 0.25	6.47 ± 0.13

for all columns number of observations (n): $8 < n < 15$

nd value not determined due to limited data available

1) values for the nine month period

Recently, Cornelissen *et al.* (1999) discussed the desorption of PAH from field contaminated sediments in terms of slow and very slow desorption for different particle size fractions. Their results were not in good agreement with the radial diffusion model and they tentatively concluded that slow desorption from the sediments resulted from the slow release from strong sorbing sites in the organic matter. They left the possibility open that (slow) desorption is a combination of diffusion through the organic matter and the presence of different sorption sites (Cornelissen *et al.*, 1999). None of these conclusions can be supported by the results obtained in this study.

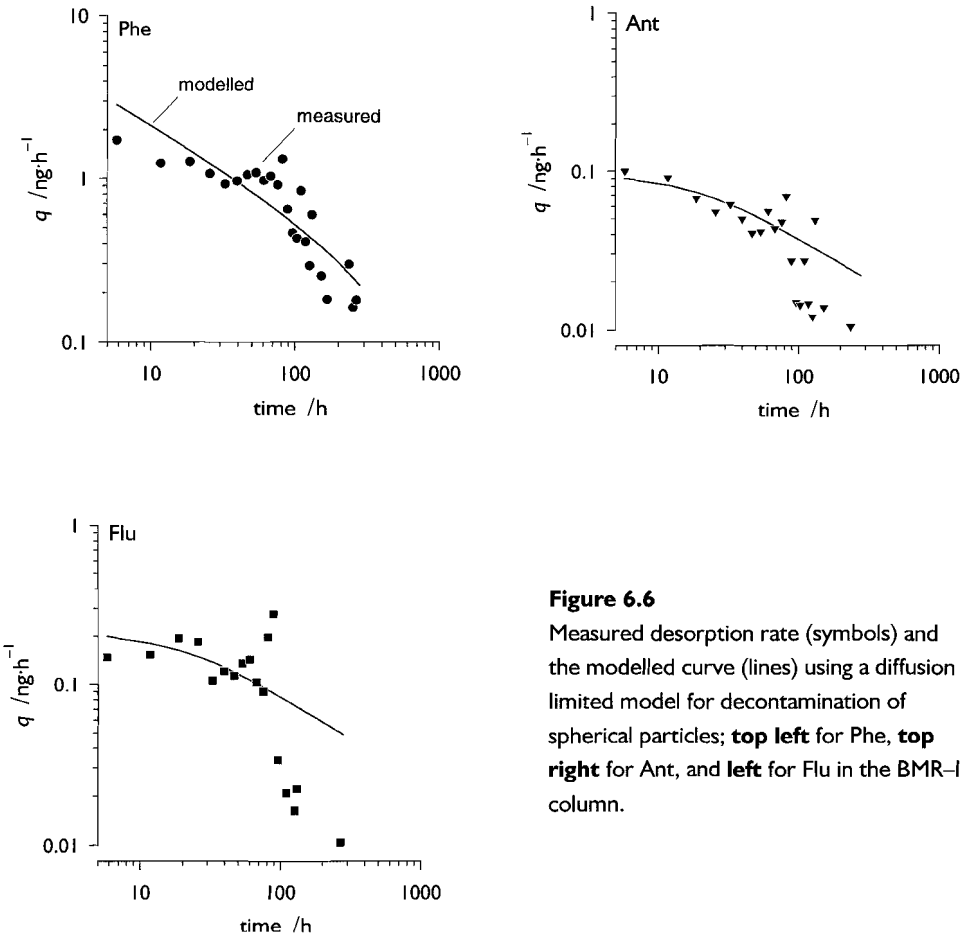

Figure 6.6
Measured desorption rate (symbols) and the modelled curve (lines) using a diffusion limited model for decontamination of spherical particles; **top left** for Phe, **top right** for Ant, and **left** for Flu in the BMR–I column.

Log K_{OC}^{app}–values for the column experiments

From the known total concentration of the individual PAH compounds within the sediment and the measured concentrations in the column effluent, apparent distribution coefficients, log K_{OC}^{app}, were calculated (Table 6.6). With the exception of Phe in the BMR columns the log K_{OC}^{app}–values for the columns are higher than the equilibrium values obtained from the batch experiments. For BMR–I and BMR–II log K_{OC}^{app} was not calculated for BbF, BkF and BaP due to the scattered appearance of their concentrations in the eluate.

Log K_{OC}^{app} in the BK columns for Phe, Flu and Ant is lower than in the BMR columns and close to the values obtained in the batch experiments. As in the BMR equilibrium is supposed to be absent, log K_{OC}^{app}–values for the BMR sludge are expected to be higher. Generally, column distribution coefficients are higher than values obtained by batch experiments (e.g. Grathwohl *et al.*, 1994).

Influence of DOM on the desorption

The analytical method used to measure the PAH content in the eluate of the columns not only measures the fraction that is actually dissolved but also the fraction of PAH bound to DOM. The association of PAH with DOM increases the apparent solubility of the compound and enhances its transport through a porous medium (Enfield *et al.*, 1989; Abdul *et al.*, 1990; Dunnivant *et al.*, 1992; Maxin & Kögel–Knabner, 1995; Totsche *et al.*, 1997). In the eluate of the four sludge columns the

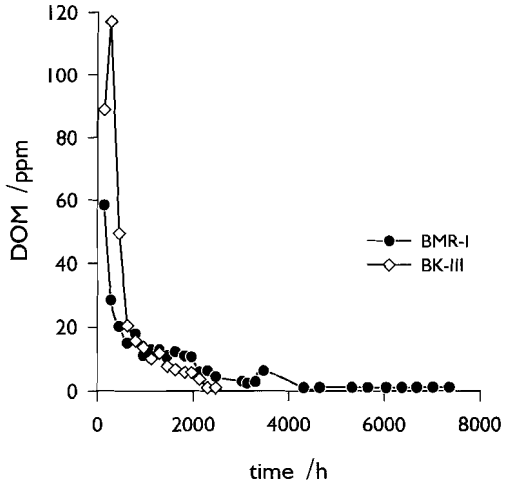

Figure 6.7
Measured DOM concentrations in the eluate of columns BMR–I and BK–III. The two other columns showed a similar decrease in DOM concentrations.

DOM concentration diminished rapidly (Figure 6.7). After approximately 2000 hours or 84 days the concentration in all columns dropped below 5 ppm. From comparison of the DOM in the eluate with the PAH elution from the BMR columns (Figure 6.3), it seems likely that most of the PAH desorbing from the BMR sludge is DOM–bound. Especially, the more hydrophobic PAH —BbF, BkF and BaP— disappear from the eluate when the the DOM concentration becomes negligible. The desorption in the BK–III and BK–IV columns remains relatively constant (Figure 6.4) and the changes in DOM concentrations are not reflected in the desorption of the PAH.

6.4 CONCLUDING REMARKS

Desorption of PAH was studied on two different sludges from the Port of Rotterdam, the Netherlands. Equilibrium log K_{OC}–values obtained from these field contaminated sediments using an ultra–centrifugation method at 4°C yielded log K_{OC} well above reported literature values. Temperature correction of the log K_{OC} could not account for the observed differences. The differences are attributed to the contact times of PAH in the sediment. The laboratory data reported in the literature were obtained after short contact times, thus underestimating the actual log K_{OC}. Our values represent contact times in excess of 3 years and therefore are more representative for the field conditions. Log K_{OC}–values obtained from column elution experiments were slightly above those obtained from the batch experiments. In the BMR columns sorption equilibrium was absent for Phe, Flu and Ant. This is attributed to the presence of a large portion of immobile water in the columns as a result of their smaller sand fraction and low pore water velocities. Elution in the BK columns occurred at near sorption equilibrium although pore water velocities were higher in these columns. However, due to large water velocity and a large sand fraction almost no immobile water was present in these columns. Assuming that desorption is diffusion controlled and that all sorption sites are covered by immobile water, observed desorption in both materials could be explained. The non–equilibrium desorption in the BMR columns could be reasonably described by a diffusion limited model assuming spherical particles.

Preliminary results of the desorption experiments were presented as: Keijzer ThJS, Middeldorp PF, Van Alphen M & Loch JPG (1998). Solid–liquid partitioning of polycyclic aromatic hydrocarbons (PAH) in column experiments on harbour sludge, at the Conference on Contaminated Soil 1998 (ConSoil 98), Edinburgh, UK, p. 857–859. A more extended manuscript is submitted for publication in *Water Air and Soil Pollution*.

7 Synthesis: Chemical osmosis in natural clayey materials

7.1 INTRODUCTION

In this chapter the performance of the experimental design will be summarised. Based on our experiments and the previous literature review (Chapters 4 & 5) the applicability of the different models for natural samples will be discussed. As this study is the first to report semipermeability of contaminated sediments, the implications on the transport of water and contaminants will be discussed in relation to the storage of harbour sludge sediments in permanent depots.

7.2 PERFORMANCE OF THE EXPERIMENTAL DESIGN

The major advantage of our experimental design in comparison to those used in most earlier studies is the direct measurement of water flow by chemical osmosis in a sample (Chapter 3). This enables the study of the evolution of semipermeability over time, as was done in one of the experiments on the BK sludge (Chapter 5). This clearly shows that σ is not an intrinsic property of a given sample at given conditions. The samples' semipermeable properties change as a result of other processes like diffusion and cation exchange that proceed simultaneously with osmosis whenever the sample is a non–ideal membrane. These processes also occur in the subsurface when a clay or a clayey sediment is not in equilibrium with a chemical gradient. The experimental design therefore allows a laboratory study of coupled flow phenomena in a setting closely related to the Dutch field situation. The use of a flexible wall permeameter allows the simulation of various overburden loads by adjusting the pressure in the cell liquid.

Problems encountered elsewhere with direct measurement of chemical osmosis like insufficient mixing of the reservoirs (e.g. Kemper & Rollins, 1966) were solved (Chapter 4). The flexible permeameter design, however, has its own limitations which

should be solved in future studies. One of these problems is leakage from the pressurised water in the cell to the reservoirs. Leakage has two different causes; firstly, the stainless steel capillaries facilitating the connection between the top of the sample and the salt water reservoir (Photo 3.2, p. 44) are vulnerable to wear and tear. This results in small cracks in the welded connection between the capillary and Serto® connector. Secondly, during the assembly of the sample in the cell and the installation of the rubber 'sleeve', small ruptures can form due to the sharp edges of the porous stones and rough outer surface. Both types of leakage resulted in an observed water flux of the same order of magnitude as induced by the chemical gradient (see e.g. Figure 4.8). Detection of the presence of a leak was sometimes only possible long after the start or even at the end of an experiment. The remedy against rupturing the rubber 'sleeve' was found in wrapping the porous stones in teflon tape. Leakage due to the wear and tear on the capillaries could not be permanently solved.

Of all criteria formulated in Chapter 3 (§3.3, p. 40) all but one were met. The choice of stainless steel Serto® components did not prove to be satisfactory. Although the reservoirs were free of leakage and more rigid than expected (Chapter 3), corrosion of the stainless steel reservoirs did occur. Cleaning the reservoirs between experiments was tedious and time consuming but necessary to eliminate the possibility of erroneous electrical conductivity signals. The stainless steel Serto® needle valves used in the reservoirs prevented the direct measurement of hydrophobic contaminants like PAH in the reservoirs because of the presence of a small teflon O–ring within the valve (Chapter 6).

In our study the time necessary to complete an experiment was not a major requirement. Generally, it took three months to complete an experiment on a given sample, including preparation of the experimental setup between different samples, calibration of the pressure transducers and electrical conductivity cell, and determination of the hydraulic conductivity. Although not considered to be a major drawback, this type of design is not suited for a quick screening on semipermeability of natural clayey materials.

7.3 APPLICABILITY OF THE MODELS ON NATURAL CLAYEY MATERIALS

The developed experimental apparatus was used to investigate the semipermeable properties of a commercially available bentonite and two contaminated harbour sludges (Chapters 4 & 5). In three of the bentonite samples chemical osmosis was observed as in one of the sludges. However, in all experiments the measured reflection coefficients were considerably lower than calculated with the models discussed in

Chapter 1. Literature reviews showed that the difference between experiment and theory is not limited to this study (Chapters 4 & 5). This raises questions about the applicability of the models for predicting semipermeability of natural materials, and to what extent the models can be tuned so that they correspond more closely with experimental conditions.

Applicability

Several assumptions made in the FMMM, Kemper–Bresler and Groenevelt–Bolt models can explain the observed difference between theory and practice (Chapter 4). For all three models these are: the assumption of a monomineral semipermeable membrane, complete dispersion of the clays within the sample, and complete occupation of the exchange complex by a monovalent cation. These assumptions limit the applicability of the models to ideal samples and make them less applicable for accurate prediction of the semipermeability of natural materials. However, the models can still be useful in indicating possible trends.

Before applying one of the models, the validity for the given porosity range and concentration should first be reviewed. Using Figure 7.1, where σ of a bentonite is plotted against c_0 for the three models —at the three assumptions above— some tentative guidelines can be derived. When studying highly compacted materials with porosities <0.3, all models predict more or less the same value for σ over the entire concentration range plotted. Thus, for studies on compacted membranes satisfying the three assumptions the choice of the model seems arbitrary. However, the model formulated by Groenevelt and Bolt is not valid for values of $\kappa_0 d_l < 1$, values generally found at low equilibrium concentrations and low porosities. Therefore, no theoretical values for σ could be obtained with the Groenevelt–Bolt model for several reported studies listed in Table 4.4 (p. 74).

The differences between the predictions by the various models increase with increasing porosities, and with decreasing CEC as is illustrated in Figure 7.1. For membranes with a high porosity, e.g. ~0.8, and c_0 below 1 mol·L^{-1}, the Kemper–Bresler model yields conservative or low estimations for σ. At higher c_0 values —above 1 mol·L^{-1}— both models, based on the Gouy–Chapman theory for a diffuse double layer, approach each other. In Figure 7.1 the curve calculated using the FMMM gradually increases with c_0 beyond a minimum σ–value. A minimum in the predicted σ is also observed when plotting σ versus porosity, see also Figure 1.5 (p. 16) or 4.1 (p. 60) and was explained by Fritz and co–workers as 'negative anomalous osmosis' (Marine & Fritz, 1981). However, the rise of the FMMM curves beyond the minimum σ–value is probably a mathematical artefact. For this reason the FMMM should be

used with caution for high porosity membranes at higher concentrations, e.g. above 2 mol·L^{-1}.

For most situations, in the laboratory and in the field, the porosity of the sample will be around 0.5 with equilibrium concentrations generally between 0.1 and 1 mol·L^{-1}. In these situations the Kemper–Bresler model again yields conservative estimates. The FMMM yields values between the Kemper–Bresler and Groenevelt–Bolt model. In this range the FMMM is recommended for an average estimate of σ.

The relatively straightforward model by Kemper (Kemper & Rollins, 1966; Kemper, 1972) and Bresler (Bresler, 1972) can be used across the entire concentration and porosity range. However, according to Bolt (1982b) this model underestimates σ at high values of $\kappa_0 d_l$, i.e. at high concentrations and porosities. For AWy the Groenevelt–Bolt model —for porosities of 0.5, 0.8 at the entire c_0–range— predicts

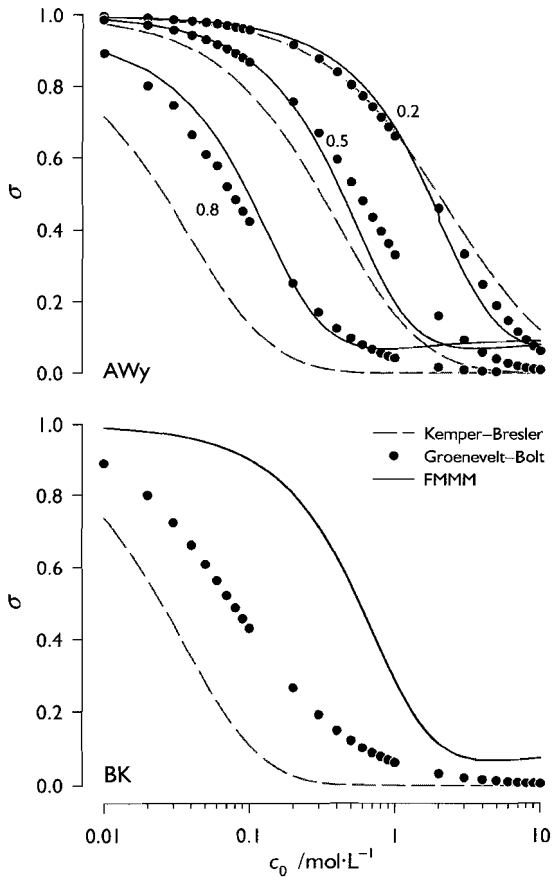

Figure 7.1
Predicted reflection coefficient as a function of the equilibrium concentration; **top** for the AWy bentonite at different porosities according the FMMM, the Kemper–Bresler and Groenevelt–Bolt models. Curves were calculated for porosities of 0.2, 0.5 and 0.8, CEC is 68 cmol$_c$·kg^{-1} and A_s is 556 m^2·g^{-1}, and **bottom** for the clayey sediment from the *Beerkanaal* at a porosity of 0.2, CEC 24 cmol$_c$·kg^{-1} and A_s 30 m^2·g^{-1}.

higher values of σ than to the Kemper–Bresler model (Figure 7.1). It is, however, especially for the samples with a high porosity subjected to high values of c_0 that experimentally determined σ's have low values (Chapter 4; Kemper & Rollins, 1966; Kemper & Quirk, 1972). Kemper (1972) also observed the underestimation of experimental values by his model whenever $\sigma<0.3$. Consequently, he introduced an empirical fitting parameter for a water film thickness of $250 \cdot 10^{-10}$ m in monomineral bentonites in order to obtain higher values for σ. Because of the limited applicability of this fitting parameter, it is better to use the Groenevelt–Bolt model if experimental σ values are underestimated by the Kemper–Bresler model than the approach by Kemper (1972).

The choice of a model is often based on how well it is described in the literature, its ease of application, and the experience of others with the model. Of the three models discussed in this thesis, the best documented and most transparent is the FMMM, published in a series of articles (Marine & Fritz, 1981; Fritz & Marine, 1983; Fritz, 1986). It is also the easiest to use; straightforward calculations yield relations between σ and influencing factors which are easily interpretable (e.g. Figure 1.5). In the opinion of the authors of the FMMM, the model is best used for deep subsurface (ground water) situations (e.g. Fritz, 1986). The model was indeed applied to evaluate semipermeability in these situations (e.g. Alexander 1990; Horseman *et al.*, 1996; Osborne & Swarbrick, 1997). The model by Groenevelt–Bolt also is well documented (Groenevelt & Bolt, 1969; 1972; Bolt, 1982b). Although, for the deriviation of Eq. 1.19 and 1.20 (p. 19) reference is made to unpublished work. Generally, the model is less transparent than than FMMM, but Figure 1.7 (p. 18) helps to clarify details of the model. Understanding the derivation of the theoretical salt sieving effect by Bresler (1973) requires a thorough knowledge of diffuse double layer theory but his description of parameters to be used in the DDL lacks transparency. Reflection coefficients based on his work were derived from Fig. 1 in Bresler (1973), e.g. by Keijzer *et al.* (1999) and Neuzil (2000). The simplicity and elegance of the model was recognised after reviewing the work by Kemper and co–workers summarised by Kemper (1972). The Kemper–Bresler model is probably the best choice when estimating the semipermeability of natural clayey sediments. It offers a simple but straigthforward approach based on the widely accepted Gouy–Chapman theory of the diffuse double layer, without dividing the double layer in a mobile and immobile part and thus complicating matters unnecessarily. The observation that the Kemper–Bresler model underestimates σ is not convincing since experimental reflection coefficients were generally lower than expected on basis of the other models (Chapters 4 & 5). Most natural clayey materials like shales, and the sludges in this study, could be best described with the Kemper–Bresler model (Keijzer *et al.*, 1997; 1999; Cey, 1999; Neuzil, 2000).

Tuning the models

Although the Kemper–Bresler model provides the best estimate for σ in natural clay rich materials, the assumption of complete dispersion often does not hold. The Kemper–Bresler and Groenevelt–Bolt models allow the use of the primary A_s as determined by the N_2–BET method instead of the secondary A_s, as determined by adsorption of EGME. Using the lower value of A_s circumvents the assumption of complete dispersion. For both the bentonites and harbour sludges this yielded theoretical reflection coefficients more in correspondence with the experimentally determined values (Chapters 4 & 5).

In the FMMM the surface area can not be tuned directly. In this model there are, however, more parameters that are of influence on σ than in the other models. The influence of R_{wm} and R_w on the reflection coefficient is given in Figure 7.2, their values were discussed in Chapter 1. Contrary to the approach in the FMMM we

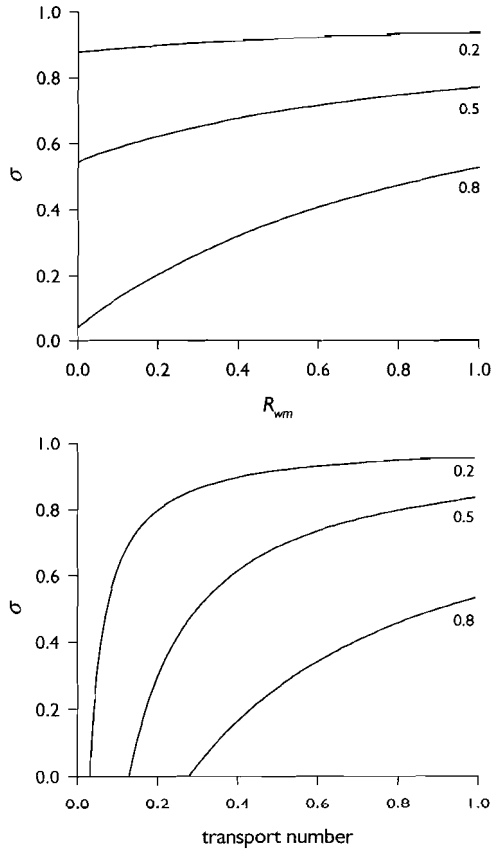

Figure 7.2
The relation between the reflection coefficient and the frictional coefficients according to the FMMM; **top** σ as a function of the friction coefficients of the anions with the membrane, R_{wm}, and **bottom** σ as a function of the transport number which is taken as a measure for R_w. Both graphs are calculated for the AWy bentonite with a CEC of 68 $cmol_c \cdot kg^{-1}$ and an average concentration of 0.5 $mol \cdot L^{-1}$ for porosities of 0.2, 0.5 and 0.8.

let R_{wm} decrease linearly between 0.1 and 0 in the porosity range of 0 and 0.4. Above a porosity of 0.4, R_{wm} was taken to be zero. This yields lower values of σ than calculated with a constant R_{wm} of 0.1 and corresponds more closely with the decrease in friction as the porosity of the membrane increases. The influence of the R's on the reflection coefficient increases for membranes with increasing porosity.

The decrease of the reflection coefficient whenever the major cation on the exchange complex is not Na^+ can be derived from the curve representing σ as a function of the transport number, t_0 (Figure 7.2). For example, values for t_0^{Ca} in the $CaCl_2$+H_2O system are typically above 0.42(Robinson & Stokes, 1959), thus $t_0^{Cl} = 0.58$, resulting in a lower σ for a membrane with Ca^{2+} as the major cation. The use of the cation transport number for calculation of σ can be confusing because the salt sieving effect is based on anion exclusion. Therefore, in Figure 7.2 the t_0^{Cl} in the $CaCl_2$+H_2O system should be used instead of the t_0^{Ca} to assess the influence of Ca^{2+} on the reflection coefficient.

Of the two models based on the Gouy–Chapman theory of the DDL the model by Kemper–Bresler can probably be best adjusted to incorporate the effect of divalent cations on the exchange complex. Bresler (1970; 1972) already studied the influence of mixed mono– and divalent ionic systems on the swelling pressure for interacting diffuse double layers.

7.4 IMPLICATIONS OF CHEMICAL OSMOSIS ON THE STORAGE OF CONTAMINATED SLUDGE

Since harbour sludge can act as a semipermeable membrane (Chapter 5) and hydrophobic contaminants do desorb under low convective flow regimes in these sediments (Chapter 6), the storage of contaminated sediments in sludge depots does not eliminate the risk of further dispersion in the environment.

Currently, the sludge layer in *De Slufter* approaches a thickness of 20 m. The water expelled from the sludge is present as a fresh/brackish layer on top, and a fresh/brackish lens in the salt water aquifer underneath the depot. Over time this lens will dissipate by diffusion and horizontal convective transport within the aquifer and its supply will run out as the depot becomes completely consolidated. The consolidated situation resembles our experimental simulation. The depot is designed to minimise the hydraulic pressure gradient across the sludge layer. Applying the average measured value for the reflection coefficient of BK (Table 5.3, p. 90) to a sludge layer with an average thickness of 20 m and a hydraulic conductivity of 10^{-9} $m{\cdot}s^{-1}$ —because of a lower consolidation grade than in our experimental samples— yields a water flux of

approximately 1.5 $mm \cdot y^{-1}$. This flux is in the same order of magnitude as the maximum water flux from a sludge in depot of 2 $mm \cdot y^{-1}$ allowed by Dutch legislation (VROM, 1993). Therefore, the tentative conclusion can be drawn that a minimisation of the hydraulic pressure gradient, as now is customary to the operation of the depot, does not automatically minimise the water flux. Separation of the relatively clean sand and the more contaminated clay fraction before storage in the depot as now is customary, will only enhance the semipermeable properties of the sludge stored, it will also reduce the hydraulic conductivity. This can result in a larger osmotic water flux than predicted here.

The fate of semipermeable sludge in depot

In the previous discussion several assumptions were made, the most important of which is the ideality of the sludge layer. Contrary to the assumption, semipermeability is not constant in time. In Chapter 5 it was shown that σ of one of the harbour sludge samples decreases in time. The reduction of ideality in time was already observed for bentonite samples (Demir, 1988; Whitworth & Fritz, 1994) and originates from the

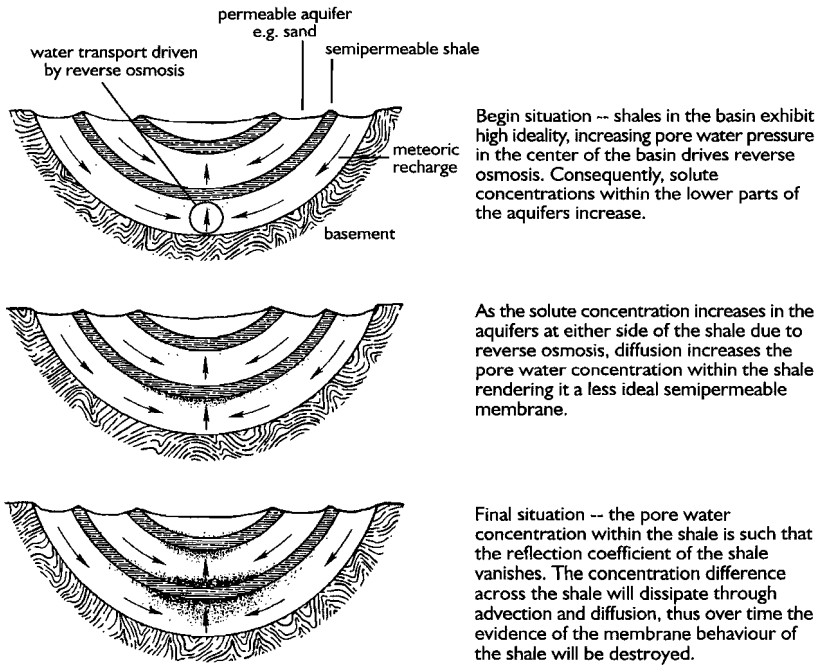

Figure 7.3 Conceptual model of the 'life cycle' of a shale with semipermeable properties in a geological setting (after Whitworth & Fritz, 1994).

samples' initial non–ideal behaviour. A natural semipermeable material goes through a 'life cycle' starting as a highly ideal membrane. Since ideality is less than 100 %, diffusion of solutes through the membrane will inevitably reduce its ideality ideal with time. The 'life cycle' will end when the pore water concentration in the membrane is sufficiently high that semipermeability is essentially absent. Given enough time, the chemical and hydraulic differences across the once semipermeable membrane will dissipate. This 'life cycle' was described by Whitworth and Fritz (1994) for a semipermeable shale in a large geological aquifer setting (Figure 7.3).

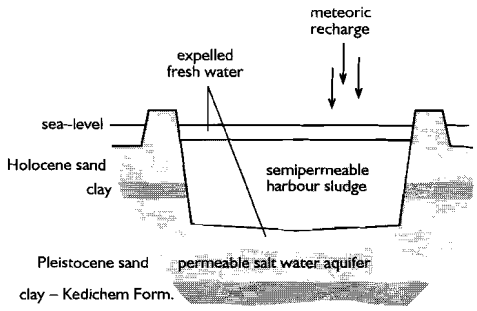

Initial situation – due to the consolidation of the sludge fresh water is expelled forming a fresh water layer on top and a lens in the salt water aquifer below the sludge.

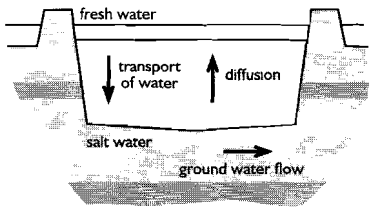

Steady-state – As the fresh water lens underneath the consolidated sludge layer dissipates due to diffusion and ground water flow, water transport will be induced as a result of the chemical gradient present. Diffusion will slowly render the sludge a less ideal semipermeable membrane

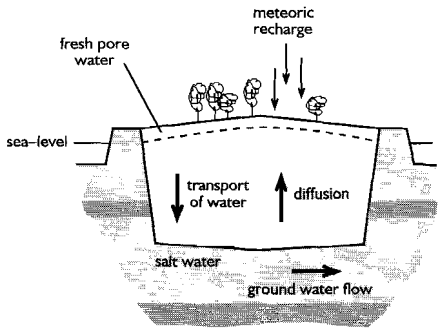

Final stage – When the depot is completely filled the sludge layer will be above sea-level; on top of the layer a recreational park will be built. However, as long as there is no impermeable layer between the protective soil cover and the sludge it will still act as a semipermable membrane, as is shown here.

Figure 7.4 Conceptual model of the stages of a contaminated harbour sludge with semipermeable properties in a setting similar to *De Slufter*, the Netherlands.

The possible 'life cycle' of a harbour sludge depot is different. A conceptual model involving chemical osmosis for a completely filled sludge depot like *De Slufter* is visualised in Figure 7.4. During and after filling the depot, the sludge will go through a consolidation stage in which water is expelled (Flohr, 1995). In this stage contaminants will be mobile and transported out of the depot. The horizontal water flux in the salt water aquifer will dissipate the brackish water lens underneath the depot. Consequently, salt will diffuse upward in the depot, whereas an osmotic gradient will transport water out of the depot into the aquifer. The water on top of the sludge layer will remain fresh to brackish as a result of rainfall and evaporation. It is in this stage that the initially high σ slowly drops. Given enough time, the system will reach a steady–state with the sludge having a low σ. In this situation the sludge will continue to act as a non–ideal semipermeable membrane over a substantial period of time, because of the constant flushing in the aquifer and refreshing of the water on top of the sludge.

One of the ultimate objectives for the depot includes a recreational park on top of the sludge layer which will lie above sea–level (Figure 7.4). This will, however, not drastically change the steady–state as the pore water in the top part of the layer will remain fresh by rainwater. Only the installation of a really impermeable layer between the sludge layer and the protective cover soil will eliminate any water flow and solute emission to the surrounding groundwater.

7.5 CONCLUDING REMARKS

Based on the model assumptions and other theoretical or practical considerations a range of conditions and properties can be given in which the models can be used. There are some possibilities discussed to tune the models for a closer approach of the conditions encountered in natural materials. Both the Fritz–Marine Membrane Model and the Groenevelt–Bolt model can only be used for certain porosity and/or concentration ranges. The Kemper–Bresler model appears to be valid over the entire porosity and concentration range encountered in geological systems. The model predicts relatively low reflection coefficients close to those measured in natural clayey materials in this and other studies.

Based on the observed semipermeability of the *Beerkanaal* sludge chemical osmosis in a harbour sludge depot like *De Slufter* is to be expected. A conceptual model is used in which the evolution of a sludge membrane is given. It is concluded that the water flux by osmosis can be in the same order of magnitude as the maximum allowed water flux in Dutch legislation. It is therefore likely that environmental

criteria of the depot will be exceeded. Because of the refreshing of the water on top and continous flushing of the salt water aquifer underneath the depot, the sludge layer can almost indefinitely act as a semipermeable membrane.

It is currently impossible to estimate or measure the contribution of chemical osmosis on water transport in a field situation. Due to the complex nature of coupled flow phenomena it is, in the author's opinion, not possible to determine exactly which fraction of a given flux is contributed by a hydraulic and by a chemical gradient. On a laboratory scale, however, the influences of coupled phenomena on transport mechanisms can be accurately separated and measured as was shown in this and other studies (e.g. Olsen, 1972; Elrick *et al.*, 1976; Yeung & Mitchell, 1993; Yeung, 1994, Soler, 1999). Experimental work in this area should be done to validate and increase the accuracy of the models, especially when the samples are 'real world mixtures' of clay minerals with different cations on the exchange complex. Experimental work in this field will also increase the awareness that water and solute transport is never governed by only one driving force.

Summary and general conclusions

Semipermeable properties of clayey natural materials can have a significant impact on a range of geological and geochemical processes on laboratory and field scale. The importance of chemical osmosis in semipermeable natural clays for transport of contaminants was first discussed in the Netherlands in relation to the environmental aspects of contaminated harbour sludge depots. One of the main depots, *De Slufter* near the Port of Rotterdam, is constructed in a salt water aquifer without a bottom liner. The clayey harbour sludge itself acts as a layer of low hydraulic conductivity, restricting advective transport of contaminants. However, the construction also enables the sludge layer to act as a semipermeable membrane.

The main objective of this study was to develop and apply instrumentation for the direct measurement of the semipermeability of materials like contaminated harbour sludge and other clayey materials under unconsolidated conditions.

In **Chapter 1** the origin of semipermeable behaviour of clayey materials is discussed within the framework of the diffuse double layer theory (DDL). A characteristic for the semipermeable properties of a material is its reflection coefficient (σ). Three models are introduced from which a reflection coefficient can be calculated. These models are:

- The Fritz–Marine Membrane Model (FMMM) based on the Donnan concept of the DDL (e.g. Fritz, 1986).
- A model formulated by Kemper (1972) and Bresler (1973) based on the Gouy–Chapman theory for a DDL.
- A model by Groenevelt and Bolt also based on the Gouy–Chapman concept of the DDL but modified for an immobile part in the DDL adjacent to a clay platelet (e.g. Bolt, 1982b).

These models are used throughout this thesis and their applicability are discussed on the basis of own experiments and reported laboratory and field studies on the semipermeable behaviour of natural clayey material. A comprehensive review of these studies is presented in Chapter 1.

In our experiments a commercially available Na–montmorillonite (bentonite) and contaminated harbour sludge samples were used. Their properties are analysed and described in **Chapter 2**. The harbour sludges were sampled at different locations in the Port of Rotterdam, the Netherlands, and reflect the different types of sludge that may be stored in permanent sludge depots. The sludge from the *Beerkanaal* contained a large clay size fraction with predominantly smectite and illite. Two third of the cation exchange complex (CEC) was occupied by mono–valent cations, theoretically making this sludge a highly ideal semipermeable membrane. The sludge from the *Beneden Merwede*–river contained a much smaller fraction of clay with mainly illite and some smectite. Its exchange complex is mainly occupied by calcium, making it a less ideal semipermeable membrane. Bentonite was included because its high CEC renders it a highly ideal semipermeable membrane.

The instrumentation developed to measure chemical osmosis is described in **Chapter 3**. The design criteria are formulated and an extended description and experimental procedures are given. It is one of the first designs used to study the semipermeable behaviour of natural materials in a flexible wall permeameter. The sample, with a thickness of approximately 2 mm, is connected to two stainless steel reservoirs that can be filled with solutions of different salt concentrations. Induced chemical osmosis is measured either by pressure transducers or by calibrated standpipes. An electrical conductivity cell monitors the effect of diffusion through the sample. The solutions in the reservoirs are kept homogeneous by a magnetically coupled gear pump. The entire apparatus is placed in a temperature controlled bench top chamber to eliminate the effects of thermo–osmosis, and of changes in thermal expansion. The apparatus also allows the determination of the hydraulic conductivity of the sample under identical conditions to those present in a chemical osmosis experiment.

Experiments of chemical osmosis in both loose and compacted samples of bentonite are described and discussed in **Chapter 4**. In three of the four samples chemical osmosis was observed and reflection coefficients could be measured. In the less compacted samples, which were also subjected to the highest chemical gradient, diffusion osmosis was observed. Diffusion osmosis is the transport of water by drag in response to the diffusion of solutes. In the more compacted bentonite with a relatively low chemical gradient this phenomenon was not observed. For all experiments the measured values of σ were lower than those estimated with the theoretical models. A literature survey on the semipermeability of bentonites revealed that the differences between experimental and theoretical values are not limited to our measurements. Two major causes for this difference are given; firstly, the model assumptions do not hold for the samples investigated, and secondly the concentrations in the bulk reservoirs during the experiment may deviate from those at the sample interface. The limitations

of the models are discussed and it is concluded that several model assumptions, in particular complete dispersion of the clay and complete occupation of the exchange complex by a monovalent cation, do not hold for most samples and experimental conditions. To assess the effect of diffusion and cation exchange for the compact bentonite a semi–infinite 1–D column was modelled using PHREEQC. The observed data could be fitted using a diffusion coefficient of NaCl between 10^{-12} and 10^{-13} $m^2 \cdot s^{-1}$. This low value results from the combined effect of the retardation by cation exchange and the osmotic counter flow.

In **Chapter 5** the results of the experiments on the two harbour sludge samples are described. For the first time semipermeable behaviour of clayey contaminated sediments is reported. For the harbour sludge from the *Beerkanaal* with a clay content of approximately 56 %, semipermeability was observed in two successive experiments. No semipermeable behaviour was observed for the sludge from the *Beneden Merwede*–river with a lower clay content (~26 %). As with the experiments on bentonites the measured reflection coefficients were lower than those obtained by the models. The model by Kemper–Bresler yields values nearest to those observed in our experimental work. A review on published data on predominantly shales supports this observation. These experiments also clearly showed that the reflection coefficient of a material is not an intrinsic value under the given conditions. During one of the experiments on the *Beerkanaal* sludge the deterioration of semipermeability was followed. As the experiment progresses, semipermeability decreases due to diffusion of salt into the clay resulting in a collapse of the double layer and subsequent flocculation of the material.

Chapter 6 discusses the desorption of PAH from both harbour sludges by advection in column experiments. When water is transported either by a hydraulic or a chemical gradient in a sludge layer, desorbing contaminants like PAH can be dispersed into the environment. Separation of liquid and solid phase for batches of sludge stored for more than 3 years by ultra–centrifugation at 4°C yielded equilibrium log K_{OC}–values. Temperature effects could not account for the observed differences with literature values. The differences are attributed to the contact time of PAH in the sediment. The laboratory data reported in the literature were obtained after short contact times, thus underestimating the actual log K_{OC}. Our values represent contact times in excess of three years and are therefore more representative for the field conditions. Log K_{OC}–values obtained from column elution experiments were slightly above those obtained from the batch experiments. During column elution of the *Beneden Merwede* sludge sorption equilibrium was absent for the lighter compounds. This is attributed to the presence of a large portion of immobile water in the columns. Elution in the *Beerkanaal* columns occurred at near sorption equilibrium although

pore water velocities were higher. Assuming that desorption is diffusion controlled, observed desorption in both materials could be explained. The nonequilibrium desorption in the *Beneden Merwede* sludge could be described by a diffusion limited model assuming spherical particles.

The experiments on bentonites and harbour sludges and the literature review showed a large difference between experimental and theoretical reflection coefficients. The applicability of the three models is discussed in **Chapter 7**. Based on the model assumptions and other theoretical or practical considerations, a range of conditions and properties are given in which the models can be used. Additionally, ways to tune the models for a closer approach of the conditions encountered in natural materials are discussed. It is concluded that both the FMMM and the Groenevelt–Bolt model can only be used for certain porosity and/or concentration ranges. The Kemper–Bresler model appears to be valid over the entire porosity and concentration range encountered in geological systems. The model predicts relatively low reflection coefficients close to those measured in natural clayey materials in this and other studies.

Based on the observed semipermeability of the *Beerkanaal* sludge, chemical osmosis in a harbour sludge depot like *De Slufter* is discussed. A conceptual model is used in which the evolution of a sludge membrane is given. It is concluded that the water flux by osmosis can be of the same order of magnitude as the maximum allowed water flux in Dutch legislation. It is therefore likely that environmental criteria of the depot will be exceeded. Because of the refreshing of the water on top and continuing flushing of the salt water aquifer underneath the depot, the sludge layer can almost indefinitely act as a semipermeable membrane. The construction of a park on top of the sludge layer as it rises above sea–level will not drastically change this situation as long as there is no geotextile between the protective cover soil and the sludge.

References

Abdul AS, Gibson TL & Rai DN (1990). Use of humic acid solution to remove organic contaminants from hydrogeological systems. *Environmental Science and Technology* **24**, 328–333.

Acar YB & Alshawabkeh AN (1993). Principles of electrokinetic remediation. *Environmental Science and Technology* **27**, 2638–2647.

Achari G, Chatterji S, Joshi RC & Bentley LR (1997). Effect of ion concentration on diffusion through clay. *Soil Science* **162**, 51–55.

Aiban SA & Znidarcic D (1989). Evaluation of the flow pump and constant head techniques for permeability measurements. *Geotechnique* **39**, 655–666.

Alexander J (1990). **A review of osmotic processes in sedimentary basins**. British Geological Survey, report no. WE/90/12, Nottingham, UK.

Allison LE (1965). Organic carbon. In: **Chemical and microbiological properties**, Vol. 2 (ed. CA Black). American Society of Agronomy, Madison WI, USA, 1367–1378.

Aylmore LAG, Sills ID & Quirk JP (1970). Surface area of homoionic illite and montmorillonite clay minerals as measured by the sorption of nitrogen and carbon dioxide. *Clays and Clay Minerals* **18**, 91–96.

Ball WP & Roberts PV (1991). Long–term sorption of halogenated organic chemicals by aquifer material: 2. Interparticle diffussion. *Environmental Science and Technology* **25**, 1237–1249.

Bantignies JL, Cartier dit Moulin C, Dexpert H, Flank AM & Williams G (1995). Asphaltene adsorption on kaolonite: Characterization by infrared microspectroscopy and X–ray absorption spectroscopy. *Comptes Rendus de L'Academie des Sciences. Serie 2* **320**, 699–706.

Bantignies JL, Cartier dit Moulin C & Dexpert H (1997). Wettability contrasts in kaolonite and illite clays: Characterization by infrared and X–ray adsorption spectroscopies. *Clays and Clay Minerals* **45**, 184–193.

Barbour SL & Fredlund DG (1989). Mechanisms of osmotic flow and volume change in clay soils. *Canadian Geotechnical Journal* **26**, 551–562.

Becker GF (1893). Quicksilver ore deposits. In: **Mineral resources of the United States for 1892** (ed. DT Day). United States Geological Survey, Washington DC, USA, 138–168.

Beigel C & Di Pietro L (1999). Transport of triticonazole in homogeneous soil columns: Influence of nonequilibrium sorption. *Journal of the Soil Science Society of America* **63**, 1077–1086.

Benson CH & Daniel DE (1990). Influence of clods on hydraulic conductivity of compacted clays. *Journal of Geotechnical Engineering* **116**, 1231–1248.

Benson CH & Trast JM (1995). Hydraulic conductivity of thirteen compacted clays. *Clays and Clay Minerals* **43**, 669–681.

Benzel WM & Graf DL (1984). Studies of smectite membrane behavior: importance of latter thickness and fabric at 20°C. *Geochimica et Cosmochimica Acta* **48**, 1769–1778.

Berry FAF (1969). Relative factors influencing membrane filtration effects in geological environments. *Chemical Geology* **4**, 295–301.

Berry FAF & Hanshaw BB (1960). Geological field evidence suggesting membrane properties of shales. *International Geological Congres. Report of the twenty–first session Norden*, Copenhagen, Denmark, 209.

Bishop JL, Pieters CM & Edwards JO (1994). Infrared spectroscopic analyses on the nature of water in montmorillonite. *Clays and Clay Minerals* **42**, 702–716.

Bjerrum L, Moum J & Eide O (1967). Application of electro–osmosis on a foundation problem in Norwegian quick clay. *Geotechnique* **16**, 214–235.

Blake GR (1965). Particle density. In: **Chemical and microbiological properties**, Vol. 1 (ed. CA Black). American Society of Agronomy, Madison WI, USA, 371–373.

Bolt GH (1955). Analysis of the validity of the Gouy–Chapman theory of the electric double layer. *Journal of Colloid Science* **10**, 206–219.

Bolt GH (1982a). Surface interaction between the soil solid phase and the soil solution. In: **Soil chemistry: A. Basic elements**, Developments in Soil Science Vol. 5a (ed. GH Bolt). Elsevier, Amsterdam, the Netherlands, 43–53.

Bolt GH (1982b). Electrochemical phenomena in soil and clay systems. In: **Soil chemistry: B. Physico–chemical models**, Developments in Soil Science Vol. 5b (ed. GH Bolt). Elsevier, Amsterdam, the Netherlands, 387–432.

Bolt GH & Miller RD (1955). Compression studies of illite suspensions. *Proceedings of the Soil Science Society of America* **19**, 285–288.

Borchart GA (1987). Montmorillonite and other smectite minerals. In: **Minerals in soil environments** (ed. JB Dixon & SB Weed). Soil Science Society of America, Madison WI, USA, 293–330.

Boulegue J, Bariac T, Mariotti A & De Kersabiec AM (1990). Hyperfiltration–osmosis effects in compacting sediments: isotopic and chemical changes in pore waters. *Chemical Geology* **84**, 352–353.

Boynton SS & Daniel DE (1985). Hydraulic conductivity tests on compacted clays. *Journal of Geotechnical Engineering* **111**, 465–478.

Bresler E (1970). Numerical solution of the equation for interacting diffuse double layers in mixed ionic systems with nonsymmetrical electrolytes. *Journal of Colloid and Interface Science* **22**, 278–283.

Bresler E (1972). Interacting diffuse layers in mixed mono–divalent ionic systems. *Proceedings of the Soil Science Society of America* **36**, 891–896.

Bresler E (1973). Anion exclusion and coupling effects in nonsteady transport through unsaturated soils: I. Theory. *Proceedings of the Soil Science Society of America* **37**, 663–669.

Briggs, LJ (1902). Filtration of suspended clay from solutions, *United States Bureau of Soils Bulletin* 19, 31-40.

Brusseau ML, Jessup RE & Rao PSC (1991a). Nonequilibrium sorption of organic chemicals: Elucidation of rate–limiting processes. *Environmental Science and Technology* **25**, 134–142.

Brusseau ML, Larsen T & Christensen TH (1991b). Rate–limited sorption and nonequilibrium transport of organic chemicals in low organic carbon aquifer materials. *Water Resources Research* **27**, 1137–1145.

Camerlenghi AA (1988). **Sub–surface dissolution of evaporites in the Eastern Mediterranean Sea**. M.Sc.–thesis, Texas A&M University, USA.

Campbell DJ (1985). **Fractionation of stable chlorine isotopes during transport through semipermeable membranes**. M.Sc.–thesis, University of Arizona, USA.

Caplan SR & Mikulecky DC (1966). Transport processes in membranes. In: **Ion Exchange. A serie of advances**, Vol. 1 (ed. JA Marinsky). Marcel Dekker, New York NY, 1–64.

Cey BD (1999). **Osmotic flow through a cretaceous clay in Southern Saskatchewan, Canada**. M.Sc.–thesis, University of Saskatchewan, Canada.

Chiou CT, Porter LJ & Schmedding DW (1983). Partition equilibria of nonionic organic compounds between soil organic matter and water. *Environmental Science and Technology* **17**, 227–231.

Choi JW & Oscarson DW (1996). Diffusive transport through compacted Na– and Ca–bentonite. *Journal of Contaminant Hydrology* **22**, 189–202.

Chung HI & Kang BH (1999). Lead removal from contaminated marine clay by electrokinetic soil decontamination. *Engineering geology* **53**, 139–150.

Churchman GJ & Burke CM (1991). Properties of subsoils in relation to various measures of surface area and water content. *Journal of Soil Science* **42**, 463–478.

Churchman GJ, Burke CM & Parfitt RL (1991). Comparison of various methods for the determination of specific surfaces of subsoils. *Journal of Soil Science* **42**, 449–461.

Coplen TB & Hanshaw BB (1973). Ultrafiltration by a compacted clay membrane: I. Oxygen and hydrogen isotopic fractionation. *Geochimica et Cosmochimica Acta* **37**, 2295–2310.

Cornelissen G (1999). **Mechanisms and consequences of slow desorption of organic compounds from sediments**. Ph.D.–thesis, Universiteit van Amsterdam, the Netherlands.

Cornelissen G, Van Zuilen H & Van Noort PCM (1999). Particle size dependence of slow desorption of in situ PAHs from sediments. *Chemosphere* **38**, 2369–2380.

Crank J (1975). **The mathematics of diffusion**. Clarendon Press, Oxford, UK.

Crunkilton RL & DeVita WM (1997). Determination of aqueous concentrations of polycyclic aromatic hydrocarbons (PAHs) in an urban stream. *Chemosphere* **35**, 1447–1463.

Daniel DE, Trautwein SJ, Boynton SS & Foreman DE (1984). Permeability testing with flexible–wall permeameters. *Geotechnical Testing Journal* **7**, 113–122.

De Haven JC (1982). Lowland underground water as a physicochemical system. In: **Tweede Nota Waterhuishouding**. SDU, The Hague, the Netherlands, 300–315.

De Maagd PG–J (1996). **Polycyclic aromatic hydrocarbons: Fate and effects in the aquatic environment**. Ph.D.–thesis, Universiteit Utrecht, the Netherlands.

De Maagd PG–J, Ten Hulscher DTEM, Van den Heuvel H, Opperhuizen A & Sijm DTHM (1998). Physicochemical properties of polycyclic aromatic hydrocarbons: aqueous solubilities, n–octanol/water partition coefficients, and Henry's law constants. *Environmental Toxicology and Chemistry* **17**, 251–257.

De Sitter LU (1947). Diagenesis of oil–field brines. *Bulletin of the American Association of Petroleum Geologists* **31**, 2030–2040.

Deer WA, Howie RA & Zussman J (1992). **An introduction to the rock–forming minerals**. Longman, Harlow, UK.

Demir I (1988). Studies of smectite membrane behavior: Electrokinetic, osmotic, and isotopic fractionation. *Geochimica et Cosmochimica Acta* **52**, 727–737.

DeRosa G, Whitworth TM & Lueth VW (1997). **Experimental evidence for potential natural remediation of heavy metal plumes**. *WERC/HSRC '97 Joint Conference on the Environment*, Albuquerque NM, USA, 285–288.

Domenico PA & Schwartz FW (1990). **Physical and chemical hydrogeology**. Wiley, New York NY, USA.

Dunnivant FM, Jardine PM, Taylor DL & McCarthy JF (1992). Transport of naturally occuring dissolved organic carbon in laboratory columns containing aquifer material. *Journal of the Soil Science Society of America* **56**, 437–444.

Elrick DE, Smiles DE, Baumgartner N & Groenevelt PH (1976). Coupling phenomena in saturated homo–ionic montmorillonite: I. Experimental. *Journal of the Soil Science Society of America* **40**, 490–491.

Enfield CG, Bengtsson G & Lindqvist R (1989). Influence of macromolecules on chemical transport. *Environmental Science and Technology* **23**, 1278–1286.

Everwijn TS, Hoffman FR, Ramhit H, Schultz CE & Verwaart JWA (1992). **Bodemreinigingstechnieken**. Boom, Amsterdam, the Netherlands.

Feller C, Schouller E, Thomas F, Rouiller J & Herbillon AJ (1992). N_2–BET specific surface areas of some low activity clay soils and their relationships with secondary constituents and organic matter contents. *Soil Science* **153**, 293–299.

Flohr PM (1995). Isolatie 'Slufter' voldoet. *Land + Water* **12**, 27–28.

Fritz SJ (1986). Ideality of clay membranes in osmotic processes: a review. *Clays and Clay Minerals* **34**, 214–223.

Fritz SJ & Marine IW (1983). Experimental support for a predictive osmotic model of clay membranes. *Geochimica et Cosmochimica Acta* **47**, 1515–1522.

Fritz SJ & Eady CD (1985). Hyperfiltration–induced precipitation of calcite. *Geochimica et Cosmochimica Acta* **49**, 761–768.

Fritz SJ & Whitworth TM (1994). Hyperfiltration–induced fractionation of lithium isotopes: Ramifications relating to representativeness of aquifer sampling. *Water Resources Research* **30**, 225–235.

Fritz SJ, Hinz DW & Grossman EL (1987). Hyperfiltration–induced fractionation of carbon isotopes. *Geochimica et Cosmochimica Acta* **51**, 1121–1134.

Gaber HM, Inskeep WP, Comfort SD & Wraith JM (1995). Nonequilibrium transport of atrazine through large intact soil cores. *Journal of the Soil Science Society of America* **59**, 60–67.

Gillham RW, Robin MJL, Dytynyshyn DJ & Johnston HM (1984). Diffusion of nonreactive and reactive solutes through fine–grained barrier materials. *Canadian Geotechnical Journal* **21**, 541–550.

Graf DL (1983). Chemical osmosis, reverse chemical osmosis and the origin of subsurface brines. *Geochimica et Cosmochimica Acta* **46**, 1431–1448.

Grathwohl P & Reinhard M (1993). Desorption of trichloroethylene in aquifer material: Rate limitation at the grain scale. *Environmental Science and Technology* **27**, 2360–2366.

Grathwohl P, Gewald T, Pyka W & Schüth C (1993). Determination of pollutant release rates from contaminated aquifer materials. *Contaminated soil '93* (ed. F Arendt, GJ Annokkée, R Bosman & WJ Van der Brink). Kluwer, Dordrecht, the Netherlands, 175–184

Grathwohl P, Pyka W & Merkel P (1994). Desorption of organic pollutants (PAHs) from contaminated aquifer material. *AIRH Symposium on transport and reactive processes in aquifers*, Zürich, Switzerland, 469–474.

Greene–Kelly R (1964). The specific surface areas of montmorillonites. *Clay Mineral Bulletin* **5**, 392–400.

Grim RE (1953). **Clay mineralogy**. McGraw–Hill, New York NY, USA.

Grim RE & Güven N (1978). **Bentonites. Geology, mineralogy, properties and uses**. Elsevier, Amsterdam, the Netherlands.

Groenevelt PH & Bolt GH (1969). Non–equilibrium thermodynamics of the soil–water system. *Journal of Hydrology* **7**, 358–388.

Groenevelt PH & Bolt GH (1972). Permiselective properties of porous materials as calculated from diffuse double layer theory. *First Symposium of Fundamental Transport Phenomena*, Haifa, Israel, 241–255.

Hanshaw BB (1962). **Membrane properties of compacted clays**. Ph.D.–thesis, Harvard University, USA.

Hanshaw BB & Hill GA (1969). Geochemistry and hydrodynamics of the Paradox Basin region Utah, Colorado and New Mexico. *Chemical Geology* **4**, 263–294.

Hanshaw BB & Zen E–A (1965). Osmotic equilibrium and overthrust faulting. *Bulletin of the Geological Society of America* **76**, 1379–1386.

Hanshaw BB & Coplen TB (1973). Ultrafiltration by a compacted clay membrane: II. Sodium ion exclusion at various ionic strenghts. *Geochimica et Cosmochimica Acta* **37**, 2311–2327.

Haydon PR & Graf DL (1986). Studies of smectite membrane behavior: temperature dependence, 20–80°C. *Geochimica et Cosmochimica Acta* **50**, 115–121.

He Y, Yediler A, Sun T & Kettrup A (1995). Adsorption of fluoranthrene on soil and lava: Effects of the organic carbon contents of adsorbents and temperature. *Chemosphere* **30**, 141–150.

Hegeman WJM, Van der Weijden CH & Loch JPG (1995). Sorption of benzo(a)pyrene and phenanthrene on suspended harbour sediment as a function of suspended sediment concentration and salinity: A laboratory study using the cosolvent partition coefficient. *Environmental Science and Technology* **29**, 363–371.

Hill RL & King LD (1982). A permeameter which eliminates boundary flow errors in saturated hydraulic conductivity measurements. *Proceedings of the Soil Science Society of America* **46**, 877–880.

Horseman ST, Higgo JJW, Alexander J & Harrington JF (1996). **Water, gas and solute movement through argillaceous media**. Nuclear Energy Agency, Organisation for Economic Co–operation and Development, report no. CC–96/1, Paris, France.

Hosterman JW & Patterson SH (1992). **Bentonite and Fuller's Earth resources of the United States**. United States Geological Survey, Washington DC, USA.

Karickhoff SW, Brown DS & Scott TA (1979). Sorption of hydrophobic pollutants on natural sediments. *Water Research* **13**, 241–248.

Ishiguro M, Matsuuro T & Detellier C (1995). Reverse osmosis seperation for a montmorillonite membrane. *Journal of Membrane Science* **107**, 87–92.

Kaštelan–Kunst L, Košutic K, Dananic V & Kunst B (1997). FT30 membranes of characterized porosities in the reverse osmosis organics removal from aqueous solutions. *Water Research* **31**, 2878–2884.

Katchalsky A & Curran PF (1965). **Nonequilibrium thermodynamics in biophysics**. Harvard University Press, Cambridge, MA, USA.

Keijzer ThJS, Loch JPG & Weststrate FA (1994). **Experimentele bepaling van chemische osmose in kleiige monsters**. Universiteit Utrecht, the Netherlands.

Keijzer ThJS, Kleingeld PJ & Loch JPG (1997). Chemical osmosis in compacted clayey material and the prediction of water transport. *Geoenvironmental Engineering. Contaminated ground: fate of pollutants and remediation* (RN Yong & HR Thomas). Cardiff, Wales, UK, 199–204.

Keijzer ThJS, Kleingeld PJ & Loch JPG (1999). Chemical osmosis in compacted clayey material and the prediction of water transport. *Engineering Geology* **53**, 151–159.

Kemper WD (1961). Movement of water as affected by free energy and pressure gradients: II. Experimental analysis of porous systems in which free energy and pressure gradients act in opposite directions. *Proceedings of the Soil Science Society of America* **25**, 260–265.

Kemper WD (1972). Isothermal flow of nonhomogeneous aqueous solutions. In: **Soil water** (ed. DR Nielsen, RD Jackson, JW Cary & DD Evans). Soil Science Society of America, Madison WI, USA, 121–154.

Kemper WD & Rollins JB (1966). Osmotic efficiency coefficients across compacted clays. *Proceedings of the Soil Science Society of America* **30**, 529–534.

Kemper WD & Van Schaik JC (1966). Diffusion of salts in clay–water system. *Proceedings of the Soil Science Society of America* **30**, 534–540.

Kemper WD & Quirk JP (1972). Ion mobilities and electric charge of external clay surfaces inferred from potential differences and osmotic flow. *Proceedings of the Soil Science Society of America* **36**, 426–433.

Kemper WD, Maasland DEL & Porter LK (1964). Mobility of water adjacent to mineral surfaces. *Proceedings of the Soil Science Society of America* **28**, 164–167.

Kharaka YK (1973). Retention of dissolved constituents of waste by geological membranes. *Second International Symposium on Underground Waste Management and Artificial Recharge*, New Orleans MI, USA, 420–435.

Kharaka YK & Berry FAF (1973). Simultaneous flows of water and solutes through geological membranes: I. Experimental investigation. *Geochimica et Cosmochimica Acta* **37**, 2577–2603.

Kharaka YK & Smalley WC (1976). Flow of water and solutes through compacted clays. *Bulletin of the American Association of Petroleum Geologists* **60**, 973–980.

Kicinski H–G (1992). PAH–Festphasenextraction aus Wasserproben (Trinkwasser und maessig belastetes Oberflachenwasser) durch Hyaminzusatz. *Zeitschrift für Wasser und Abwasserungs Forschung* **25**, 289–294.

Knight WC (1898). Bentonite. *The Engineering and Mining Journal* **66**, 491.

Kookana RS, Schuller RD & Aylmore LAG (1993). Simulation of simazine transport through soil columns using time–dependent sorption data measured under flow conditions. *Journal of Contaminant Hydrology* **14**, 93–115.

Kruyt HR & Overbeek JThG (1965). **Inleiding tot de fysische chemie**. HJ Paris, Amsterdam, the Netherlands.

Kuijper C, Cornellise JM & Winterwerp JC (1990). **Cohesive sediments**. Delft Hydraulics, Delft, the Netherlands.

Letey J, Kemper WD & Noonan L (1969). The effect of osmotic pressure gradients on water movements in unsaturated soils. *Proceedings of the Soil Science Society of America* **33**, 15–18.

Li Y–H & Gregory S (1974). Diffusion of ions in sea water and in deep–sea sediments. *Geochimica et Cosmochimica Acta* **38**, 703–714.

Liu H & Amy G (1993). Modeling partitioning and transport interactions between natural organic matter and polynuclear aromatic hydrocarbons in groundwater. *Environmental Science and Technology* **27**, 1553–1562.

Loch JPG (1996). Behaviour and fate of organic contaminants in soil and groundwater. In: **Soil pollution and soil protection** (ed. HFAM de Haan & MI Visser–Reyneveld). Wageningen, the Netherlands, 181–199.

Loch JPG & Keijzer ThJS (1996). Chemical osmosis in contaminated clayey materials. *1996 V.M. Goldschmidt Conference*, Heidelberg, Germany, 367.

Mackay D, Shiu WY & Ma KC (1992). **Illustrated handbook of physical–chemical properties and environmental fate for organic chemicals**. Lewis, London, UK.

Marcus Y (1997). **Ion properties**. Marcel Dekker, New York NY, USA.

Marine IW & Fritz SJ (1981). Osmotic model to explain anomalous hydraulic heads. *Water Resources Research* **17**, 73–82.

Maxin CR & Kögel–Knabner I (1995). Partitioning of polycyclic aromatic hydrocarbons (PAH) to water–soluble soil organic matter. *European Journal of Soil Science* **46**, 193–204.

McIntyre DS, Cunningham RB, Vatanakul V & Stewart GA (1979). Measuring hydraulic conductivity in clay soils: methods, techniques and errors. *Soil Science* **128**, 171–183.

McKelvey JG & Milne IH (1962). The flow of salt solution through compacted clay. *Clays and Clay Minerals* **9**, 248–259.

McNeal BL & Reeve RC (1964). Elimination of boundary flow errors in laboratory hydraulic conductivity measurements. *Proceedings of the Soil Science Society of America* **28**, 713–714.

Merten U (1966). **Desalination by reverse osmosis**. MIT Press, London, UK.

Milne IH, McKelvey JG & Trump RP (1964). Semi–permeability of bentonite membranes to brines. *Bulletin of the American Association of Petroleum Geologists* **48**, 103–105.

Mitchell JK (1993). **Fundamentals of soil behavior**. Wiley, New York NY, USA.

Neuzil CE (1986). Groundwater flow in low–permeability environments. *Water Resources Research* **22**, 1163–1195.

Neuzil CE (1994). Characterization of flow properties, driving forces, and pore–water chemistry in the ultra low permeability Pierre Shale, North America. In: **OECD Documents. Disposal of radioactive waste**. Nuclear Energy Agency, Organisation for Economic Co–operation and Development, Nottingham, UK, 65–74.

Neuzil CE (1998). Is osmosis important in the subsurface? Evidence from an in situ experiment. *Abstracts with Programs* **30**, 172.

Neuzil CE (2000). Osmotic generation of 'anomalous' fluid pressures in geological environments. *Nature* **403**, 182–184.

Olsen HW (1969). Simultaneous fluxes of liquid and charge in saturated kaolinite. *Proceedings of the Soil Science Society of America* **33**, 338–344.

Olsen HW (1972). Liquid movement through kaolinite under hydraulic, electric and osmotic gradients. *The American Association of Petroleum Geologists Bulletin* **56**, 2022–2028.

Olsen HW, Nichols RW & Rice TL (1985). Low gradient permeability measurements in a triaxial system. *Geotechnique* **35**, 145–157.

Olsen HW, Rice TL & Nichols RW (1988a). Measuring effects of permeant composition on pore–fluid movement in soil. In: **Ground–water contamination: field methods**, ASTM STP 963 (ed. AG Collins & AL Johnson). American Society of Testing and Materials, Philadelphia PA, USA, 331–342.

Olsen HW, Morin RH & Nichols RW (1988b). Flow pump applications in triaxial testing. In: **Advanced triaxial testing of soil and rock**, ASTM STP 977 (ed. RT Donaghe, RC Chaney & ML Silver). American Society for Testing and Materials, Philadelphia PA, USA, 68–81.

Olsen HW, Yearsley EN & Nelson KR (1989). Chemical causes of groundwater movement. In: **Groundwater contamination. Proceedings of the 3rd IAHS Scientific Assembly**, IAHS Publication 185 (ed. LM Abriola). IAHS, Baltimore MA, USA, 65–72.

Olsen HW, Yearsley EN & Nelson KR (1990). Chemico–osmosis versus diffusion–osmosis. In: **Transportation Research Record no. 1288. Soils, Geology and Foundations**. Washington DC, USA, 15–22.

Osborne MJ & Swarbrick RE (1997). Mechanisms for generating overpressure in sedimentary basins: A reevaluation. *The American Association of Petroleum Geologists Bulletin* **81**, 1023–1041.

Oscarson DW, Hume HB, Sawatsky NG & Cheung SCH (1992). Diffusion of iodine in compacted bentonite. *Journal of the Soil Science Society of America* **56**, 1400–1406.

Padmanabhan E & Mermut AR (1995). The problem of expressing the specific surface areas of clay fractions. *Clays and Clay Minerals* **43**, 237–245.

Parker JC & Van Genuchten MT (1984). **Determining transport parameters from laboratory and field tracer experiments**. U.S. Salinity Laboratory, Bulletin 84–3, Riverside CA, USA.

Parkhurst DL (1995). **User's guide to PHREEQC – A computer program for speciation, reaction path, advective–transport, and inverse geochemical calculations**. US Geological Survey, Water Resources Investigations Report no. 95–4227, Lakewood CO, USA.

Petersen LW, Moldrup P, Jacobsen OH & Rolsten DE (1996). Relations between specific surface area and soil physical and chemical properties. *Soil Science* **161**, 9–21.

Phillips FM & Bentley HW (1987). Isotopic fractioning during ion filtration: I. Theory. *Geochimica et Cosmochimica Acta* **51**, 683–695.

Puchelt H & Bergfeldt B (1992). Major and trace element concentrations in waters entrifuged from unsaturated soils. *Proceedings of the 7th international symposium on water–rock interaction. Vol. 1, Low temperature environments* (ed. YK Kharaka & AS Maest). Park City UT, USA, 751–752.

Robinson RA & Stokes RH (1959). **Electrolyte solutions**. Butterworths, London, UK.

Russell WL (1933). Subsurface concentration of chloride brines. *Bulletin of the American Association of Petroleum Geologists* **17**, 1213–1228.

Schrap SM & Opperhuizen A (1992). On the contradictions between experimental sorption data and the sorption partitioning model. *Chemosphere* **24**, 1259–1282.

Schüth C & Grathwohl P (1994). Nonequilibrium transport of PAHs: A comparison of column and batch experiments. *AIRH Symposium on transport and reactive processes in aquifers*, Zürich, Switzerland, 143–148.

Schwarzenbach RP, Gschwend PM & Imboden DM (1993). **Environmental organic chemistry**. Wiley, New York NY, USA.

Shackelford CD (1991). Laboratory diffusion testing for waste disposal – A review. *Journal of Contaminant Hydrology* **7**, 177–217.

Shackelford CD & Daniel DE (1991). Diffusion in saturated soil. I: Background. *Journal of Geotechnical Engineering* **117**, 467–484.

Soler JM (1999). **Coupled transport phenomena in the Opalinus Clay: Implications for radionuclide transport**. Paul Scherrer Institute, report no. 99–07, Villingen, Switzerland.

Sposito G (1989). **The chemistry of soils**. Oxford University Press, New York NY, USA.

Srasra E, Bergaya F & Fripiat JJ (1994). Infrared spectroscopy study of tetrahedral and octahedral substitutions in an interstratified illite–smectite clay. *Clays and Clay Minerals* **42**, 237–241.

Stigliani WM, Jaffe PR & Anderberg S (1993). Heavy metal pollution in the Rhine basin. *Environmental Science and Technology* **27**, 786–793.

Sun L, Perdue EM & McCarthy JF (1995). Using reverse osmosis to obtain organic matter from surface and ground waters. *Water Research* **29**, 1471–1477.

Tavenas F, Leblond P, Jean P & Leroueil S (1983a). The permeability of natural soft clays. Part I: Methods of laboratory measurements. *Canadian Geotechnical Journal* **20**, 629–644.

Tavenas F, Leblond P, Jean P & Leroueil S (1983b). The permeability of natural soft clays. Part II: Permeability characteristics. *Canadian Geotechnical Journal* **20**, 645–660.

Totsche KU, Danzer J & Kögel-Knabner I (1997). Dissolved organic matter enhanced retention of polycyclic aromatic hydrocarbons in soil miscible displacement experiments. *Journal of Environmental Quality* **26**, 1090–1100.

Van Beek CGEM & Pal RAJ (1978). The influence of cation exchange and gypsum solubility on the transport of sodium, calcium and sulphate through soils. *Journal of Hydrology* **36**, 133–142.

Van Cauwenberghe L (1997). **Electrokinetics**. Ground Water Remediation Technologies Analysis Center, report no. TO–97–03, Pittsburgh PA, USA.

Van den Berg GA & Loch JPG (1993). **De chemie van verontreinigd baggerslib in depot. Een kennisinventarisatie**. Ministerie van Verkeer en Waterstaat, Directoraat Generaal Rijkswaterstaat DFl Flevoland & DWW Delft, Flevobericht 342, Lelystad, the Netherlands.

Van Olphen H (1963). **Clay colloid chemistry**. John Wiley & Sons, London, UK.

Van Reeuwijk LP (1995). **Procedures for soil analysis**. International Soil Reference and Information Centre, Wageningen, the Netherlands.

Van Zoest R & Van Eck GTM (1993). Historical input and behaviour of hexachlorobenzene, polychlorinated biphenyls and polycyclic aromatic hydrocarbons in two dated sediment cores from the Scheldt estuary, SW Netherlands. *Marine Chemistry* **44**, 95–103.

Veder C (1979). **Rutschungen und ihre Sanierung**. Springer Verlag, Vienna, Austria.

VROM (1993). **Beleidsstandpunt verwijdering baggerspecie**. Ministerie van VROM, Tweede Kamer der Staten Generaal, vergaderjaar 1993–1994, 23450 nr. 1, The Hague, the Netherlands.

Walter T, Ederer HJ, Forst C & Stieglitz L (2000). Sorption of selected polycyclic aromatic hydrocarbons on soils in oil–contaminated systems. *Chemosphere* **41**, 387–397.

Warkentin BP, Bolt GH & Miller RD (1957). Swelling pressure of montmorillonite. *Proceedings of the Soil Science Society of America* **21**, 495–497.

Whitworth TM (1993). **Hyperfiltration–induced isotopic fractionation: mechanisms and role in the subsurface**. Ph.D.–thesis, Purdue University, USA.

Whitworth TM & Fritz SJ (1994). Electrolyte induced solute permeability effects in compacted smectite membranes. *Applied Geochemistry* **9**, 533–546.

Whitworth TM & DeRosa G (1997). **Geological membrane controls on saturated zone heavy metal transport**. New Mexico Water Resourses Research Insitute, WRRI Technical Completion Report No. 303, Las Cruses NM, USA.

Wilkens BJ (1995). **Evidence of groundwater contamination by heavy metals through soil passage under acidifying conditions**. *Geologica Ultraiectina* **129**, Ph.D.–thesis, Universiteit Utrecht, the Netherlands.

Wood WW (1976). A hypothesis of ion filtration in a potable–water aquifer system. *Ground Water* **14**, 233–244.

Wu S–C & Gschwend M (1986). Sorption kinetics of hydrophobic organic compounds to natural sediments and soils. *Environmental Science and Technology* **20**, 717–725.

Yearsley EN (1989). **Transport properties and coupled flow phenomena in Salton Sea Scientific Drilling Program Cores**. M.Sc.–thesis, Colorado School of Mines, Golden CO, USA.

Yeung AT (1990). Coupled flow equations for water, electricity and ionic contaminants through clayey soils under hydraulic, electrical and chemical gradients. *Journal of Non–Equilibrium Thermodynamics* **15**, 247–267.

Yeung AT (1994). Effects of electro–kinetic coupling on the measurements of hydraulic conductivity. In: **Hydraulic conductivity and waste contaminant transport in soils**, ASTM STP 1142 (ed. DE Daniel & SJ Trautwein). American Society of Testing and Materials, Philadelphia PA, USA, 569–585.

Yeung AT & Mitchell JK (1993). Coupled fluid, electrical and chemical flows in soil. *Geotechnique* **43**, 121–134.

Yeung AT & Datla S (1995). Fundamental formulation of electrokinetic extraction of contaminants from soil. *Canadian Geotechnical Journal* **32**, 569–583.

Yeung AT, Sadek SM & Mitchell JK (1992). A new apparatus for the evaluation of electro–kinetic processes in hazardous waste management. *Geotechnical Testing Journal* **15**, 207–216.

Young A & Low PF (1965). Osmosis in argillaceous rocks. *Bulletin of the American Association of Petroleum Geologists* **49**, 1004–1008.

Symbols and abbreviations

Symbols

a_w	activity of water		
A	cross sectional area of a sample		m^2
b	water film thickness		m
c_i	initial concentration of a solute in a RO experiment		$mol \cdot L^{-1}$
c_e	concentration of a solute in the effluent of a RO experiment		$mol \cdot L^{-1}$
$\overline{c}_s$	average solute concentration across a membrane in the FMMM		$mol \cdot m^{-3}$
c_0	concentration of a solute in the equilibrium solution		$mol \cdot L^{-1}$
c_w	concentration of a PAH in the aqueous phase		$g \cdot L^{-1}$
C	concentration of a solute in a BTC		$mol \cdot L^{-1}$
$\overline{C}_a$	anion concentration in the membrane pores in the FMMM		$mol \cdot m^{-3}$
$\overline{C}_c$	cation concentration in the membrane pores in the FMMM		$mol \cdot m^{-3}$
C_0	initial concentration of a solute in a BTC		$mol \cdot L^{-1}$
d_l	thickness of a water film on a charged surface		m
D	diffusion–dispersion coefficient		$m^2 \cdot s^{-1}$
D_0	diffusion coefficient of a solute in the free solution		$m^2 \cdot s^{-1}$
D^{app}	apparent diffusion coefficient		$m^2 \cdot s^{-1}$
$D^{\star}$	effective diffusion coefficient		$m^2 \cdot s^{-1}$
E	filtration efficiency from the TMS		%
f_{OC}	fraction organic carbon of a soil or sediment		
F	Faraday constant	$96.4853 \cdot 10^3$	$C \cdot mol^{-1}$
g	gravitational constant	9.8066	$m \cdot s^{-2}$
H_s^e	enthalpy		$J \cdot mol^{-1}$
i	hydraulic pressure gradient		
I_0	ionic strength of the equilibrium solution		$mol \cdot m^{-3}$
J_i	flux of the component i		$mol \cdot m^{-2} \cdot s^{-1}$
J_s	flux of the solute		$mol \cdot m^{-2} \cdot s^{-1}$
J_v	flux of the solvent		$m \cdot s^{-1}$

J_w	water flux		$m \cdot s^{-1}$
K_d	distribution coefficient of a compound between the solid phase and the aqueous solution; K_d^{eq} represents the value at equilibrium		$dm^3 \cdot kg^{-1}$
K_h	hydraulic conductivity		$m \cdot s^{-1}$
K_s	measure for the salt exclusion properties in the FMMM		
K_{OC}	distribution coefficient normalised on the fraction organic carbon of a compound; K_{OC}^{eq} represents the value at equilibrium; K_{OC}^{app} represents the apparent value		$dm^3 \cdot kg^{-1}$
K_{OW}	distribution coefficient of a compound between octanol and water, a measure of hydrophobicity		
L	length of a column or length of a diffusional path		m
L_{ii}	conductivity coefficient of component i resulting from driving force i		
L_{ij}	coupling coefficient of component i resulting from driving force j		
L_e	effective length of a diffusional path		m
L_p	hydraulic permeability coefficient		$m^3 \cdot N^{-1} \cdot s^{-1}$
m	molality		$mol \cdot kg^{-1}$
M	molarity		$mol \cdot L^{-1}$
M_0	initial content of a solute in a sphere		$g \cdot g^{-1}$
n	porosity		$m^3 \cdot m^{-3}$
n_0	concentration of ions in the equilibrium solution		$ions \cdot m^{-3}$
N_A	Avogadro constant	$6.02214 \cdot 10^{23}$	mol^{-1}
p	hydraulic pressure		Pa
P_c	Peclet number		
q	desorbing contaminant flux		$g \cdot g^{-1} \cdot s^{-1}$
Q_h	hydraulic flux		$m \cdot s^{-1}$
Q_s	solute flux		$mol \cdot s^{-1}$
r	radius of a sphere or aggregate		m
R	gas constant	8.31451	$J \cdot K^{-1} \cdot mol^{-1}$
R_m	ratio of frictional coefficients of the anions and cations with the membrane wall in the FMMM		
R_w	ratio of frictional coefficients of the anions and cations with the water in the membrane in the FMMM		
R_{wm}	ratio of frictional coefficients of the anions with the matrix and the water in the membrane in the FMMM		
S	slope of a breakthrough curve at $C / C_0 = ½$		

t	time or the mathematical expression for $\sqrt{u-1}/\sqrt{u+1}$	
t_0	transport number of an ion in free solution	
t_d	mathematical expression for $\sqrt{u-1}/\sqrt{u+1}$ at the truncation plane of a double layer	
t_s	mathematical expression for $\sqrt{u-1}/\sqrt{u+1}$ at the shear plane of a double layer	
T	absolute temperature	K
u	Boltzmann accumulation factor for monovalent counterions	
v	pore water velocity	$m \cdot s^{-1}$
$\bar{V}_W$	partial molar volume of water	$m^3 \cdot mol^{-1}$
W_w	molecular weight of the solvent	$mol \cdot kg^{-1}$
x	thickness or distance	m
X_i	driving force of component i	
X_j	driving force of component j	
y	dimensionless potential function in the DDL	
α	first order mass transfer coefficient	s^{-1}
α'	factor in the tortuosity to account for the increasing viscosity of the water directly adjecent to a clay platelet	
β	constant in the DDL at 298.15 K: $10.80 \cdot 10^{15}$	$m \cdot mol^{-1}$
γ	factor in the tortuosity to account for anion exclusion	
Γ	counter charge per unit surface area	$mol_c \cdot m^1$
δ	distance of an imaginary plane of infinite charge and potential behind the surface of a clay particle in the DDL	m
ε_r	dielectric constant of water at 298.15 K: 78.54	
ε_0	permittivity of vacuum $8.85419 \cdot 10^{-12}$	$C \cdot V^{-1} \cdot m^{-1}$
θ	volumetric water content	$cm^3 \cdot cm^{-3}$
κ_0	Debije–Hückel reciprocal thickness of a diffuse double layer	m^{-1}
λ	dispersion length	m^{-1}
ν	number of ions in which an electrolyte dissociates	
π_0	osmotic pressure in the equilibrium solution	Pa
π	osmotic pressure in the pore water of the clay	Pa
ρ	fluid density	$g \cdot cm^{-3}$
ρ_b	bulk density	$g \cdot cm^{-3}$
ρ_p	particle density	$g \cdot cm^{-3}$
σ	reflection coefficient of a semipermeable membrane	
τ	tortuosity	
τ_a	apparent tortuosity	

ϕ	molal osmotic coefficient	
χ	double layer charge	$C \cdot m^{-2}$
ω	solute permeability coefficient	$mol \cdot N^{-1} \cdot s^{-1}$

Abbreviations

Ant	anthracene	
AgTU	silver thiourea	
A_S	specific surface area	$m^2 \cdot g^{-1}$
AWy	Ankerpoort Wyoming bentonite	
BaP	benzo[a]pyrene	
BbF	benzo[b]fluoranthrene	
BET	Brunauer–Emmett–Teller theory for adsorption	
BgP	benzo[ghi]perylene	
BK	harbour sludge from the *Beerkanaal*	
BkF	benzo[k]fluoranthrene	
BMR	harbour sludge from the *Beneden Merwede*–river	
BTC	breakthrough curve	
CEC	cation exchange capacity	$mol_c \cdot kg^{-1}$
DDL	diffuse double layer (theory)	
DOM	dissolved organic matter	
Ec	electrical conductivity	$mS \cdot cm^{-1}$
EGME	adsorption technique with ethylene glycol monoethyl ether	
HPLC	high performance liquid chromatography	
Flu	fluoranthrene	
FMMM	Fritz–Marine Membrane Model	
FTIR	Fourier transform infrared spectroscopy	
ICP–AES	inductively coupled plasma atomic emission spectroscopy	
InP	indeno[1,2,3 cd]pyrene	
PAH	polycyclic aromatic hydrocarbons	
Phe	phenanthrene	
POM	polyoxymethylene	
RO	reverse osmosis	
SPE	Bakerbond solid–phase extraction columns	
SWy	Source clay Wyoming bentonite	
TMS	Teorell–Meyer–Siever model for hyperfiltration	
XRD	X–ray diffractometry	

Samenvatting

Deze samenvatting is zo geschreven dat iedereen kennis kan nemen van dit onderzoek. Voor een wetenschappelijke samenvatting wordt de lezer verwezen naar de *Summary and general conclusions*, p. 129.

WAT IS CHEMISCHE OSMOSE?

Water stroomt van hoog naar laag. Iedereen kent wel de proef met twee buizen waarin water met een verschillende hoogte met elkaar worden verbonden. Water stroomt dan van de hoge naar de lage kant, net zolang tot het water in beide buizen even hoog staat. Logisch! Veel minder bekend is dat water ook kan stromen als gevolg van een verschil in (chemische) samenstelling van de oplossingen aan weerszijden van een halfdoorlatende laag. Dit watertransport heet chemische osmose en de halfdoorlatende laag wordt een semipermeabel membraan genoemd. In het ideale geval is zo'n membraan wél doorlatend voor het water en helemaal níet doorlatend voor de opgeloste stoffen in het water. In twee wetenschappelijke vakgebieden worden materialen bestudeerd die semipermeabele eigenschappen bezitten: biologie en geologie. Het bekendste biologische semipermeabele membraan is de varkensblaas. In de geologie zijn het de kleien en kleiige sedimenten/gesteenten die semipermeabel gedrag kunnen vertonen. Maar hoe werkt dat?

KLEIEN EN HUN EIGENSCHAPPEN

Waardoor zijn kleien in staat om als een semipermeabel membraan te werken? Kleideeltjes zijn electrisch negatief geladen door kleine onregelmatigheden in hun kristalrooster. Wanneer ze in aanraking komen met water, trekken zij positief geladen opgeloste deeltjes (kationen) uit het water aan. Negatief geladen deeltjes (anionen) in het water worden door de klei afgestoten. Hierdoor onstaat in de directe omgeving van het kleideeltje een hogere concentratie kationen dan in de rest van het water.

Verder van het kleideeltje weg neemt het aantal kationen af omdat de invloed van het kleideeltje minder sterk wordt. De kationen die door de klei worden aangetrokken èn oppervlak van het kleideeltje noemen we samen de Diffuse DubbelLaag (DDL). De mate waarin kleimineralen kationen kunnen binden varieërt sterk omdat de onregelmatigheden in het kristalrooster bij elk kleimineraal anders zijn. De mate waarin kationen gebonden worden heet de kationuitwisselingscapaciteit (*Cation Exchange Capacity*, CEC). Belangrijk voor de omvang van de dubbellaag is de lading van het kation. Kationen met een enkele lading —zoals natrium— hebben een dikke dubbellaag tot gevolg, omdat de klei deze kationen niet sterk aantrekt. Kationen met een dubbele lading —zoals calcium— worden veel sterker aangetrokken en geven daardoor een dunnere dubbellaag.

Wanneer de klei samengedrukt wordt, komen de kleideeltjes zo dicht bij elkaar te liggen dat de dubbellagen elkaar overlappen. Hierdoor wordt de ruimte tussen de kleideeltjes zo klein dat transport door de klei volledig beïnvloed wordt door de dubbellaag. Door de grote hoeveelheid positieve en negatieve lading worden de kationen en anionen in een oplossing die de klei willen passeren als het ware buiten de deur gehouden. Het water zelf en opgeloste stoffen zònder lading ondervinden geen hinder van de dichte opéénstapeling van lading in de klei en kunnen het membraan wel passeren. De klei werkt dan als een semipermeabel membraan!

De mate waarin een semipermeabel membraan ondoorlatend is voor opgeloste stoffen in een oplossing noemen we de idealiteit van een membraan en wordt uitgedrukt als de reflectiecoëfficiënt, σ. Veel biologische membranen zijn perfect in staat om de opgeloste stoffen in het water tegen te houden. We spreken dan van een ideaal membraan; σ is dan gelijk aan 1. Veel geologische membranen zijn niet zo goed in het tegenhouden van de opgeloste stoffen in het water. We spreken dan van niet–ideale membranen, waardoor de waarde van σ tussen 0 en 1 ligt. Bij een membraan met een σ–waarde van 0 is er geen sprake meer van semipermeabiliteit. De idealiteit van natuurlijke semipermeabele materialen wordt voornamelijk bepaald door de volgende factoren.

- De kleimineralen die aanwezig zijn in het gesteente of sediment. Sommige kleimineralen hebben een veel grotere CEC dan andere. Het kleimineraal montmorilloniet (bentoniet) bijvoorbeeld heeft een 10 keer grotere CEC–waarde dan kaoliniet, een kleimineraal in boetseerklei.
- De kationen die gebonden zijn aan de klei. Deze bepalen de dikte van de dubbellaag. Hoe dikker deze is, hoe eerder de dubbellagen van naburige kleideeltjes zullen overlappen.
- De mate waarin de klei is samengedrukt (compactie). Hoe hoger de compactie, hoe meer de dubbellagen van naburige kleideeltjes overlappen.

- De concentraties in de oplossingen aan beide zijden van het semipermeabele membraan. Hoe groter de concentratieverschillen hoe slechter de klei gaat werken als semipermeabel membraan.

Veel geologische semipermeabele membranen zijn niet–ideale membranen en zijn dus niet in staat om alle opgeloste stoffen in het water tegen te houden. Bij deze membranen kunnen opgeloste stoffen op twee verschillende manieren passeren. Ten eerste 'door mee te liften' met het water dat door osmose wordt verplaatst. Dit 'meeliften' heet advectie en bij chemische osmose gaat dit van de minder naar de meer geconcentreerde oplossing. Ten tweede bewegen ze zich van de geconcentreerde naar de minder geconcentreerde oplossing. Dat heet diffusie. In het geval van chemische osmose werken advectie en diffusie dus in tegengestelde richting. Wanneer het verschil in concentratie aan beide kanten van een niet–ideaal membraan groot is, gaat diffusie snel. Het concentratieverschil wordt daardoor kleiner, totdat het helemaal verdwenen is. Als het concentratieverschil over het semipermeabel membraan is verdwenen, is de motor achter chemische osmose stilgevallen.

WAAROM DEZE STUDIE?

In Nederland wordt op grote schaal gebaggerd. In de Rotterdamse haven is dat om de bereikbaarheid voor grote zeeschepen te behouden. Het opgebaggerde slib (baggerspecie) is in sommige gevallen zó verontreinigd dat het permanent moet worden opgeslagen. Een voorbeeld van een opslagplaats is het depot De Slufter op de Maasvlakte ten westen van Rotterdam. Het waterniveau in De Slufter wordt op dezelfde hoogte gehouden als daarbuiten. Hierdoor is het transport van water door de baggerspecielaag als gevolg van de verschillen in waterhoogte minimaal. Men veronderstelt dat hierdoor verspreiding van verontreinigingen in de baggerspecie wordt voorkomen. Echter de situatie van De Slufter —met zout water aan de onderkant, en zoet water aan de bovenkant— zorgt ervoor dat de baggerspecie gaat werken als een semipermeabel membraan. Er is immers een verschil in zoutconcentratie aan beide zijden van de baggerspecie. Die baggerspecie bevat bovendien klei waarvan bekend is dat het kan werken als een semipermeabel membraan. Hierdoor kan transport van water door osmose optreden en kunnen verontreinigingen in de baggerspecie alsnog door advectie —het 'meeliften' met het water— in het grondwater terecht komen. Zo kunnen bijvoorbeeld verontreinigingen zoals polycyclische aromatische koolwaterstoffen (PAK) zich toch verspreiden. PAK hebben geen lading en kunnen daardoor vrijwel ongehinderd een semipermeabel membraan passeren. Dit probleem doet zich niet alleen voor bij De Slufter maar kan ook in andere situaties nadelige

effecten hebben op de verspreiding van verontreinigingen. Bijvoorbeeld bij de toepassing van klei in afdichtende lagen onder vuilstorten.

De invloed van semipermeabiliteit van klei en kleiige sedimenten en de invloed daarvan op het transport van water en de verspreiding van verontreinigingen, is in Nederland niet eerder onderzocht.

DIT PROEFSCHRIFT

Het doel van het onderzoek was het ontwikkelen van een laboratoriumopstelling waarin de semipermeabiliteit van kleiige materialen gemeten kan worden en de invloed van semipermeabiliteit op het transport van water en verontreinigingen.

In **hoofdstuk 1** wordt de theorie van semipermeabel gedrag van kleiige materialen besproken. Drie rekenmodellen waarmee een schatting van de semipermeabiliteit kan worden gemaakt worden geïntroduceerd. Deze drie modellen, het Fritz–Marine Membraan Model (FMMM), het model geformuleerd door Kemper en Bresler en een model geformuleerd door Groenevelt en Bolt, worden in het hoofdstuk uitgebreid beschreven. Daarnaast wordt een overzicht gegeven van eerder werk op het gebied van de semipermeabiliteit van natuurlijke materialen, de factoren die daarop van invloed zijn en de consequenties op geologische processen.

Alle experimenten in deze studie zijn uitgevoerd met bentoniet en verontreinigde baggerspecie. De eigenschappen van deze monsters worden beschreven in **hoofdstuk 2**. Bentoniet is gekozen omdat deze klei in de praktijk toegepast wordt als een slecht doorlatende laag in situaties waar de verspreiding van verontreinigingen ongewenst is, bijvoorbeeld onder vuilstorten. Uit eerdere studies is bekend dat bentoniet heel goed als semipermeabel membraan kan werken. De baggerspeciemonsters zijn representatief voor de baggerspecie die gestort wordt in De Slufter en komen van twee verschillende lokaties uit het havengebied van Rotterdam.

Een uitgebreide beschrijving van de opstelling voor het meten van chemische osmose wordt gegeven in **hoofdstuk 3**. In de opstelling staat het monster —met een dikte van ongeveer 2 mm— in contact met oplossingen van verschillende concentratie. Wanneer het monster werkt als een semipermeabel membraan, kunnen het osmotisch gedreven watertransport en de veranderingen in de concentraties in de reservoirs, bijvoorbeeld door diffusie gemeten worden.

De experimenten met bentoniet worden beschreven in **hoofdstuk 4**. In drie van de vier experimenten is chemische osmose waargenomen en konden de waarden voor σ van de monsters worden bepaald. Naast chemische osmose werd eveneens diffusie–osmose waargenomen. Diffusie–osmose is transport van water dat wordt

'meegesleept' tijdens diffusie. In alle experimenten werd een σ gemeten die beduidend lager was dan de door de modellen voorspelde waarde. Uit een vergelijking met literatuurwaarden bleek het verschil tussen berekende en gemeten waarden voor bentonieten niet beperkt te zijn tot deze studie. Er zijn twee oorzaken 1) de aannamen die ten grondslag liggen aan de modellen zijn niet van toepassing op de gebruikte monsters en 2) onnauwkeurigheden in de metingen tijdens de experimenten maken dat σ lager is dan de theorie voorspelt.

Om het effect van diffusie op het semipermeabel gedrag te kwantificeren, is één experiment gemodelleerd met het computerprogramma PHREEQC. Hieruit bleek dat de diffusiesnelheden in een klei die werkt als semipermeabel membraan lager zijn dan normaal in kleien en sedimenten.

In **hoofdstuk 5** worden de resultaten van de experimenten met de twee baggerspeciemonsters beschreven. Het is de eerste keer dat het semipermeabel gedrag van verontreinigd kleiig sediment wordt beschreven. De baggerspecie uit het Beerkanaal met een kleigehalte van ongeveer 56 % vertoonde osmotisch gedreven watertransport. In de baggerspecie uit de Beneden Merwede daarentegen werd geen semipermeabel gedrag waargenomen. Deze specie heeft een beduidend lager kleigehalte, ongeveer 26 %. Het verschil in gedrag is toegeschreven aan de verschillen in het kleigehalte tussen de baggerspeciemonsters en de aanwezige kleimineralen.

Evenals bij de experimenten aan bentoniet was de gemeten σ voor de baggerspecies lager dan de door de modellen voorspelde waarde. Het model van Kemper–Bresler gaf de beste voorspelling van de experimentele reflectiecoëfficiënt. Deze waarneming wordt ondersteund door resultaten uit vergelijkbare studies aan geologische materialen. Uit de experimenten aan baggerspecie werd eveneens duidelijk dat σ geen vaste eigenschap is van een gegeven natuurlijk kleiig materiaal. Gedurende een experiment neemt σ af als gevolg van diffusie.

In **hoofdstuk 6** wordt de uitspoeling van acht polycyclische aromatische koolwaterstoffen (PAK) uit de baggerspeciemonsters besproken. PAK komen vaak voor als verontreinigingen in bodems en sedimenten. De mobiliteit van deze verontreinigingen kan worden uitgedrukt in de partitiecoëfficiënt (K_{OC}). Twee verschillende experimenten werden uitgevoerd om K_{OC} te bepalen in de baggerspecie onder omstandigheden die vergelijkbaar zijn met die in een baggerspeciedepot 1) centrifuge *batch*–experimenten en 2) kolomexperimenten, beide bij 4°C. De K_{OC}–waarden waren hoger dan meestal gevonden wordt met traditionele bepalingsmethoden, zoals bij *batch*–experimenten waarin de monsters gedurende een korte periode geschud worden bij 25°C. Ook de waarden afgeleid uit de kolomexperimenten waren hoger. De verschillen kunnen niet volledig verklaard worden door het temperatuursverschil. De langdurige verontreiniging van de baggerspecies met PAK is waarschijnlijk van

doorslaggevend belang. Uit de kolomexperimenten bleek ook dat, zelfs bij zeer lage doorstroomsnelheden van water, PAK uit de baggerspecie kunnen spoelen. De hogere waarden van K_{OC} duiden er op dat de hoeveelheden lager zullen zijn dan geschat op basis van de traditionele bepalingsmethoden.

In **hoofdstuk 7** wordt de toepasbaarheid van de drie rekenmodellen voor het bepalen van σ geëvalueerd. De experimenten aan de baggerspecie en de bentoniet èn de literatuurwaarden lieten een groot verschil zien tussen experiment en theorie. Op basis van enkele theoretische en praktische overwegingen en de aannamen in de modellen wordt voor de afzonderlijke modellen een toepassingsgebied gegeven. Daarnaast worden mogelijkheden aangedragen om de modellen beter af te stemmen op de specifieke omstandigheden van geologisch semipermeabele membranen.

Op basis van de gemeten σ van de baggerspecie uit het Beerkanaal wordt de invloed van semipermeabiliteit op het transport van water in het baggerspeciedepot De Slufter besproken. Hieruit blijkt dat het osmotich gedreven watertransport in dezelfde orde van grootte is als het wettelijke maximaal toelaatbare, hydraulische watertransport. Het is daarom te verwachten dat de door het beleid gehanteerde milieucriteria met betrekking tot het watertransport in het depot worden overschreden. Bovendien kan door de specifieke omstandigheden in en om De Slufter de baggerspecie in het depot oneindig lang werken als een semipermeabel membraan met alle mogelijke nadelige gevolgen voor mens en milieu.

Dankwoord / Acknowledgements

Met dank aan: • Mijn promotor, CH van der Weijden voor de mogelijkheid om te promoveren op een interessant, bijna vergeten onderwerp en de vrijheid die hij mij gegeven heeft om het onderzoek in te vullen naar eigen inzicht. • Mijn co–promotor, Guus Loch. Guus, dank je voor je aanstekelijke enthousiasme voor Nederlandse bodems en de processen die zich daarin afspelen. Voor gek heb ik je versleten op de Asselse Heide op een heldere voorjaarsochtend toen je lyrisch begon te vertellen over een podzol. Nu betrap ik mijzelf hierop! Voor de prettige discussies die we gevoerd hebben over soms moeilijk te interpreteren resultaten. Ik heb er veel van geleerd en veel van de inzichten staan in dit proefschrift. • *Steven Fritz. Steven, thank you for your support. Without our discussions in the cold, february air of Indiana I wouldn't have had the motivation to finish this thesis.* • Pieter Kleingeld. Pieter, je bleek onmisbaar. Zonder jouw veelzijdigheid en enthousiasme had er waarschijnlijk nooit een 'kippenhok' gestaan met daarin een werkende opstelling. • Mark van Alphen. Mark, bedankt voor alle analyses. Er zijn momenten geweest dat je moet hebben gedacht dat er nooit een einde zou komen aan de CEC bepalingen. Mijn kamergenoten: Berend Wilkens, Pim Middeldorp, Gerard van der Berg en Arthur Schmidt. Dankzij jullie ben ik niet alleen bezig geweest met chemische, maar ook met sociale osmose. • De projectgroep Geochemie: Alle aio's, oio's, post–docs en vaste staf. • Sandra.

Curriculum vitæ

Thomas Jillerd Simon Keijzer werd op 16 september 1966 geboren te Bramsche in de Bondsrepubliek Duitsland. Na een omzwerving door het Nederlandse onderwijssysteem, waarbij hij een MAVO–diploma behaalde aan de RK MAVO De Nijehove te Leeuwarden en een HAVO–diploma aan het RK Veurs College te Leidschendam, begon hij in 1985 aan de opleiding tot chemisch analist aan de voormalige Haagse Analisten School te 's–Gravenhage. In 1989 werd deze afgesloten en na een aantal maanden werkzaam te zijn geweest als chemisch analist begon hij aan de studie Geochemie aan de Faculteit Aardwetenschappen van de Universiteit Utrecht. Deze opleiding werd in het voorjaar van 1993 afgesloten met een afstudeeronderzoek naar de verspreiding van een fungicide in de Groningse Veenkoloniën. Eind 1993 kwam hij in dienst van de Faculteit Aardwetenschappen, Universiteit Utrecht, als toegevoegd onderzoeker. Een *pilot*–onderzoek naar chemische osmose in samenwerking met Grondmechanica Delft (het huidige GeoDelft) werd circa een jaar later afgesloten. In de periode 1995–1999 was Thomas werkzaam als assistent in opleiding aan dezelfde faculteit en werd het promotieonderzoek uitgevoerd, waarvan de resultaten beschreven worden in dit proefschrift.

Van de maan af gezien, zijn we allen even groot.
Voor een weter zou er geen verschil merkbaar zijn tussen de kennis van 'n kind
en van de wijsgeer die 't meest en 't zuiverst gedacht heeft.
Multatuli – Idee 155

P